

Glucose Responsive Microgel Modified Quartz Crystal Microbalances as a Glucose  
Sensor

by

Chung Yeon Cho

A thesis submitted in partial fulfillment of the requirements for the degree of

Master of Science

Department of Chemistry  
University of Alberta

© Chung Yeon Cho, 2015

## **Abstract**

The Serpe group has shown that optical devices can be fabricated by layering poly (N-isopropylacrylamide) (pNIPAm) microgels onto a gold-coated glass substrate and then depositing another gold layer on top. These devices, called etalons, exhibit optical properties that depend on many characteristics, primarily temperature. Temperature is the most basic property of pNIPAm-based microgels, as it changes their solvation state. In this study, we modified pNIPAm-based microgels with 3-aminophenylboronic acid (APBA), which renders them responsive to glucose; i.e., they change size in a glucose-dependent fashion. By modifying the Au surface of a quartz crystal microbalance (QCM) with etalons composed of these microgels, we can make QCM-based devices that shift frequency as a function of glucose concentration in buffer solution. Again, this is a result of the microgels' changing solvation state in response to glucose. It was determined that glucose-responsive pNIPAm microgel-based QCM can be used as a glucose sensor. This dissertation will detail the work done on these systems.

## ACKNOWLEDGEMENTS

First of all, I would like to thank Dr. Michael J. Serpe for giving me the opportunity to join and work in his group. He has always encouraged and supported me to broaden the scope of my chemistry environmental work and my project. He always gave me lots of comments for what I got from my project and ready to help me to handle problems. He has appreciation of the student's problem from his experience and he was an excellent teacher, life coach and a research supervisor. He trusted his students and kept cheering them up to reach excellent level. Whenever I had the discussions with him, he helped me a lot and gave me a wider perspective of science in general. He also always thinks great idea I cannot imagine.

I also would like to thank everyone in Serpe group, Xue Li who helped me and organized general group atmosphere as a senior student, and especially, Molla. Islam who has helped me a lot with my troubles in every single thing in a lab. I would like to thank my friends in the department of Chemistry for their help and support. I would also like to thank Korean Graduate Student's Association (KGSA) helped and supported me during my master study, especially Inseok Chae who gave me lots of lessons about life and working in the lab, advices for my future career. I would like to thank my friends in Edmonton, Hyeongjin Kim, Andrew Jo, Anne JH Lim, and Carmen Wong and I would like to thank my parents and my sister for their unconditional support and love all through my life.

# Table of Contents

CHAPTER 1	STIMULI RESPONSIVE POLYMERS, POLY (N-ISOPROPYLACRYLAMIDE) MICROGEL BASED ETALONS, AND QUARTZ CRYSTAL MICROBALANCES .....	1
1.1	Introduction.....	1
1.2	Stimuli-Responsive Polymers.....	6
1.2.1	Physical Stimuli Responsive Polymers .....	7
1.2.2	Chemical Stimuli-Responsive Polymers .....	8
1.2.3	Biological Stimuli-Responsive (Bioresponsive) .....	9
1.2.4	Multi Stimuli Responsive .....	14
1.3	Stimuli-Responsive Hydrogel.....	14
1.4	Poly (N-isopropylacrylamide) Microgels .....	15
1.4.1	Synthesis of pNIPAm Microgels.....	17
1.4.2	pNIPAM Microgel-Based Etalon .....	18
1.4.3	pNIPAm Microgel Applications.....	20
1.5	Quartz Crystal Microbalance .....	24
1.5.1	Etalon Fabrication on a QCM.....	28
1.5.2	Surface Chemistry in QCM study .....	29
1.5.2.1	Physisorption on QCM .....	29
1.5.2.2	Chemisorption on QCM .....	30
1.5.2.3	Plasma-Polymerized Films (PPFs) .....	32

1.5.3 QCM Applications.....	33
1.5.3.1 Detection of Gaseous Species.....	33
1.5.3.2 Detection of Carbohydrates .....	34
1.5.4 Previous QCM studies.....	35
1.5.4.1 DNA Sensing.....	35
1.5.4.2 <i>Protein Sensing</i> .....	37
1.6 Outline of the Thesis.....	41
 CHAPTER 2 POLY (N-ISOPROPYLACRYLAMIDE) MICROGEL BASED ETALONS FOR GLUCOSE DETECTION.....	 42
2.1 Introduction.....	42
2.1.1 The Development of a Glucose Biosensor .....	42
2.1.1.1 First Generation of Glucose Biosensors .....	44
2.1.1.2 Second Generation of Glucose Biosensors.....	46
2.1.1.3 Third Generation of Glucose Biosensors.....	48
2.1.2 Current Glucose-Sensing Technology.....	49
2.1.3 Glucose-Responsive Microgels .....	51
2.2 Materials and Methods.....	53
2.3 Results and discussion .....	60
2.4 Conclusions.....	69
 CHAPTER 3 MICROGEL MODIFIED QUARTZ CRYSTAL MICROBALANCES AS A GLUCOSE SENSOR.....	 70
3.1 Introduction.....	70

3.2 Materials and Methods.....	71
3.3 Results and Discussion .....	76
3.3.1 <i>Selectivity Performance</i> .....	76
3.3.2 <i>Reproducibility Performance</i> .....	80
3.4 Conclusions.....	84
CONCLUSIONS.....	85
FUTURE DIRECTION .....	86

## LIST OF TABLES

Table 2.1 The resonant frequency shift in different diameter pNIPAm- <i>co</i> -APBA microgels after 0.6 g/dL of glucose buffer solution (pH 9.5).....	68
Table 3.1 The resonant frequency shift in different glucose concentrations and the reproducibility of each concentration .....	83

## LIST OF FIGURES

Figure 1.1 Biosensor components and steps of measurement. ....	1
Figure 1.2 Schematic of an LFA.....	2
Figure 1.3 Schematic of an ELISA.....	4
Figure 1.4 Classified Stimuli-Responsive Polymer.....	7
Figure 1.5 Temperature-responsive polymers change their forms when the temperature changes.....	8
Figure 1.6 Chemical Stimuli-Responsive Polymer, scheme of swelling/deswelling mechanism activated by pH changes in pH-Responsive Polymer.....	9
Figure 1.7 The scheme of the DNA-responsive hydrogel photonic beads. ....	11
Figure 1.8 The scheme of a mechanism for the swelling of semi-IPN hydrogel in response to a free antigen.....	11
Figure 1.9 The illustration of the genetically engineered cysteine site near the receptor-active site and the binding capacity of the ligand in the polymer's hydrated or collapsed state. ....	12
Figure 1.10 Chemical Structure of pNIPAm. Amide group side and isopropyl side group showed hydrophilic (Blue) and hydrophobic (Yellow) properties, respectively. ....	16
Figure 1.11 Different comonomers with their pKa.....	17
Figure 1.12 The synthesis of a pNIPAM-based microgels using an APS initiator.....	18
Figure 1.13 A scheme of a Fabry-Pérot interferometer.....	19
Figure 1.14 The scheme of drug loading and release process in pNIPAm-based controlled drug release. ....	23

Figure 1.15 The side-view of coated material modified QCM crystal .....	25
Figure 1.16 pNIPAm-based microgel etalon fabrication .....	28
Figure 1.17 Scheme of Self-Assembled Monolayers' deposition on QCM crystal.....	31
Figure 1.18 Schematic illustration of QCM-based DNA detection by immobilized DNA probe on the QCM surface.....	36
Figure 1.19 $\Delta f$ vs $t$ and $\Delta D$ vs $t$ for the adsorption of Hb on the QCM surface at pH 6.5 and 7.0 The influence of pH on the Hb adsorption kinetics is also illustrated by the D-f plot (c). The simple linear behavior at pH 7.0 is replaced by a two-phase behavior at pH 6.5, where the total mass uptake and final dissipation shift are larger. ....	38
Figure 2.1 The glucose oxidation and generating electrons in membranes on the platinum electrode.....	44
Figure 2.2 Glucose Oxidase electrochemistry in second-generation glucose biosensors' mediated system.....	47
Figure 2.3 The three generation of glucose biosensors based on amperometric enzyme electrodes. ....	49
Figure 2.4 The single-use blood glucose meter strip. Adapted from <sup>170</sup> . Copyright 2008, ACS Publications.....	50
Figure 2.5 The illustration of glucose biosensing based on a graphite electrode. ....	51
Figure 2.6 The mechanism of glucose binding to hydroxylated boronic acid at pH 9.5..	52
Figure 2.7 The scheme of the glucose responsivity of a pNIPAm- <i>co</i> -APBA microgel-based etalon at pH 9.0. ....	53
Figure 2.8 Scheme of pNIPAm- <i>co</i> -ABPA microgel on QCM crystal.....	60

Figure 2.9 The microscopic image of pNIPAm- <i>co</i> -APBA microgels on the glass substrate. .....	61
Figure 2.10 The AFM image of a APBA microgel layer after glucose solution addition A) 0min, B) 15 min, and C) 30 min. ....	62
Figure 2.11 The height of the pNIPAm- <i>co</i> -APBA microgel layer on the QCM crystal before glucose was added .....	63
Figure 2.12 The height of the pNIPAm- <i>co</i> -APBA microgel layer on the QCM crystal 15 min after glucose was added. ....	63
Figure 2.13 The height of the pNIPAm- <i>co</i> -APBA microgel layer on the QCM crystal after 30 min glucose addition. ....	64
Figure 2.14 UV-VIS absorption spectra of pH 9.5 buffer solutions containing pNIPAm- <i>co</i> -APBA microgels before and after the addition of the indicated amount of glucose. ....	65
Figure 2.15 The variation of the absorbance at 300nm as a function of glucose addition. .....	66
Figure 2.16 The resonant frequency shift of pNIPAm containing 10 % and 15 % APBA with different amounts of glucose added .....	67
Figure 3.1 The Molecular Structure of A) $\alpha$ -D Glucose, B) Galactose, and C) Sucrose.	77
Figure 3.2 Equilibria between the favorable form (left) and the form that contains a syn-periplanar anomeric hydroxyl pair (right) of D-fructose A), D-glucose B) and D-galactose C).....	77
Figure 3.3 The selectivity performance in pNIPAm- <i>co</i> -APBA microgels. Glucose-, sucrose-, and galactose-responsive measurement by resonant frequency shift. ....	79

Figure 3.4 The resonant frequency shift for each A) 0.05 g/dL and B) 0.11 g/dL of glucose buffer solution (pH 9.5) added at 25 °C..... 80

Figure 3.5 The resonant frequency shift for each A) 0.125 g/dL and B) 0.140 g/dL of glucose buffer solution (pH 9.5) added at 25 °C..... 81

Figure 3.6 The resonant frequency shift for each A) 0.155 g/dL and B) 0.175 g/dL of glucose buffer solution (pH 9.5) added at 25 °C..... 82

Figure 3.7 The resonant frequency shift for each A) 0.199 g/dL of glucose buffer solution (pH 9.5) added and B)..... 82

## LIST OF ABBREVIATIONS

AAc – Acrylic Acid

AC – Alternating Current

ADDL –  $\alpha$ -Amyloid  $\beta$ -Derived Diffusible Ligands

AFM – Atomic Force Microscopy

APBA – 3-Aminophenylboronic Acid

APS – ammonium persulfate

BIS – N,N'-methylenebisacrylamide

CAP – Cell-Adhesive Peptide

CTAB – Cetyltrimethyl Ammonium Bromide

DI – Deionized

DLS – Dynamic Light Scattering

DMAEMA – N-Dimethylamoniethyl methacrylate

ECM – Extracellular Matrix

EDC – 1-ethyl-3-(3-dimethylaminopropyl) carbodiimide

ELISAs – Enzyme-Linked Immunosorbent Assays

ESP – Enzyme-Sensitive Peptide

FAD – Flavin Adenine Dinucleotide

FIA – Flow Injection Analysis

GDH-PQQ – pyrrole-quinolinequinone

GOx – Glucose Oxidase

GMOs – Genetically Modified Organisms

Hb – Hemoglobin

HEMA – 2-hydroxyl methacrylate

IFA – Immunofluorescent Assay

IPN – Interpenetrating Polymer Network

LFAs – Lateral Flow Assays

LBL – Layer-By-Layer

LCST – Lower Critical Solution Temperature

LSPR – Local Surface Plasmon Resonance

Mb – Myoglobin

MC – Microcantilever

NW – Nanowire

ODN – oligodeoxyribonucleotides

P35S – CaMV 35S promoter sequence

PA – polyacetylene

PAHs – Polycyclic Aromatic Hydrocarbon

PANI – polyaniline

PBA – Phenylboronic Acid

PDADMAC – poly (diallyldimethyl-ammonium chloride)

PEG – polyethylene glycol

poly(GMA-co-VFc) – poly (glycidyl methacrylate-co-vinylferrocene)

pNIPAm – Poly(N-Isopropylacrylamide)

pNiPAm-co-AAc – Poly(N-Isopropylacrylamide-co-acrylic acid)

PPFs – Plasma-Polymerization Films

PPy – poly (pyrrole)  
PrA – Protein-A  
PrG – Protein-G  
PSA – Prostate-Specific Antigen  
PSS – sulphonated-polystyrene, poly (sodium 4-styrenesulfonate)  
PT – poly (thiophene)  
QCM – Quartz Crystal Microbalance  
QCM-D – Quartz Crystal Microbalances Dissipation  
rcf – relative centrifugal force  
SAMs – Self-Assembled Monolayers  
SILs – Sensing Ionic Liquids  
SMBG – Self-Monitoring Blood Glucose  
SPR – Surface Plasmon Resonance  
TCNQ – Tetracyanoquinodimethane  
tPSA – total Prostate-Specific Antigen  
TTF – Tetrathiafulvalene  
TRAIL – TNF-Related Apoptosis-Inducing Ligand  
TSM – Thickness Shear Mode  
UV – Ultraviolet  
VIS – Visible  
VPTT – Volume Phase Transition Temperature  
WHO – World Health Organization

# CHAPTER 1 STIMULI RESPONSIVE POLYMERS, POLY (N-ISOPROPYLACRYLAMIDE) MICROGEL BASED ETALONS, AND QUARTZ CRYSTAL MICROBALANCES

## 1.1 Introduction

Over the past 50 years, sensor research has had an impact on medical and environmental science.<sup>1</sup> Biosensors that can detect biological compounds such as glucose, urea, and cholesterol in blood can be used to diagnose diseases.<sup>2</sup> The general biosensing concept relies on a physical signal that is triggered by interactions between immobilized species and target molecules. Biosensors generally operate according to the following process:

- 1) A biological element (i.e., analyte) is recognized by a binding element.
- 2) Each binding triggers a signal.
- 3) Each signal is recorded
- 4) The records for all of the signals are collected.
- 5) Each signal is processed and connected to the appropriate analyte concentration.

Figure 1.1 schematically depicts the biosensor process.<sup>2</sup> Biosensor studies have been developed to detect biomolecules such as microorganisms,<sup>3</sup> enzymes,<sup>4</sup> antibodies, and antigens,<sup>5</sup> and to detect diseases.<sup>1-6</sup>

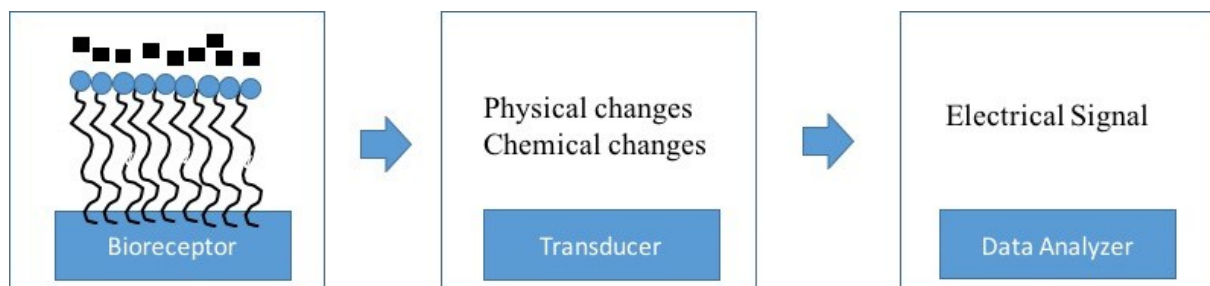


Figure 1.1 Biosensor components and steps of measurement. Adopted from <sup>2</sup>. Copyright Intech Publications.

Two kinds of biosensors are frequently used in lateral flow immunochromatographic assays (LFAs) and enzyme-linked immunosorbent assays (ELISAs).<sup>7</sup> The LFA uses bio-recognition probes and chromatography to detect the presence (or absence) of a targeted analyte in a sample. LFAs are commonly used for urine-based pregnancy tests, antibody-antigen interactions,<sup>7</sup> and to detect cancer biomarkers.<sup>8</sup> An LFA schematic is shown in figure 1.2.

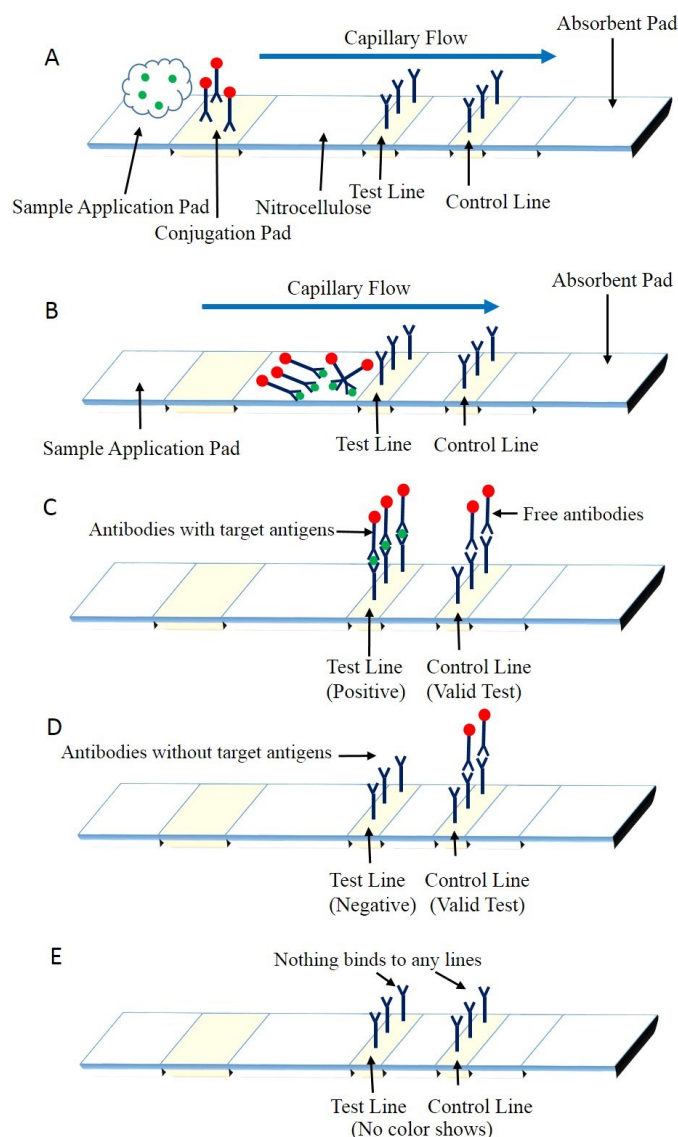


Figure 1.2 Schematic of an LFA: A) The sample with the target analyte is applied to the sample application pad. B) The sample flows over the strip under capillary action. C) Labeled probe biomolecules (antibodies) capture the target analyte (antigen), and the color appears at the test and control lines. D) Color appearing only at the control line means the target analyte is not present in sample, i.e., the results are negative. E) No color at test and control lines shows that the antibody is damaged. Adopted from<sup>9</sup>. Copyright 2013, MDPI publications.

LFA is performed on a strip with different components assembled on the surface. The pre-immobilized reagents located on different parts of the strip become active when they contact target analytes in the liquid sample.<sup>10</sup> When a sample containing a target analytes are applied to the sample application pad (figure 1.2 A), the probe biomolecules (usually labeled with gold nanoparticles or fluorophores) capture the analyte species and flow along the strips under capillary action (figure 1.2 B). Once the captured analytes reach the test line, the acceptors capture the conjugated analytes and a line of color appears. After more of the fluid sample flows along the strip, colored species that bind to analytes accumulate at the test line. Unbound probe biomolecules accumulate at the control line, as seen in figure 1.2 C. If the sample does not contain target biomolecules, the color shows up not at the test line but at the control line.

The ELISA is commonly used in serological tests to look for specific antigens or antibodies. It provides a color change to identify an antigen in a liquid sample. Figure 1.3 shows a schematic of the ELISA. The ELISA is typically performed in a 96-well polystyrene plate, which allows the probe proteins to adsorb onto the well surface (figure 1.3 A). Next, the liquid sample is added to the well to detect the target antigens, which bind to the primary surface-bound antibodies (figure 1.3 B). After rinsing the well to remove unbound antigens (figure 1.3 C), secondary antibody aliquot is added. These antibodies are modified with a reporter enzyme (figure 1.3 D) so that they change color when the enzyme reacts with its substrate (figure 1.3 E and F).<sup>11</sup>

The advantages of the LFA are its quick analysis time (a few minutes), ease of use, and low cost. However, its detection limit is near 0.1  $\mu\text{M}$ , which is not low enough to detect many biological molecules of interest in samples. The ELISA analysis time is longer (approximately one hour) than that of the LFA but its sensitivity is  $10^6$  higher. Ideally, biosensor technologies should have a low limit of detection and fast analysis time.<sup>7</sup>

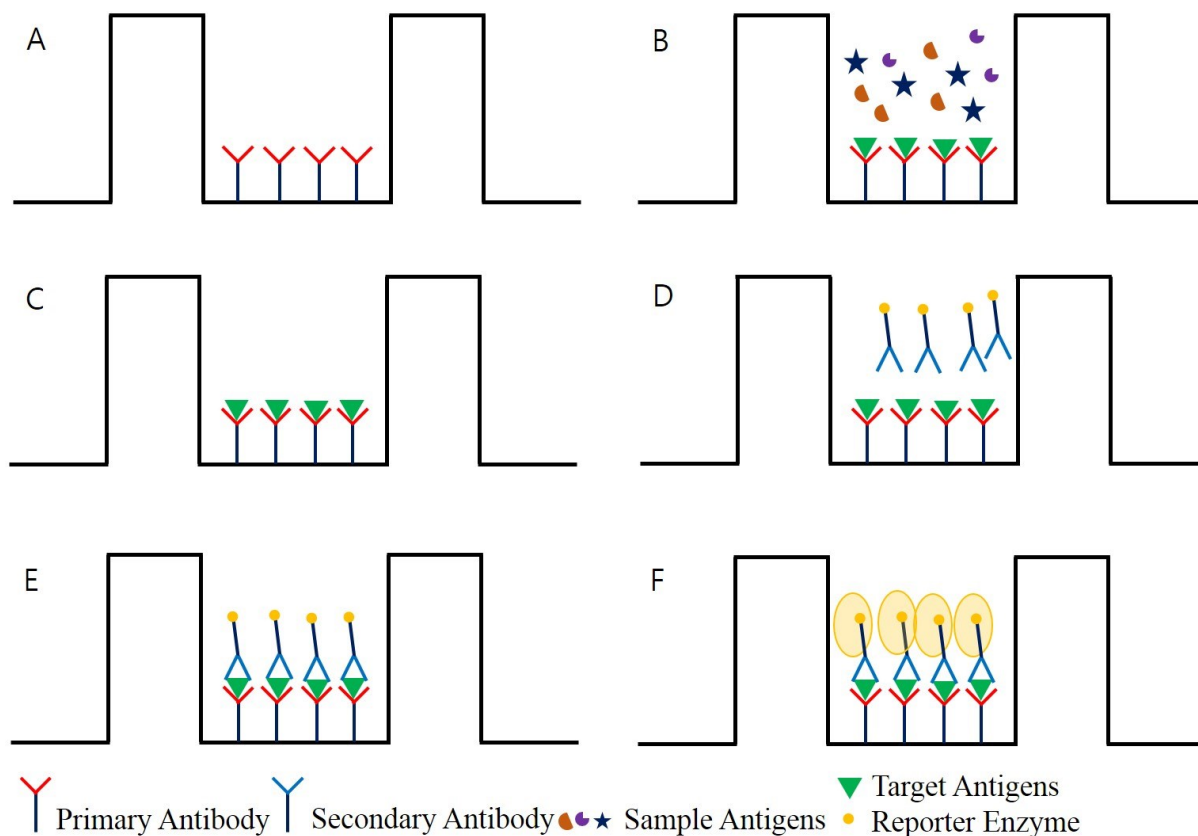


Figure 1.3 Schematic of an ELISA: (A) Primary antibodies are precoated on the well sides. (B) Sample antigens, including antigens targeted by the antibodies, are introduced into the well. (C) Primary antibodies bind to target antigens. The solution is removed from the well. (D) Secondary antibodies with reporter enzymes are introduced into the well. (E) Primary antibodies bind to immobilized secondary antibodies. (F) The wells are washed and filled with antibodies modified with reporter enzymes that produce a color when they bind to the target antigen. The amount of labelled antigens is calculated by measuring the color intensity.

Surface plasmon resonance (SPR) has been used for many years to detect biomolecules and biomolecular interactions.<sup>12</sup> SPR-based biosensors can detect refractive index changes near an Au sensor surface when a molecule that binds to this surface induces a change in the refractive index at the interface between the molecule and the sensor surface.<sup>13</sup> SPR is able to characterize binding interactions in real-time without biomolecule labeling and therefore has been widely adopted to determine the specificity and affinity of macromolecules (e.g., protein-protein,<sup>14</sup> protein-DNA,<sup>15</sup> receptor-drug,<sup>16</sup> and enzyme-substrate or enzyme-inhibitor).<sup>17</sup> The Van Duyne group developed localized surface plasmon resonance (LSPR), a detection technique that relies on the unique properties of metal nanoparticles.<sup>18</sup> This group also

introduced a biosensor for the early detection of biomolecules that indicate Alzheimer's disease. They used silver nanoparticles to help determine the interaction between amyloid beta-derived diffusible ligands (ADDL) and anti-ADDL antibodies, which are thought to be involved in the development of Alzheimer's.<sup>19</sup>

The SPR signal is strongly affected by optical thickness changes in the metal film on the sensor surface and by changes ( $\sim 200$  nm) in the refractive index of the light that strikes the metal surface.<sup>20</sup> Kim et al. used this information to develop an antibody chip with conformational specificity; the Bax protein is bound to the chip with specific rotated structure to provide this conformational specificity. The Bax protein plays a main role in the mitochondrial pathway for apoptosis. Kim et al. showed that the TNF-related apoptosis-inducing ligand (TRAIL) induced conformational changes in the Bax protein which can be represented in SPR images. Only structural alterations in the conformation of the Bax protein were shown in these results.<sup>21</sup>

Biomarkers are biomolecules that are indicative of disease. They can be detected if they can be immobilized on the surface of SPR sensors and the binding changes the refractive index of the light at the metal sample interface. Uludag et al. used SPR to detect total prostate-specific antigen (tPSA),<sup>22</sup> a biomarker for prostate cancer. An increase of  $4 \text{ ng mL}^{-1}$  of prostate-specific antigen (PSA) over the normal level in human blood indicates the possible presence of a prostate tumor. Biomarkers exist in low concentrations in blood samples, and the limit of detection of SPR in biosensors is  $0.29 \text{ ng mL}^{-1}$  ( $8.5 \text{ pM}$ ).<sup>22</sup> To overcome this limitation, nanoparticles have been used to amplify the signal. SPR signals are enhanced by using antibody-modified nanoparticles to increase the surface's refractive index.<sup>22</sup>

Other approaches to biosensing have used polymers modified with various functionality/biomolecules to improve the biosensor detection limit, stability, and sensitivity.<sup>1,23</sup> For example, stimuli-responsive polymers<sup>24</sup> are able to "sense" and "respond" to

external stimuli (i.e., temperature<sup>25</sup> and pH<sup>24</sup>) by undergoing a change in their conformation, size, shape, optical properties, solubility, degradation, and/or bond cleavage.<sup>24</sup> Stimuli-responsive polymers have beneficial properties for biosensor research, such as structure stability, biocompatibility, and processability.<sup>26</sup> Biosensor studies are useful in investigating antibody-antigen<sup>5</sup> and probe-target protein<sup>27</sup> interactions and enzyme-substrate binding.

## **1.2 Stimuli-Responsive Polymers**

Stimuli-responsive polymers can respond in specific ways to stimuli such as changes in temperature and pH.<sup>28-29</sup> These polymers change their hydrophilicity/hydrophobicity, solubility, and conformation in the presence of certain stimuli<sup>8</sup> and their responses are reversible. Stimuli-responsive polymer systems are easy to modify with functional groups that can be tailored for specific applications. For example, weak polyelectrolytes conjugated with stimuli-responsive polymers show pH-responsive properties. At the molecular level, intra/intermolecular interactions in the polymer chains lead to changes in properties such as charge or hydrophilicity. Stimuli can be physical, chemical, and biological (figure 1.4).<sup>24</sup> Temperature, pH, chemical, and multi-responsive polymer systems are described in sections 1.2.1 to 1.2.4.<sup>24-29</sup>

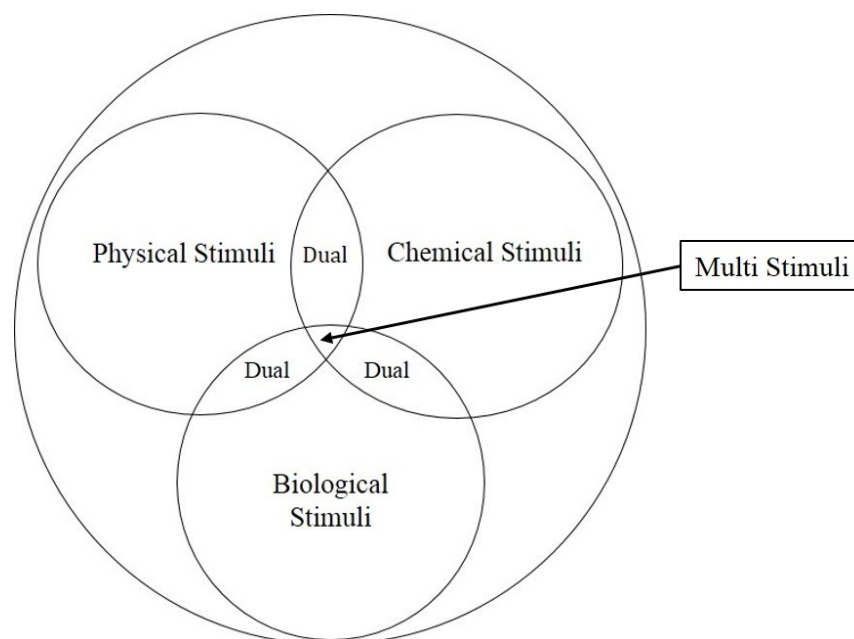


Figure 1.4 Classified Stimuli-Responsive Polymer Adopted from<sup>24</sup>. Copyright 2006, Elsevier Ltd.

### 1.2.1 Physical Stimuli Responsive Polymers

Physical stimuli, which contain light, temperature, magnetic, electrical, and mechanical deformation, affect polymer structure and chain dynamics, such as the energy level of the polymer-solvent system. In biomedical engineering and sensing applications, temperature-responsive polymers are commonly used because certain diseases manifest physiological temperature changes in the human body.<sup>24,25</sup> The commonly used physical stimulus is temperature stimulus. Generally, temperature-responsive polymers are characterized by a lower critical solution temperature (LCST) where the phase separation occurs. At this temperature, the polymer becomes insoluble in water because of increased hydrophobic interactions. Thus, the polymer chains form a compact structure by dehydration and have a phase separation above the LCST (figure 1.5). A well-known temperature-responsive polymer is poly (N-isopropylacrylamide) (pNIPAm).<sup>24,28</sup> In pNIPAm, temperature changes lead to conformational changes such as swelling or shrinking. The temperature is a critical factor in polymer

performance and it should be considered in biosensor applications. Thermo-responsive properties in pNIPAm will be discussed in Section 1.3.

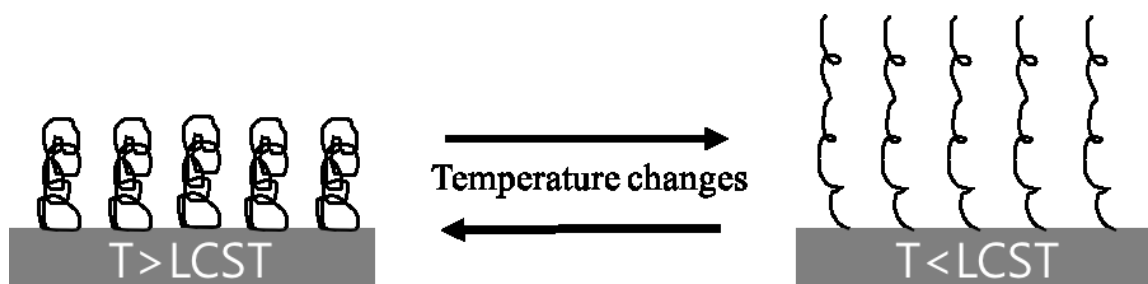


Figure 1.5 Temperature-responsive polymers change their forms when the temperature changes.

### 1.2.2 Chemical Stimuli-Responsive Polymers

Ionic strength and pH-responsive polymers are the mostly widely used chemical stimuli-responsive polymers.<sup>28-29</sup> pH is one of the most important physiological factors in disease detection because acid and base disorders can lead to dysfunctional homeostasis in the human body. Each compartment in the human body has a different pH range: for example, the stomach has a pH of 1-3 and the intestine has a pH of 5-8. The pH in chronic wounds ranges from 5.4-7.4.<sup>30</sup> pH changes can cause severe damage to the human body. In general, pH-responsive polymers have an ionisable group, such as polyelectrolytes. These groups possess the weak acidic or basic parts attached to the polymer's main hydrophobic backbone.<sup>24,31</sup> After the acidic or basic moieties are ionized, electrostatic repulsions (Coulombic repulsion) take place between generated charges, causing an extension of the random coil in the polymer network (figure 1.6).<sup>31</sup> Another characteristic of pH-responsive polymers is that they show protonation or deprotonation by changing pH. In a polymer network, pH changes lead to a distribution of the charges over the ionisable groups, such as carboxyl or amino groups. When a pH change is induced, charges are generated and phase transition occurs. Generally, pH-responsive properties are obtained by copolymerization with weak polyelectrolytes, e.g., electrolytes that

are not fully charged in solution. The electrolytes' charges [poly (acrylic acid) (AAc)<sup>24,25</sup> and poly 3-aminophenylboronic acid (APBA)<sup>32</sup>] depend on changes in the solution pH.<sup>33</sup> APBA is commonly used as a comonomer for glucose detection.<sup>32</sup> In this thesis, we focus primarily on APBA-functionalized pNIPAm-based microgels in glucose detection. This will be discussed in Chapter 2.

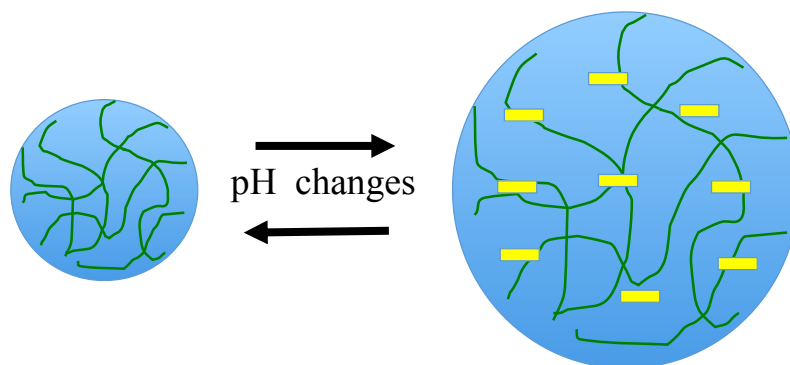


Figure 1.6 Chemical Stimuli-Responsive Polymer, scheme of swelling/deswelling mechanism activated by pH changes in pH-Responsive Polymer

Ionic strength (salt concentration) -responsive polymers include cationic or anionic groups in the polymer side chain. They show ionic strength-dependent solubility. In low ionic strength, the polymers are soluble due to the domination of electrostatic interaction between cationic groups. However, the polymers' solubility decreases with the increase of ionic strength due to the screening effect of free ions, which decreases the electrostatic interactions between cationic groups.<sup>34</sup> The different ionic strengths change the diameter of the polymer particles, the solubility of the polymers, and the phase transition.<sup>35</sup>

### 1.2.3 Biological Stimuli-Responsive (Bioresponsive)

Biological stimuli-responsive polymers change their form by recognizing biological interactions that act as stimuli. These polymers mimic the properties of biological activities, such as enzyme actuation,<sup>36</sup> glucose sensitivity<sup>37</sup>, and drug release.<sup>36</sup>

Bio-responsive hydrogels have been developed for controlled drug release, e.g., to release insulin in response to increased blood sugar levels, providing autonomous treatment for insulin-dependent diabetes.<sup>38</sup> One approach for controlled drug release uses immobilized glucose oxidase (GOx) on the polymer network. After the GOx-glucose interaction, gluconic acid is formed. This lowers the pH, and the basic groups in the polymer are protonated. These actions induce polymer swelling and promote insulin release.<sup>39</sup>

Another sensor with an optical signal uses microlenses made of poly (N-isopropylacrylamide)-*co*-acrylic acid (pNIPAm-*co*-AAc). The biotin-functionalized pNIPAm-*co*-AAc microlenses detect avidin and anti-avidin antibodies. Binding these proteins to surface-bound biotin causes additional cross-linking in the gel and increases the local refractive index of the hydrogel. This change in optical properties can be measured qualitatively; the higher the concentration of avidin or anti-avidin, the larger the increase in the refractive index.<sup>40</sup>

Highly sensitive and selective DNA detection is very important for forensic science,<sup>41</sup> disease diagnosis,<sup>42</sup> water analysis (for bacteria),<sup>43</sup> and many other applications. Pelton et al. studied DNA oligonucleotide-conjugated microgels and their applications.<sup>44</sup> They fabricated DNA-microgel-based bioassays to investigate whether DNA-microgel conjugates were compatible with enzymatic reactions. They used two enzymes, T4 DNA ligase and Phi29 DNA polymerase, and covalently coupled DNA molecules on the microgel. After they amplified DNA chain development, they used DNA-processing enzymes to manipulate the DNA-microgel-based conjugate, and used the conjugate for the DNA-sensing application.<sup>44</sup>

Another DNA-detection technique employed probe DNA-target DNA-interaction as a cross-linker. pNIPAm-based beads were constructed into a photonic structure, which can convert physicochemical changes from probe- and target-DNA binding into spectral signals.<sup>45</sup> N,N'-methylenebisacrylamide (BIS), which is a general cross-linker in the hydrogel, and single strand DNA are used as cross-linkers. After being polymerized with acrylamide, BIS, single

strand DNA, and a photoinitiator, the target DNA is introduced into the gel network and specific hybridization occurs between the probe and target DNA. This process causes the hydrogel to collapse, which can be detected from the blue shift of the Bragg diffraction peak position shown in figure 1.7.

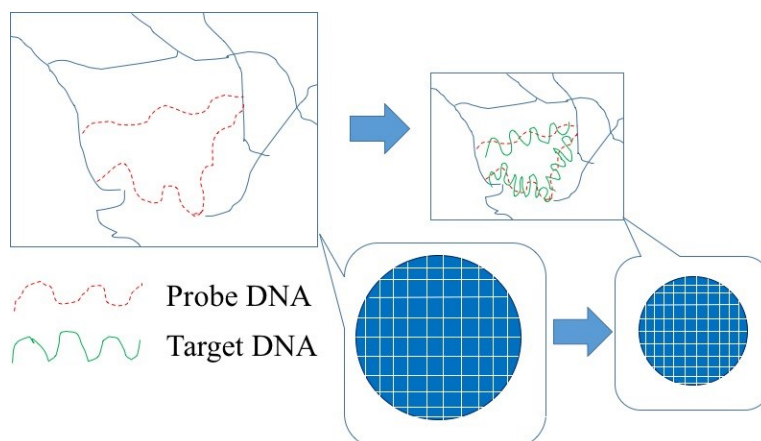


Figure 1.7 The scheme of the DNA-responsive hydrogel photonic beads. Adapted from <sup>45</sup>. Copyright 2010, WILEY-VCH Verlag GmbH & Co. KGaA, Weinheim.

Antigen-antibody bonding can also serve as a cross-linker to build up antigen-responsive hydrogels based on a semi-interpenetrating polymer network (IPN).<sup>46-47</sup> The hydrogel-containing antibody shows a higher affinity with the free antigen than with the immobilized antigen in hydrogel. An immobilized antibody will bind to a free antigen. The free antigen then replaces immobilized antigen, causing the hydrogel to swell. The mechanism for the swelling of semi-IPN hydrogel is shown in figure 1.8.

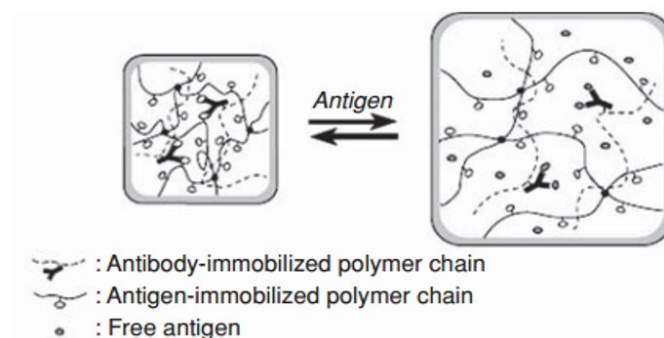


Figure 1.8 The scheme of a mechanism for the swelling of semi-IPN hydrogel in response to a free antigen. Adapted from <sup>46</sup>. Copyright 1999, Nature Publishing Group.

The hydrogel can swell because of the presence of free antigens, which leads to the dissociation of immobilized antigen by the exchange of the free antigens. In the absence of the free antigens, the hydrogel shrinks. The immobilized antigen-antibody interactions serve as a crosslink among the chains. However, after the immobilized antigens change to free antigens, due to the decrease in crosslinking density, the microgel can swell.<sup>46</sup>

In another example of bioresponsive polymer, protein-pNIPAm conjugates show LCST behavior.<sup>47</sup> In Hoffman's work, streptavidin was generated to contain a single cysteine near the biotin binding site for the specific conjugation of a vinyl-sulfone at the end of a pNIPAm chain.<sup>48</sup> Generally, the binding interaction between biotin and streptavidin in pNIPAm occurs below the LCST, while above LCST the pNIPAm collapses and blocks the binding. Figure 1.9 shows the biotin-binding capacity of the pNIPAm conjugate below and above LCST.

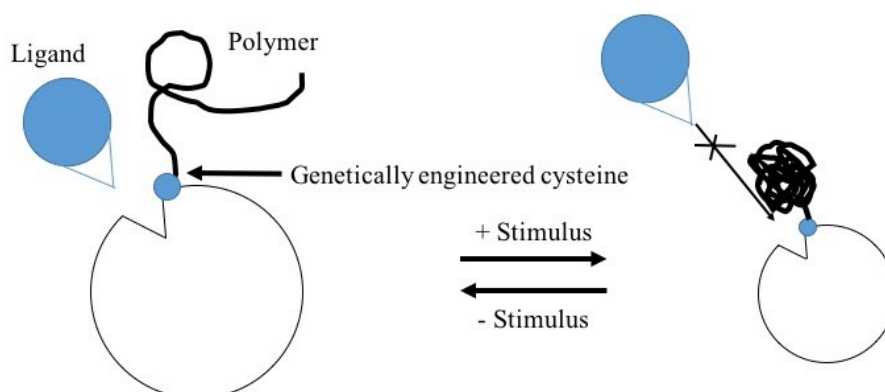


Figure 1.9 The illustration of the genetically engineered cysteine site near the receptor-active site and the binding capacity of the ligand in the polymer's hydrated or collapsed state. Adapted from <sup>48</sup>. Copyright 1995, Nature Publishing Group.

Because they are biocompatible and biodegradable, hydrogel scaffolds can promote cell adhesion in tissue engineering. The commonly studied polyethylene glycol (PEG) hydrogel is modified with bioactive molecules such as cell-adhesive peptide (CAP), enzyme-sensitive peptide (ESP) and growth factors to mimic extracellular matrix (ECM) biofunctions such as cell adhesion, enzyme sensitive degradation, and growth factor bindings. This hydrogel scaffold

was used to drive the formation and maintenance of 3D tissue structures. The scaffold can be tailored so that it repairs tissues and organs that need to be replaced.<sup>49-50</sup>

Conventionally, cells are harvested using proteolytic enzymes such as trypsin and dispase. These enzymes degrade cell adhesion. They then deposit ECM, which detaches the cultured cells. They also degrade cell-cell junction proteins, so that the monolayer cells are harvested as single cells. In this study, temperature-responsive polymers were used to detach cells from surfaces, yielding a single cell sheet. This was done by using temperature-responsive polymers deposited on the culture dishes. When the temperature decreases below the LCST, the cells spontaneously lifted up from the surface without the help of proteolytic enzymes.<sup>51-52</sup>

A study by You and Auguste provides another example of bio-responsive polymers. They synthesized pH-responsive nanoparticles comprised of N-dimethylamoniethyl methacrylate (DMAEMA) and 2-hydroxyl methacrylate (HEMA).<sup>53</sup> DMAEMA is a pH-responsive polymer that has a tertiary amine group with a  $pK_a$  of 7.5.<sup>54</sup> When exposed to a low pH environment, this pH-sensitive DMAEMA-HEMA nanoparticles-encapsulating paclitaxel swells. For example, when exposed to a tumor, the particle swells and releases a drug.<sup>55</sup>

A similar approach used nanoparticles for gene delivery, where the triggered release of plasmid DNA at the low pH endosome was optimized.<sup>56</sup> The nanoparticles encapsulated the plasmid DNA for green fluorescent protein. The particles were used for gene carrier transport into the cell via endocytosis and endosome forms. When the endosome was in a low pH environment, its particles swelled and released genes, leading to gene transfection at the target nucleus.<sup>56</sup>

GOx was conjugated to a pH-responsive polymer to make glucose-responsive polymers. When GOx oxidizes glucose to gluconic acid, the pH change occurs in the environment. Then, the pH-responsive polymer shows a phase transition as a response to the decreased pH.<sup>33,57</sup> A

new approach, involving pH-responsive polymers using APBA as a glucose-responsive polymer, will be introduced in Chapter 2.

#### **1.2.4 Multi Stimuli Responsive**

Stimuli-responsive polymers have been developed for biomedical applications. The technology has evolved to the point where systems that respond to multiple stimuli can be achieved. These techniques are mainly used for drug delivery systems, temperature- and pH-responsive polymers, or magnetic and temperature-responsive polymers for self-regulated insulin delivery.<sup>24,58</sup> We can obtain magnetic/temperature-responsive polymers from the doping process of polymeric material with magnetic nanoparticles. These nanoparticles consist of magnetic iron oxide ( $\text{Fe}_3\text{O}_4$ ). The magnetic particles provide inductive heating, which behaves as a stimulus by promoting the phase transition of temperature-responsive polymers that release encapsulated drug molecules.<sup>59</sup> In this thesis, we are using pH- and glucose-responsive polymers for glucose detection.

### **1.3 Stimuli-Responsive Hydrogel**

Hydrogels are made up of a crosslinked network of hydrophilic polymers.<sup>31,60</sup> Hydrogels are categorized into two classes of hydrogels; physically cross-linked and chemically cross-linked.<sup>61</sup>

Physically cross-linked hydrogels are based on non-covalent bonds such as hydrophobic and electrostatic interactions or hydrogen bonding. They are formed by dynamic cross-links made of synthetic or natural building blocks.<sup>61</sup> In particular, hydrophilic hydrogels are most naturally inert material and they allow minimal non-specific interaction with proteins, DNA, cells, or biomolecules.<sup>62</sup> Chemically cross-linked hydrogels, however, are formed by covalent bonds and do not dissolve in water without breaking those bonds.<sup>63</sup> Hydrogels are easily modified, typically by grafting with various functional groups or by copolymerization to yield stimuli-responsive hydrogels that can respond to physical, chemical, or biochemical stimuli.

When these hydrogels are exposed to external stimuli, they undergo reversible changing, behavior such as swelling or deswelling. The magnitude of change is determined by the hydrogel composition, cross-linking type, and degree of cross-linking.<sup>61,64</sup> A molecular interaction triggered by the sudden change in the polymer network leads to an internal stimulus, causing stimuli-responsive hydrogels to undergo a volume-phase transition: in other words, the hydrogels swell or collapse.<sup>61</sup>

Stimuli-responsive hydrogels are prepared using methods including temperature-initiated radical polymerization,<sup>64</sup> addition reaction,<sup>65</sup> or UV-initiated polymerization.<sup>66</sup> The hydrogels' responsive rate depends on their composition. To increase the responsive rate, it is necessary to decrease the crosslinking density<sup>67</sup> or increase a number of ionic groups in the hydrogel matrix.<sup>68</sup> For example, increasing the number of ionic groups using pH-responsive polymers leads to a better response to analyte.

#### **1.4 Poly (N-isopropylacrylamide) Microgels**

pNIPAm based microgels (or hydrogels) are the most well-known stimuli-responsive polymers.<sup>24, 29, 69</sup> pNIPAm is fully water soluble and hydrophilic below  $\sim 32$  °C, existing as a random coil, but it becomes water insoluble and relatively hydrophobic above  $\sim 32$  °C,<sup>70</sup> the LCST. Wu et al. first observed the LCST with homopolymer chains of pNIPAm in water.<sup>71,72</sup> Figure 1.10 shows the chemical structure of pNIPAm. The polymer conformation in a solvent depends on the interaction between the polymer-polymer, polymer-solvent, and solvent-solvent. Those interactions create a balance in the system. pNIPAm in water shows solvation changes because one interaction increases while the other decreases.<sup>73</sup> When pNIPAm is in water, the water molecules bind to the amide side group through hydrogen bonding at room temperature. However, the isopropyl side groups in pNIPAm make the water structure around them. The structured water leads to an entropically driven polymer-polymer interaction supported by the hydrophobic effect.<sup>73</sup> When the water is heated, it becomes a poor solvent, and the hydrogen

bond between pNIPAm and the water is interrupted, causing the polymer chain to collapse. At room temperature, polymer-solvent interactions are stronger than polymer-polymer interactions, and the pNIPAm becomes swollen.<sup>74-75</sup>

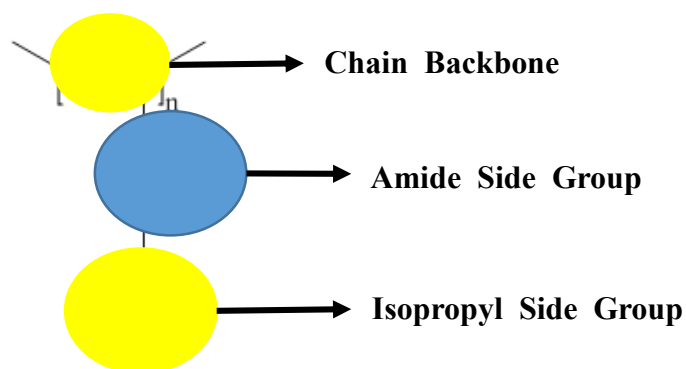


Figure 1.10 Chemical Structure of pNIPAm. Amide group side and isopropyl side group showed hydrophilic (Blue) and hydrophobic (Yellow) properties, respectively. Reprinted from <sup>73</sup>. Copyright © 2005 WILEY-VCH Verlag GmbH & Co. KGaA, Weinheim.

pNIPAm-based microgels are easily tunable by adding a comonomer to the polymer network. The commonly used comonomers that have been copolymerized with NIPAm are AAc<sup>28</sup> and APBA.<sup>28</sup> AAc is widely used and easily copolymerized with NIPAm.<sup>28</sup>

AAc is a weak acid, with a  $pK_a$  of  $\sim 4.25$ . Therefore, at  $pH < pK_a$ , the pNIPAm-*co*-AAc microgels become fully responsive; however, at  $pH > pK_a$ , the microgels become less responsive.<sup>76-77</sup> Namely, at  $pH > pK_a$  the Coulombic repulsion occurs between deprotonated AAc groups in the AAc microgels and the pNIPAm-*co*-AAc microgels become swollen.<sup>78</sup>

The Serpe group uses AAc or APBA as a comonomer. The  $pK_a$  value of each compound is 4.25,<sup>76</sup> and 8.2,<sup>79</sup> respectively. This is shown on a pH scale in figure 1.11. Researchers use pNIPAm modified with APBA for glucose sensing because boronic acids bind easily to glucose.<sup>71</sup> The following sections will describe the pNIPAm synthesis as a micrometer diameter, the Fabry-Pérot etalon device and its fabrication in the pNIPAm microgels system, and pNIPAm microgels applications.

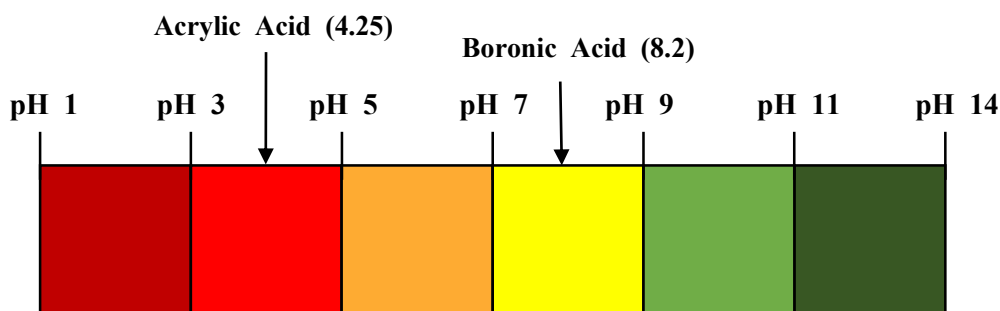


Figure 1.11 Different comonomers with their pKa

### 1.4.1 Synthesis of pNIPAm Microgels

In sensor applications, pNIPAm must be visible by optical microscopy and influenced by thermal changes. Homogeneous pNIPAm particles provide enhanced optical properties.<sup>80</sup> To make the particles homogenous, we should investigate the possibility of synthesizing pNIPAm microgels.

pNIPAm-based microgels can be synthesized using various methods such as precipitation polymerization (heterogeneous bulk polymerization),<sup>77</sup> anionic copolymerization,<sup>81</sup> emulsion polymerization<sup>82</sup>, and free radical precipitation polymerization (homogeneous polymerization).<sup>83</sup> Free radical precipitation polymerization is a general approach for the polymerization of pNIPAm microgels with homogenous nucleation.<sup>83</sup> This thesis focuses on the synthesis of pNIPAm-based microgels using free radical precipitation polymerization. This will be discussed in detail in Chapter 2. In free radical precipitation polymerization, NIPAm is a major monomer. BIS is a commonly used cross-linker.<sup>84</sup> Under the 65 °C, the commonly used initiator, ammonium persulfate (APS), starts to polymerize pNIPAm microgels (figure 1.12).<sup>82</sup>

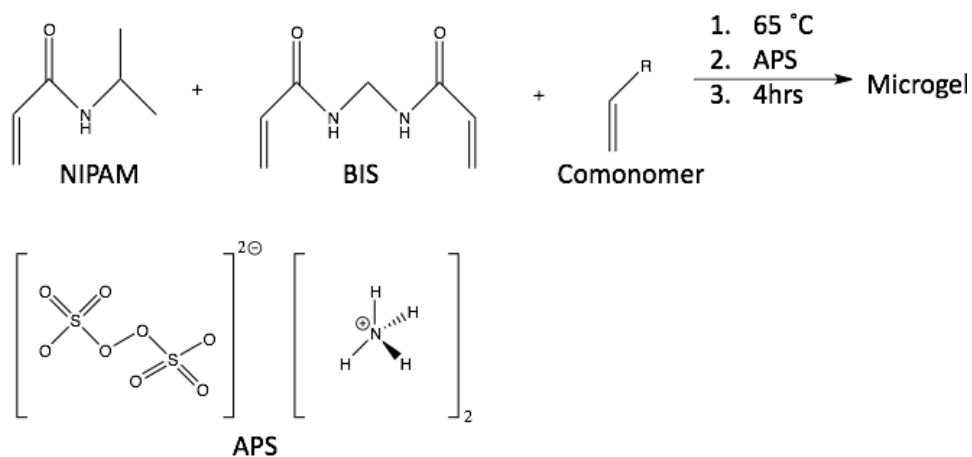


Figure 1.12 The synthesis of a pNIPAM-based microgels using an APS initiator. The functional group R in the comonomer with a double bond can involve radical polymerization in an aqueous solution.

Polymerization works by APS generating sulphate radicals that initiate the polymerization. After the initiation, pNIPAm polymer chains start to grow, until they reach a critical chain length. The growing chain collapses because the polymerization temperature is much higher than the LCST of the pNIPAm, resulting in a phase transition. The growing chains become colloiddally unstable precursor particles. These particles behave as nuclei to seed the polymerization and the growing pNIPAm microgel. Eventually the reaction is halted by termination steps, then after the monomer/cross-linker solution is depleted. The process generates particles that have been stabilized by the electrostatics from the sulfate groups on APS.<sup>83, 85</sup> The electrostatic stabilization creates a repulsive barrier to prevent aggregation of the microgels.<sup>86</sup>

#### 1.4.2 pNIPAM Microgel-Based Etalon

A Fabry-Pérot interferometer (etalon) is made by sandwiching a dielectric material between two semitransparent mirrors. When light strikes the etalon, it is reflected at each interface. Some light is "trapped" between the two Au layers and resonates, leading to constructive/destructive interference. This in turn leads to certain wavelengths of light being

enhanced, while others are not, leading to specific wavelengths of light being reflected/transmitted.<sup>87-88</sup> This interference is realized as peaks in a reflectance spectrum, and can be described by equation 1. It is shown schematically in figure 1.13.

$$\lambda m = 2nd \cos \theta$$

Equation 1

where  $\lambda$ , is the maximum wavelength of the peak(s),  $m$  is the peak order,  $n$  is the refractive index of the dielectric material,  $d$  is the distance between mirrors, and  $\theta$  is the angle of incidence.

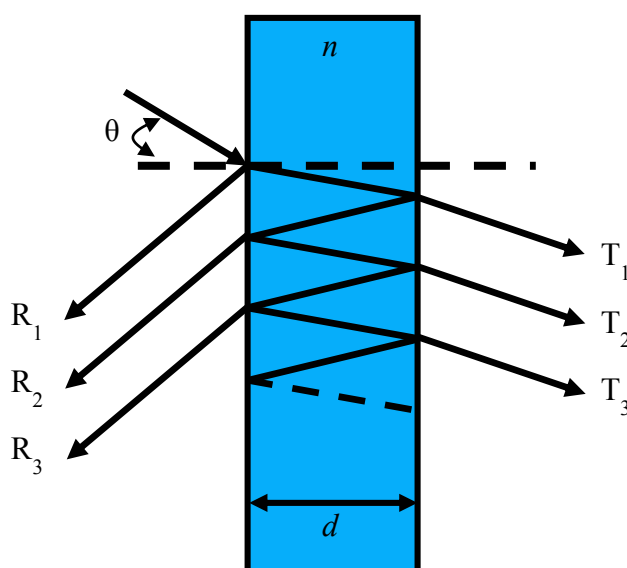


Figure 1.13 A scheme of a Fabry-Pérot interferometer

From equation 1, the wavelength  $\lambda$  is proportional to  $d$ . Thus, an increase in  $n$  for a provided peak of order  $m$  triggers a red-shift. In other words, the distance between two mirrors increases, which means a red-shift in  $\lambda$  for order  $m$ . Previous studies on the etalons using pNIPAm-based microgels have demonstrated that when the device is immersed in different pH solutions, the color changes due to the change in distance between the two reflective mirrors.<sup>87</sup> According to equation 1, the distance is directly proportional to the wavelength. As the distance decreases, the peak wavelength of the reflected light changes, which means that the microgels have collapsed.<sup>87-88</sup>

Previously, the Serpe group was able to show that pH responsive pNIPAm-based microgels could be used to generate optical devices that have visual color, exhibit unique reflectance spectra, and contain multiple reflectance peaks.<sup>89</sup> They demonstrated that the pNIPAm-based microgel between two Au layers showed better performance than the non-etalon-pNIPAm microgel platform.<sup>28, 88</sup> This suggests that the etalon device contributes to pNIPAm-based microgel sensor applications.

### 1.4.3 pNIPAm Microgel Applications

pNIPAm-based microgels can be used for a wide variety of applications, including biosensing,<sup>90</sup> water remediation,<sup>91</sup> and drug delivery.<sup>92</sup> Glucose-responsive pNIPAm-based microgels are functionalized with APBA groups. Pelton et al. showed that APBA microgels demonstrated glucose-dependent swelling responses at physiological pH and temperature.<sup>93</sup> APBA microgels are amphoteric, charge-switching polymers; they can be designed to either swell or shrink in response to glucose, depending on the pH of the system. By functionalizing pNIPAm microgels with APBA, the Serpe group was able to show that the microgels have the potential to detect glucose. In the Serpe group's studies, pNIPAm-co-AAc microgels were functionalized with APBA by coupling them with 1-ethyl-3-(3-dimethylaminopropyl) carbodiimide (EDC).<sup>88</sup> APBA microgel-based etalons showed a 110-150 nm red shift in response to a 3 mg/mL glucose solution in 5 mM pH 9 buffer solution at 15 °C. Also, before binding with glucose, the etalons had a volume phase transition temperature (VPTT) of 18-20 °C, which changed to 24-26 °C after glucose was added.<sup>32,93-94</sup>

The Serpe group showed that pNIPAm-based microgels could be used to remove organic dye from water, specifically that pNIPAm-co-AAc microgels could remove the organic dye molecule Orange II from an aqueous solution at room temperature.<sup>91</sup> The dye removal efficiency depends on the concentration of AAc and the microgel. The concentration of BIS in the microgel aggregates affects the uptake efficiency. Furthermore, the size of the microgels

significantly impacts the efficiency of the dye removal. The Serpe group's work will be used to remove the contaminants (including polycyclic aromatic hydrocarbons (PAHs), metals, and naphthenic acids) from water.<sup>95</sup>

The Pelton group was able to show that carboxylic acid functionalized pNIPAm-based microgel-uptake cationic drugs.<sup>96</sup> A high degree of drug uptake was observed when the microgels were protonated at pH 4. A low degree of drug release was observed when the acid-base interactions were eliminated.<sup>96</sup> However, uncharged microgel and anionic drugs showed better uptake than cationic drugs, because, in microgels, hydrophobic partitioning plays an important role in drug uptake.

The Richtering group developed biosensor applications that involved microgel/enzyme thin films that adsorbed on conductive substrates.<sup>97</sup> The microgels adsorbed under the appropriate condition: a hydrophobic non-charge state. The microgel and the enzyme were oppositely charged under certain pH conditions. After the subsequent electrostatic interaction between the microgel and enzyme, the larger amount of enzyme could bind to microgel during the subsequent adsorption. This is not only a surface adsorption; the materials also absorb the enzyme molecules inside the microgel, similar to a sponge soaking up a liquid. This approach is used for surface modification in biosensor applications.<sup>97</sup>

In Section 1.2.3, we explained that pNIPAm has cell-adhesive bioresponsive properties that show adhesion, as well as mechanical properties, and it can be used as a switchable cell culture substrate.<sup>98</sup> Because the pNIPAm microgels have a LCST close to body temperature, they have been used in cell culture engineering applications. Schmidt et al. seeded L929 mouse fibroblasts on microgel film in a cell culture and incubated cell culture for 48 hours at 37 °C. After being incubated in the cell culture and cooled to 25 °C, nearly all of the cells were detached from the pNIPAm films by gentle rinsing.<sup>98</sup> This shows that using a pNIPAm

microgel-coated surface makes it possible to efficiently switch from cell-adhesion to cell-detachment using simple temperature stimulus.<sup>98</sup>

The Serpe group and others have demonstrated that optical sensors can be very useful for sensing and biosensing.<sup>99</sup> Marzán et al. introduced gold nanoparticles into pNIPAm microgel particles.<sup>100</sup> The use of surfactants, such as cetyltrimethyl ammonium bromide (CTAB) has proven efficient for synthesizing a variety of sizes of gold (metal) nanoparticles.<sup>101</sup> Marzán et al. used encapsulated CTAB-coated gold nanoparticles within pNIPAm microgels to make a core-shell structure. These microgels showed a thermo-responsivity similar to that of pure pNIPAm microgels. The temperature-dependent solvation state was preserved, and was reversible. Gold (metal) nanoparticles can be grown in the microgel network. Different CTAB concentrations will result in different morphologies. Encapsulating the gold (metal) particles in pNIPAm is a useful approach in applications involving optical sensing of temperature or pH in intracellular imaging.<sup>102</sup>

The Pichot group showed that DNA could be immobilized on pNIPAm microgels by synthesizing the microgels with amine functionality; the oligo-deoxyribonucleotides (ODN) with an amine on the 5' end reacted with 1,4-phenylene diisocyanate in a 1:2 ratio so that one of the isocyanates was coupled to the ODN, leaving the other isocyanate side free. After purification, the DNA was able to be coupled to the microgel by the free isocyanate, where it reacted with the amine on the particle surface. The immobilized DNA on the microgel was used for specific target DNA detection.<sup>103</sup>

As shown in figure 1.14, the Needham group introduced the controlled release of a drug from a microgel copolymerized with methacrylic acid.<sup>92</sup> This process followed general pH-responsive microgel properties. When the microgels were swollen, the drug, doxorubicin, was loaded into the microgel network. The particles were coated with a lipid bilayer to prevent the drug from leaking out of the polymer when the particles condensed at a pH value below the

methacrylic acid  $pK_a$ . After the pH was reduced to less than the  $pK_a$  of the methacrylic acid, the microgel collapsed and the lipid bilayer coated its surface to prevent the drug from leaking. To release the drug, the Needham group used an ion exchange to make pores on the microgel surface.<sup>92</sup>

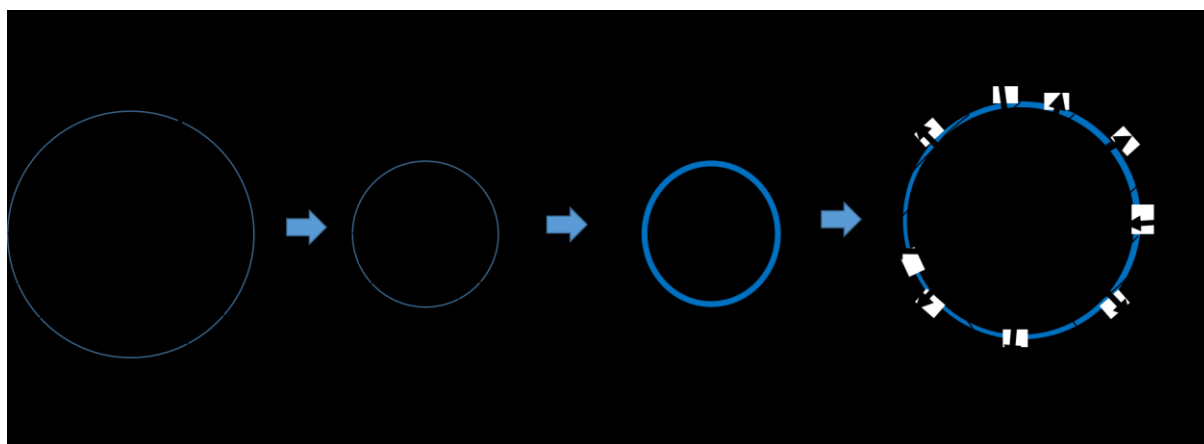


Figure 1.14 The scheme of drug loading and release process in pNIPAm-based controlled drug release. Reprinted from <sup>92</sup>. Copyright 1998, Nature Macmillan Publishers Ltd.

The Lyon group explored microgels for targeted drug release by generating folic acid-modified pNIPAm core-shell microgels that can localize at cancer cells.<sup>104</sup> Folic acid is a well-known ligand for targeting cancer cells because most cancer cells overexpress folate receptors. The Lyon group labeled the microgel core with a fluorophore. The pNIPAm shell contained a primary amine, which could be used to attach the folic acid to the microgel shell. The pNIPAm microgels were then incubated with cancer cells that overexpressed the folate receptor. The microgels were taken up in the cells, where they exhibited cytotoxicity.<sup>104</sup>

The Lyon group's work generated glucose-responsive core-shell microgels that could respond by changing the solvation state in the presence of various concentrations of glucose.<sup>105</sup> The microgels could be used to detect glucose levels in solution (or blood), which suggests that they are a potential glucose sensor. The development of the glucose sensor for diabetes

diagnosis and the selectivity of glucose are the focus of this thesis and are discussed in detail in Chapter 3.

## 1.5 Quartz Crystal Microbalance

The main technique used in the work in this thesis is quartz crystal microbalance (QCM). This section will discuss the basic QCM principle and its applications in biosensor studies. In the work for this thesis, pNIPAm microgels were coated on QCM crystal surfaces and used to sense glucose.

Many techniques are available for sensing applications, such as microcantilevers (MC), nanowires (NW), immunofluorescent assays (IFA), and ELISA.<sup>7</sup> QCM can be used for biosensing due to its resonant frequency shift in response to mass and viscosity changes at its surface.<sup>7</sup> QCM provides qualitative and quantitative information about biomolecular interactions by monitoring the change in mass on the quartz crystal surface's functionalized layer. The mass changes lead to a resonant frequency shift of the quartz crystal.<sup>106</sup> QCM has many advantages, including sub-nanogram detection capabilities. It is inexpensive to create and can characterize diverse interactions.<sup>106</sup> Its limit of detection ranges from micro- to sub-nanogram and the mass is determined by the viscoelasticity of the deposited materials.<sup>106</sup>

QCM's operation mechanism is based on the converse piezoelectric effect. Piezoelectricity comes from the Greek word, *piezein*, which means to press. Piezoelectricity is the process by which electrical charges are generated when a mechanical force is applied to the surface of crystalline materials.<sup>7</sup> The surface of the QCM crystal can be modified with any number of coatings and/or biomolecular receptors and used for sensing and biosensing. The coating material interacts chemically or physically with the targeting materials.<sup>106-107</sup> Consequently, QCM crystal is not disturbed by any unintended molecules that could bind to its surface, a process that leads to an unintended resonant frequency shift.<sup>106, 108</sup> Generally, the electrodes consist of gold, silver, platinum, aluminum or nickel, and cover the quartz crystal from top to

bottom. Also, wire leads are attached to the electrodes and connected to oscillator circuit.<sup>7</sup> Figure 1.15 shows the coated materials on QCM crystal's surface. The top layer contains a gold electrode. Coating materials are deposited on the top gold electrode.

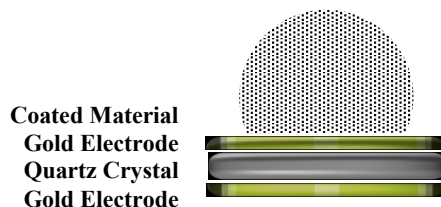


Figure 1.15 The side-view of coated material modified QCM crystal

Generally, QCM crystal is AT-cut form and its structure allows the crystal to oscillate stably at room temperature. Its thickness shear mode (TSM) is almost temperature-independent and responds to pressure fluctuations in the resonant frequency of the quartz crystal. AT-cut quartz crystals are commonly used as a sensor because of their piezoelectric properties, resonance behavior, and sensing mass changes. When alternating current (AC) voltage is applied to a pair of electrodes (typically Au) sandwiching a specially cut QCM crystal, QCM crystal can be excited electrically. Then QCM crystal undergoes an oscillating shearing motion at a certain resonant frequency. The frequency is highly dependent on mass and viscosity.<sup>109-</sup>  
<sup>110</sup> This resonant frequency and mass shift value are calculated using a Sauerbrey equation,<sup>111</sup> as shown in equation 2:

$$\Delta f = -\frac{2f_0^2}{A\sqrt{\rho_q\mu_q}}\Delta m = -n\frac{1}{c}\Delta m \quad \text{Equation 2}$$

where  $f_0$  is the initial resonant frequency (Hz) value of the QCM crystal,  $\Delta f$  is the frequency (Hz) shift measured by the QCM,  $\Delta m$  is the change in mass (g),  $A$  is the area of the electrode ( $\text{cm}^2$ ),  $\rho_q$  is the density of quartz ( $2.648 \text{ g/cm}^3$ ),  $c$ , for a 5 MHz resonator oscillation at its fundamental mode ( $n=1$ ) is  $17.7 \text{ ng/cm}^2\cdot\text{Hz}^{-1}$  and  $\mu_q$  is the shear modulus of quartz ( $2.947 \times 10^{11}$

g/cm<sup>2</sup>). From the Sauerbrey equation, it is possible to consider that an increase in mass on the electrode surface results in a linear decrease in the quartz crystal's resonant frequency. This equation provides that the change in mass ( $\Delta m$ ) is the significant component in the equation, affecting the crystal's resonant frequency value ( $\Delta f$ ). It also demonstrates that QCM is able to detect mass changing with near nanogram sensitivity, which is more than 1000 times better than a conventional electronic balance, which has 0.1 microgram sensitivity.<sup>111</sup>

The advantage of a QCM sensor is that it can be used to monitor adsorbing analytes on the QCM crystal surface in real-time. QCM measurements provide quantitative and qualitative information about biomolecular interactions between analytes and a modified surface. In addition, QCM provides mass shift on a nanogram scale by detecting the mass of material that binds to the QCM crystal surface. This mass shift is also calculated by the Sauerbrey equation. Mostly, the sensor is modified with specific surface chemistry and it interacts with analytes.<sup>106</sup> However, QCM can only serve a function as a mass sensor in the gas phase. Even though QCM crystal can be modified by liquid and solid materials, the Sauerbrey equation is only valid for gas phase processes. It may provide information about the liquid and solid phases but cannot be applied if the mass is deposited under liquid and inelastic conditions. QCM can be used in the liquid phase only if the bulk's properties have conductivity, a dielectric constant, viscosity, and density. Kanazawa and Gordon demonstrated and verified when QCM is operated under this specific condition and derived the following equation, equation 3, for calculating the resonant frequency shift measured in the liquid phase.<sup>106</sup>

$$\Delta f = \frac{C_f f_0^2 \Delta m}{A} + C_f f_0^2 \sqrt[3]{(\Delta \eta_L \Delta \rho_L)} \quad \text{Equation 3}$$

The same as equation 2,  $\Delta f$  represents the measured resonant frequency change (Hz),  $C_f$  represents the Sauerbrey constant that depends on  $f_0$  and increases proportionally by increasing the overtone number or the integrated QCM/mass sensitivity,  $f_0$  is the fundamental

frequency (Hz) of an AT-cut quartz crystal,  $\Delta m$  is the change in mass (g),  $\mu_q$  is the shear modulus of an AT-cut quartz crystal ( $2.947 \times 10^{11} \text{ g/cm}^{-1}\text{s}^{-2}$ ), and  $\rho_q$  is the density of quartz crystal ( $2.648 \text{ g/cm}^{-3}$ ). The  $\eta_L$  indicates the absolute viscosity of the liquid, and  $\rho_L$  represents the absolute density of the liquid.

This modified equation demonstrates that the measuring resonant frequency shift of QCM performing in the liquid phase depends on the square root of the product of the density and viscosity of the liquid.<sup>112</sup> Generally this viscous liquid is called viscoelastic material and this material has both properties: density and viscosity. The QCM operation can take place under both the gas phase and the viscoelastic phase. As shown in equation 3, the resonant frequency of QCM crystal decreases as the viscosity of the viscoelastic material on the quartz crystal increases. When it comes to the pNIPAm polymer in QCM, pNIPAm changes its conformation to the collapsed state: in other words, increased viscosity leads to an increased resistance of QCM oscillation, decreasing the quartz crystal's resonant frequency. However, when pNIPAm reaches a low viscous state, it promotes QCM crystal's oscillations and QCM shows increased resonant frequency. This suggests that a resonance frequency shift has occurred, since pNIPAm shows a transition from a swollen state to the deswollen state (low viscosity to high viscosity) or from a deswollen state to the swollen state (high viscosity to low viscosity).<sup>110</sup>

The QCM measurement is based on an interaction between binding materials and the top gold electrode of the QCM crystal. Of the other sensors, the biosensor in particular focuses on surface chemistry, measuring specific binding events on functionalized surfaces. This makes QCM an excellent candidate as a biosensor, as well as for protein adsorption,<sup>109</sup> antibody-antigen interaction,<sup>113</sup> and cell attachment or adhesion to a surface.<sup>114</sup> Furthermore, QCM measurement with dissipation technology allows quantitative analysis in a thermal metal evaporator to monitor the thickness of the deposited metal on the surface. If the mass coverage

is uniform, the film thickness is easily calculated by dividing the mass per unit area provided by the Sauerbrey equation. Equation 4 is shown below:

$$T_f = \Delta m / \rho_f$$

where  $T_f$  is the thickness of the film material in cm,  $\rho_f$  is the density of the film material in  $\text{g/cm}^3$ , and  $\Delta m$  is the change in mass per unit area in  $\text{g/cm}^2$ .<sup>115</sup>

### 1.5.1 Etalon Fabrication on a QCM

Etalon fabrication with pNIPAm microgels enhances the sensitivity of Equation 4 the microgels' stimuli-responsivity. Figure 1.16 shows a pNIPAm microgel-based etalon.<sup>87-88</sup> Microgels are sandwiched between two chromium/gold layers. The Serpe group has demonstrated that the presence of an Au overlayer of etalon interacting with microgels on the quartz crystal leads to enhanced sensitivity.<sup>81,82</sup> For instance, above the LCST and  $\text{pH} < \text{pK}_a$ , the microgels enter a collapsed state and the Au overlayer of the etalon gets close to the QCM crystal, causing the crystal to sense the mass of the Au overlayer and resist oscillation. As a result, the QCM measures an initial resonant frequency shift that is lower than what it would be compared to a microgel without an AU overlayer. In this case, the quartz crystal senses the microgel's viscosity only and its initial resonant frequency is not as low as is observed for etalon fabricated on a QCM crystal.<sup>116</sup>

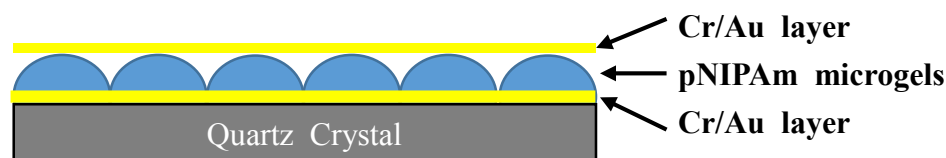


Figure 1.16 pNIPAm-based microgel etalon fabrication

In both cases, however, the microgels become swollen when the temperature is below the LCST or  $\text{pH} > \text{pK}_a$  and the resonant frequency increases at approximately the same value. This is because even though the microgels are swollen, the QCM crystal cannot detect the Au layer. This proves that etalon fabricated on a QCM crystal shows a much larger resonant frequency shift from the collapsed state than from the swollen state, which is in contrast with what happens to microgels coated only on the QCM crystal. In other words, the Au overlayer makes the QCM device much more sensitive to temperature or pH deviations, because it provides a larger frequency shift and allows many applications in pNIPAm microgel-based biosensors.<sup>116</sup>

### **1.5.2 Surface Chemistry in QCM study**

Etalon must be fabricated on the surface of QCM crystal. The surface refers to the QCM electrode that is exposed to the gas or liquid environment. The surface chemistry of QCM involves adsorption of functional group on the surface of crystal. Two different adsorption methods, physical and chemical, are used in the QCM system. Physical adsorption includes non-specific interactions, such as hydrophobic bonds, and hydrogen bonds, all of which are weak or non-covalent bonds. Chemical adsorption includes specific interactions, such as self-assembled monolayers (SAMs), plasma-polymerized films (PPFs), and photochemistry, which are strong covalent bonds between the crystal's substance and surface. The advantages of physical adsorption are that it requires a simple experimental preparation, and has the potential for reversibility. Surface chemistry in physical and chemical adsorption for QCM will be discussed following sections.<sup>106</sup>

#### **1.5.2.1 Physisorption on QCM**

##### ***Hydrophobic bonds***

The most common use of a non-covalent bond is in a hydrophobic interaction between a functionalized layer and an electrode surface. This functionalized layer is usually bounded on the gold electrode. Generally, the hydrophobic interaction takes place between the protein and

the layer. The hydrophobic interactions based on QCM used a cholesterol biosensor such as cholesterol oxidase attached directly to the electrode surface,<sup>117</sup> and an influenza virus hemagglutinin antigen immunosensor based on the direct attachment of an anti-hemagglutinin antibody on the electrode surface.<sup>106, 118</sup> The binding of any proteins to the QCM crystal surface decreases resonant frequency, which suggests that the frequency changes to detect the presence of the proteins. However, hydrophobic interactions provide a weak bond between the electrode and the very first protein layer. Appropriate potential is required for continuing the incubation steps needed for the protein to be successfully adsorbed.<sup>106</sup>

### ***Ionic Bonds***

Another physical adsorption method based on surface chemistry uses electrostatic interactions for polyelectrolyte/electrostatic layer-by-layer (LBL) assembly. In this LBL assembly, thin films are deposited by alternate adsorption of opposite-charged polyions such as cationic chitosan and anionic hyaluronic acid.<sup>119</sup> Surface chemistry based on polyelectrolyte/electrostatic LBL assembly is useful in developing clinical immunosensors.<sup>120</sup> The immobilized LBL assembly on the electrode surface and the very top layer create an electrostatic interaction against the targeting material. Each layer has a positive or negative charge, and the charges alternate from layer to layer. The QCM is able to monitor the assembly process of polyionic layers. Also, by measuring the resonant frequency changes, it detects when the anti-substance layer from the surrounding solution interacts with the immobilized layer. These polyelectrolyte/electrostatic LBL assembled multilayers have great thermal and mechanical stability, and their constituent molecules are not damaged by layer deposition. However this system has a propensity to leak.<sup>121</sup>

### **1.5.2.2 Chemisorption on QCM**

#### ***Self-Assembled Monolayers (SAMs)***

SAMs consist of a single layer of surface molecules. SAMs are precisely ordered and oriented immobilized molecules. Generally, alkane-thiols are bound parallel on a gold surface. The gold group in alkane-thiols is attached to the gold surface until the alkane chains are close enough to have interactions with each other. The alkane groups are lifted up from the surface but remain packed to the gold electrode by the thiol groups. Consequently, the surface of the gold electrode is covered by a single alkane-thiol layer, which is oriented at an angle of  $30^\circ$  from the gold electrode (figure 1.17).<sup>106</sup>

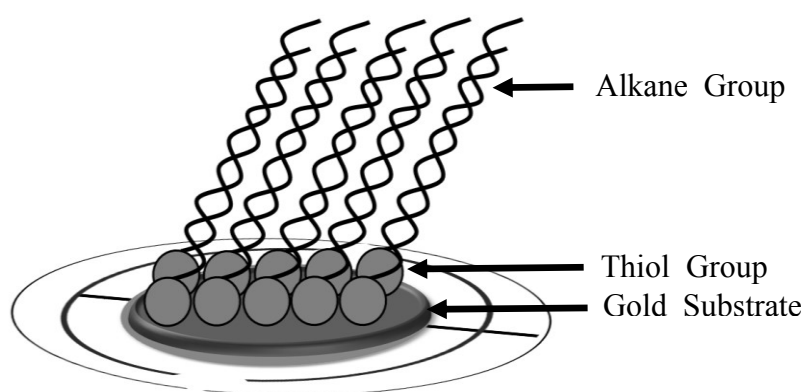


Figure 1.17 Scheme of Self-Assembled Monolayers' deposition on QCM crystal. Adapted from <sup>122</sup>. Copyright 2001, Science Publication.

As mentioned above, the single SAMs consist of long-chain alkane-thiols, which are generally at least 11 carbon atoms in length. Because of the alkane chain's hydrophobicity, hydrophobic interactions between alkyl chains and these alkane-thiol chains are highly ordered and well-packed.<sup>122</sup> These well-packed SAMs are used in a majority of QCM devices.

The advantage of SAM-based device surface chemistry is that it is simple to prepare. The preparation requires only a washing-off process after the SAMs' deposition. In addition, SAMs are allowed to have a reproducibility as a QCM device. In fact, from the recent study, SAMs based QCM is regenerated more times than Protein A (PrA)-modified on QCM crystal. SAMs

also can be used to facilitate biological membranes and prohibit non-specific adsorption of proteins.<sup>106, 123</sup>

### **1.5.2.3 Plasma-Polymerized Films (PPFs)**

Another method for depositing a layer on a QCM uses plasma-polymerized films (PPFs). Some examples of PPF include Protein-A (PrA) or Protein-G (PrG). Depositing a PPF on the surface of a QCM and other biosensors requires a special apparatus, which is generally used in research labs. The apparatus contains a gas bomb or liquid reservoir and mass-flow controller. The controller leads to a closed chamber containing the substrate that operates the apparatus. There is a vacuum pump at the bottom of the closed chamber and a radio frequency generator and matching network near the substrate. The first step for depositing PPFs on the surface is to supply vaporizing gas or liquid monomer using a gas bomb or liquid reservoir, respectively. Once the plasma pressure and the flow rate of the monomer are controlled, electromagnetic power is applied to inductive coils or capacitance to initiate the monomers for polymerization. Then, the thin film is deposited on the electrode surface of the quartz crystal.<sup>124</sup>

PPF surface chemistry in QCM devices has been studied to detect antigens and DNA. In order to detect ovalbumin, which is allergenic egg protein, Papadopoulou-Bouraoui et al. designed DNA hybridization with an immobilized ssDNA probe for DNA detection and active amino group deposition using plasma-polymerization of polyallylamine on the gold surface of a QCM.<sup>125-126</sup> Polyallylamine with a PPF can also detect albumin and it may be useful as a QCM to sense allergenic food proteins.<sup>127</sup> Fabricating PPFs on a gold electrode can lead to numerous biosensor applications. The functionalized PPFs on the electrode surface are thin, generally less than 1  $\mu\text{m}$ . This provides great adhesion onto substrates and flat surfaces. The PPFs' highly branched polymer network also makes the mechanically and chemically stable. Another advantage is that PPFs are biocompatible with enzymes and antibodies. Furthermore, plasma-polymerized amines do not shrink or swell as poly (acrylamide) hydrogels do and are

not odorous as thiol SAMS are.<sup>126</sup> However, even though the PPF method has many advantages, organic vapors are not stable, do not last long, and are not highly oriented and arranged as SAMs are. Also, if the sample is exposed to air after the reaction begins, amine PPFs may react with oxygen and generate peroxides.<sup>106, 125</sup>

### 1.5.3 QCM Applications

QCM can provide information about biomolecular interactions by showing changes in mass at the probe-immobilized surface of the quartz crystal. The change can be shown by the quartz crystal's resonant frequency shift. The QCM is commonly used as a biosensor for protein and DNA adsorption, as mass changes can be detected on its surface.<sup>106</sup> The surface chemistry that has been used to functionalize the QCM surface suggests that QCM has numerous applications.<sup>128</sup> In biological sensors, proteins such as bacteria, fungi, antibodies, antigens, and viruses are adsorbed on a QCM surface<sup>129-130</sup> The QCM has a wide variety of applications. In this section, we introduce two of those: the detection of gaseous species,<sup>131-132</sup> and the detection of carbohydrates.<sup>133-134</sup> Most QCM crystal surfaces are coated with polymeric film. Depending on the film's physical or chemical response, it becomes hydrophilic or hydrophobic when they are exposed to reaction.<sup>106</sup> Similarly, the simple process of coating (painting) pNIPAm-based microgels on QCM crystal provides numerous biosensing applications. This thesis focuses on making a glucose sensor using pNIPAm-*co*-APBA microgels modified using QCM.

#### 1.5.3.1 Detection of Gaseous Species

QCM is generally used in gas phase material sensing. As Marx showed,<sup>111</sup> QCM has been used to detect volatile/vapor-phase species and for sensing environmental contaminants.<sup>131-132</sup> A special technique, sensing ionic liquids (SILs), can be used to thin-coat the QCM surface for the chemoselective real-time detection of aldehyde, ketone, and amine gases.<sup>132</sup> This SILs technique does not require dilution with solvents. Also, once the coated film is deposited on the surface, it is easily removed using methanol, and a new film can then replace the old one.

SILs does not encounter problems related to porous solid materials used as adsorbents for gas adsorption. The commonly known problems include pore size and shape, surface area, thermal stability, and complex adsorption behaviors. This technique is able to overcome these problems. Also, it is easy to coat and remove the film, which makes it possible to regenerate the surface simply by washing. Because it provides an analytical signal to the QCM, the chemical reaction between gaseous species analytes and coated film on the QCM crystal can provide the resonant frequency shift that indicates that mass changes have occurred.<sup>106</sup>

### **1.5.3.2 Detection of Carbohydrates**

Hyperglycemia and diabetes, which result from poor insulin homeostasis in the body, have led to serious medical problems for WHO. The ability to monitor the concentration of glucose in the blood serum is critical for the management of diabetes.<sup>133</sup> Two different methods for detecting glucose will be introduced, the first of which is graphene nanosheets deposited on the QCM crystal surface and QCM biosensor. After the nanosheets are adsorbed, phenoxydextran is injected into the nanosheets. Phenoxydextran has a lower binding affinity than glucose to Concanavalin A. This method showed that due to  $\pi$ - $\pi$  stacking interactions, phenoxydextran molecules were capable of adsorption on the graphene surface. Concanavalin A was added, and its molecules started to conjugate to dextran. When glucose was added to the QCM cell, it competed for binding sites on Concanavalin A and dextran. Dextran has a relatively low binding affinity with Concanavalin A. Therefore dextran was detached from the graphene nanosheets and glucose-bound to Concanavalin A. As a result, a resonant frequency shift occurred and the limit of detection was 5.0  $\mu$ M.<sup>106,125</sup>

Another glucose detection technique was conjugated to gold nanoparticles carbohydrates. This technique used a polymer containing boronic acid. This polymer is commonly used as a glucose sensor, and can selectively and sensitively detect various carbohydrates. A polymer containing boronic acid was coated on the surface of the QCM crystal, and gold nanoparticles

and carbohydrates conjugated with each other to form multivalent carbohydrates. When they bound to the boronic acid, the electrical signal was amplified.<sup>106,134</sup> This suggests that two different methods can be used for carbohydrate detection by QCM. One, the graphene nanosheet deposited on QCM crystal, introduced the material with a lower binding affinity with analytes on the p surface. After the analytes were added, the material was detached and the analytes bound to the probe. The other method introduced the material with great binding affinity to analytes on the immobilized probe on the surface. Once the analytes bound to the probe, the frequency shift was amplified.<sup>134</sup>

#### **1.5.4 Previous QCM studies**

QCM is widely used in many applications including interactions between molecules, depositing layers on the surface of quartz crystal, and nanogram scale mass changes. Surface and coating chemistry are closely related to QCM techniques. QCM can be used as a sensor to monitor mass changes or adsorption on the surface layer.

##### **1.5.4.1 DNA Sensing**

DNA sensing, immobilization, hybridization, and hydrolytic cleavage are monitored in real-time from frequency shifts through an electrode on quartz crystal.<sup>135-136</sup> This study showed that it is possible to use a QCM-based biosensor in immunosensor research. İ. Karamollaoğlu et al.,<sup>76</sup> investigated a mass-sensitive QCM-based DNA biosensor to detect the hybridization of a CaMV 35S promoter sequence (P35S) to study the screening of genetically modified organisms (GMOs). The food industry has focused on detecting specific DNA sequences in order to screen target sequences for genetically modified organisms. The İ. Karamollaoğlu et al. study is based on the immobilization of probe sequences coated on the gold surface on the QCM crystal and used a thiol group, because of thiol's excellent interaction with gold and its

ability to immobilize on a QCM surface. There is a transgene in a certain region of the CaMV 35S promoter sequence. This transgene performs as a probe to detect GMOs. After the probe detects GMOs and hybridization occurs, the resonance frequency in QCM decreases.<sup>137</sup> In this study, the QCM showed that the immobilized probes on the gold surface with thiol groups can detect GMOs. Their hybridization shows that mass changes on the QCM crystal surface decrease resonant frequency.

The QCM-based DNA sensor has attracted attention because it is time-resolved, has the sensitivity to detect non-labeled DNA or single mismatched DNA, and can perform multi-analysis. The principle of QCM-based DNA biosensors is the complementary interaction between the specific DNA sequences and the DNA probe. It is necessary to use an immobilized DNA probe on the surface of quartz crystal (figure 1.18).

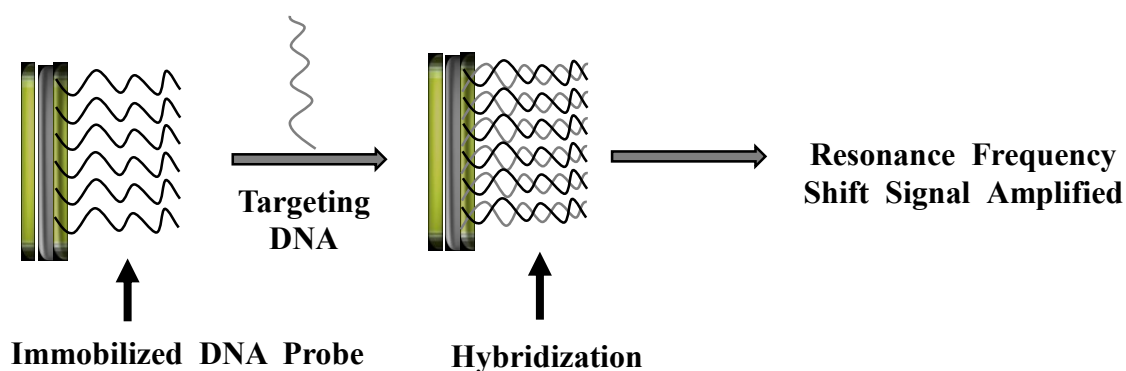


Figure 1.18 Schematic illustration of QCM-based DNA detection by immobilized DNA probe on the QCM surface. Reprinted from<sup>138</sup>. Copyright 2001, Elsevier LTD.

Zhou et al. demonstrated that different types of biotin-DNA probes immobilized in the film on the QCM surface affect sensor sensitivity.<sup>138</sup> It was suggested that six different layers of film, either single or multi-layers, were immobilized on the surface of the QCM crystal. As a result, the multi-layer film-based biotin-DNA probe showed the highest frequency shift around 350Hz. This shows that targeting DNAs can penetrate into multi layers of film, allowing the film to detect more targeting DNAs and thus enhancing sensitivity. The multi-layered film

showed a faster response, and high hybridization and sensitivity. This study investigated that a biotin-based DNA probe showed a different efficiency, which depended on the level of covalent or electrical adsorption on single or multi layers.<sup>138-139</sup>

Diagnosis using QCM has a great advantage over the more conventional method, fluorescence-labeling. First, it is not necessary to require pre- or after-treatment of the sample, and it is possible to monitor the sample's hybridization *in-situ*. Other advantages include the speed of the measurement instrument, low cost, and simple instrumental setup.<sup>138-139</sup>

#### 1.5.4.2 Protein Sensing

Höök performed protein adsorption on QCM under liquid conditions. As discussed in Section 1.5, in general, QCM has been used in gas or liquid conditions, and only if rigid material on the the surface is applied using a Sauerbrey equation. However, it is difficult to analyze QCM results using the Sauerbrey equation. The protein adsorption in aqueous solutions is such that the assumptions under the Sauerbrey equation cannot be applied. The non-rigid nature of protein molecules implies that the energy dissipation of the system could be affected. Another possible reason that it is difficult to analyze QCM results using the Sauerbrey equation is that the protein molecules could trap the water molecules, leading to an increase in mass.<sup>130</sup> In order to obtain an accurate amount of protein adsorbed on the surface in the liquid system, frequency and mass shift have to be considered, as does the dissipation factor. The dissipation factor is explained after equation 5.

$$D = \frac{1}{Q} \frac{E_{lost}}{2\pi \cdot E_{stored}} \quad \text{Equation 5}$$

where  $Q$  is the quality factor of crystal,  $E_{lost}$  is the energy lost per oscillation, and  $E_{stored}$  is the energy that remains following an oscillation. The larger  $D$  value indicates the softer and more

swollen phase, while the smaller  $D$  value exhibits a relatively rigid and collapsed phase adsorbed on the crystal.<sup>140</sup>

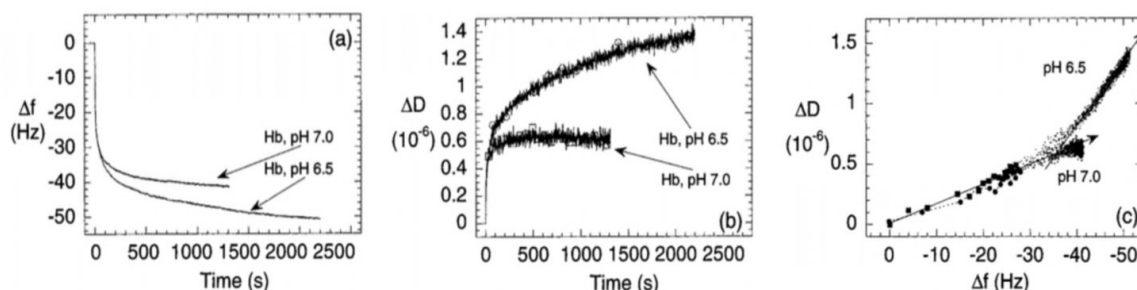


Figure 1.19  $\Delta f$  vs  $t$  and  $\Delta D$  vs  $t$  for the adsorption of Hb on the QCM surface at pH 6.5 and 7.0. The influence of pH on the Hb adsorption kinetics is also illustrated by the  $D$ - $f$  plot (c). The simple linear behavior at pH 7.0 is replaced by a two-phase behavior at pH 6.5, where the total mass uptake and final dissipation shift are larger. Reprinted from<sup>141</sup>. Copyright 1998, ACS publication.

Frequency shift ( $\Delta f$ ) and ( $\Delta D$ ) represent the mass changing and viscosity of adsorbed material, respectively. Thus, the protein adsorption measurement in QCM is affected by the relationship between  $\Delta f$  and  $\Delta D$ . In this study, Höök investigated protein adsorption, including molecules ranging in size from small to large. He tested the adsorption of hemoglobin (Hb) in pH 6.5 and 7.0. At the beginning of the study, the resonant frequency decreased due to an increase in mass. However, the rate of the increasing dissipation shift slowed because the surface of the crystal quickly became saturated. In the case of  $\Delta D$ ,  $\Delta D$  increased, which is the opposite of what happened to  $\Delta f$ , as seen in Figure 1.19.<sup>141</sup>

The protein was deposited on the surface during the fast and slow phases of adsorption because of different relative dissipation rates. This suggests that a single protein can form adlayers with different viscoelastic properties, depending on the interaction between the surface and the adlayers. Therefore it is necessary to investigate  $\Delta f$  and  $\Delta D$  in Newtonian fluid to generate accurate data during the QCM measurement shown in equations 6 and 7. When crystal is immersed in water, the dissipation factor shifts are induced by coupling the crystal shearing motion in Newtonian fluid. This was suggested by Stockbridge in 1966.<sup>141-142,143</sup>

$$\Delta f = -\sqrt{\frac{n}{\pi}} \frac{\sqrt[3]{f}}{v_q \rho_q} \sqrt{v_l \rho_l} \quad \text{Equation 6}$$

$$\Delta D = 2 \sqrt{\frac{f}{n\pi}} \frac{1}{v_q \rho_q} \sqrt{v_l \rho_l} \quad \text{Equation 7}$$

where  $v_q$  is the shear velocity of quartz,  $\rho_q$  is the density of quartz,  $v_l$  is the shear velocity of liquid, and  $\rho_l$  is the density of liquid. These two equations assume that: *i*) The fluid is coupled to the oscillatory motion of the crystal: in other words, there is a no-slip condition; *ii*) The surface is smooth enough and no liquid can be trapped in the pores. The surface of the crystal is very smooth, so nothing can be trapped in pores.<sup>141-142</sup>

Moreover, the moment the protein molecules adsorb on the surface of the QCM, the following must be considered: the interface between the liquid and the protein and the interface between the protein and the QCM crystal surface. Overall, there are three interfaces in this system for D-shifts; *i*) at the QCM surface interface and protein, *ii*) within the protein layer (including trapped water molecules), *iii*) in the protein and liquid environments. These three possible candidates may affect the mass changes. These changes include not only the amount of protein adsorption but also the additional mass shift, including trapped water molecules. In order to obtain reliable mass changes, the  $\Delta D$  concept is introduced and the ratio of  $\Delta D/\Delta f$  is measured.<sup>109</sup>

Höök also tested the material's different size and viscoelastic properties adsorbed on the QCM and measured the ratio of  $\Delta D/\Delta f$  and the small globular proteins, which are relatively dense and rigid compared to large compounds such as myoglobin (Mb) and hemoglobin (Hb).<sup>141</sup> The dense and rigid compounds showed the lowest  $\Delta D/\Delta f$  value, and the increasing  $\Delta D/\Delta f$  value ranging from the large flexible protein (fibrinogen, immunoglobulin) to larger viscoelastic and large macro molecular compounds. The latter two compounds have a relatively high viscoelasticity compared to small proteins, such as living cells and bacteria, and showed

the largest  $\Delta D/\Delta f$  value.<sup>109,141-142</sup> This result does not exclude the mass changing, which means that water molecules could be trapped by proteins or directly bound on the surface. However, the largest  $\Delta D/\Delta f$  value is focused only on  $\Delta f$ , indicating mass changes but a considered  $\Delta D$  energy loss. This indicates that the  $\Delta D/\Delta f$  value provided a much more reliable amount of protein adsorption than the amount calculated by the Sauerbrey equation. The amount of adsorbed protein from  $\Delta D/\Delta f$  value is similar data from ellipsometry or optical waveguide lightmode spectroscopy measurement.<sup>141</sup> The  $\Delta D/\Delta f$  value in the QCM measurement has a limitation: it cannot clearly state the exact amount of proteins adsorbed. This is a challenge for further QCM-based protein detection or adsorption studies.<sup>141</sup>

## 1.6 Outline of the Thesis

This thesis discusses the application of stimuli-responsive polymers on glucose sensors. Chapter 2 will explain the development of a glucose biosensor and illustrate how pNIPAm-*co*-APBA microgels can respond to glucose when a pNIPAm-based microgel is the main component in a glucose-responsive polymer that contains a boronic acid group. The pNIPAm-based microgel copolymerizes with APBA performs glucose detection in solution by responding to various pH levels. The magnitude of glucose detection will be represented by a QCM measurement, resonant frequency shift. Chapter 3 will focus on the selectivity and regeneration performance in a pNIPAm-*co*-APBA microgel-modified QCM device. This thesis's main objective is to show that the proposed pNIPAm-*co*-APBA microgel-modified glucose sensor is highly selective to glucose in other sugars and is regenerable.

# CHAPTER 2 POLY (N-ISOPROPYLACRYLAMIDE) MICROGEL BASED ETALONS FOR GLUCOSE DETECTION

## 2.1 Introduction

In Chapter 1, we introduced stimuli-responsive polymers, specifically poly (N-isopropylacrylamide) (pNIPAm)-based microgels. Microgels become pH-responsive when, during polymerization, we add comonomers containing weak polyelectrolyte groups. This chapter details the pNIPAm-*co*-(3-aminophenylboronic acid) (APBA) microgels, and their response to glucose. In our study, we fabricated etalons directly onto the surface of quartz crystal microbalance (QCM) crystal and characterized their response to glucose concentrations in solution by measuring the resonant frequency of QCM crystal. This chapter will introduce the development of a glucose biosensor and investigate different compositions of APBA in pNIPAm-*co*-APBA microgels and show how diameter affects the microgels' glucose responsivity. We also looked at how ultraviolet visible spectroscopy (UV-VIS) can be used to show how different glucose concentrations affect microgels' glucose sensitivity. Also, adding glucose changes the microgel layer on the QCM crystal. Atomic force microscopy (AFM) was used to measure the height of microgel layer.

### 2.1.1 The Development of a Glucose Biosensor

Diabetes mellitus is one of the most common endocrine disorders that affects carbohydrate metabolism, and is a major cause of human morbidity and mortality. A sedentary lifestyle has led to increased obesity. This, along with changes in (or poor) eating habits, has led to an increased occurrence of diabetes mellitus.

Glucose levels in blood vary before and after meals, and throughout the day. In general, the normal fasting glucose concentration level range for most adults is between 0.08 and 0.11 g/dL (dL=100 mL). People whose range is consistently below 0.07 g/dL are considered

hypoglycemic. Adults whose fasting blood glucose level exceeds 0.126 g/dL and whose level two hours after a meal is over 0.2 g/dL have diabetes mellitus (i.e., hyperglycemia).<sup>144</sup> Hyperglycemia occurs under two conditions: when people do not have enough insulin in their body to keep their glucose level at a normal range, and/or when people fail to take their diabetes medicine.<sup>145-146</sup> Diabetes mellitus is classified into two types; type 1 is caused by low insulin levels. Most type 1 patients are children and young people whose condition is the result of a damaged pancreas (usually caused by genetic disorder). Type 2 is caused by resistance to insulin at the cellular level, and is commonly found in older individuals. The causes of hypoglycemia are kidney failure, liver disease, starvation, and inborn error of metabolism. Hypoglycemia can be treated by taking glucose tablets or other forms of sugar to return blood glucose to a normal level.<sup>146-148</sup>

Generally, blood glucose concentration is the major diagnostic criterion for diabetes. Blood glucose monitoring, a valuable tool to manage diabetes, helps patients maintain a normal blood glucose concentration to prevent further progression or complications.<sup>149,150</sup> Patients check their blood glucose level regularly using a blood glucose monitor before or after a meal. They are required to have insulin injections three or four times in a day because it takes two to five hours for an injection to take effect.<sup>151</sup> Currently, glucose sensors are used to monitor blood glucose. These sensors use an electrochemical platform, which offers superior sensitivity, accuracy/precision, and low cost.<sup>149-150, 152-153</sup>

The first glucose biosensor was proposed and developed in 1962 by Clark and Lyon, who made an enzyme-based electrode to measure blood glucose.<sup>154</sup> The glucose is oxidized by glucose oxidase (GOx) and, in Clark and Lyon's biosensor, GOx trapped between semipermeable membranes over an oxygen electrode was used to monitor oxygen consumption.<sup>155</sup> Later, Updike and Hicks simplified and developed the electrochemical glucose assay by immobilizing GOx.<sup>156</sup> As can be seen schematically in figure 2.1, glucose is oxidized

by GOx and hydrogen peroxide is oxidized on the platinum electrode, and consequently, electrons are generated.

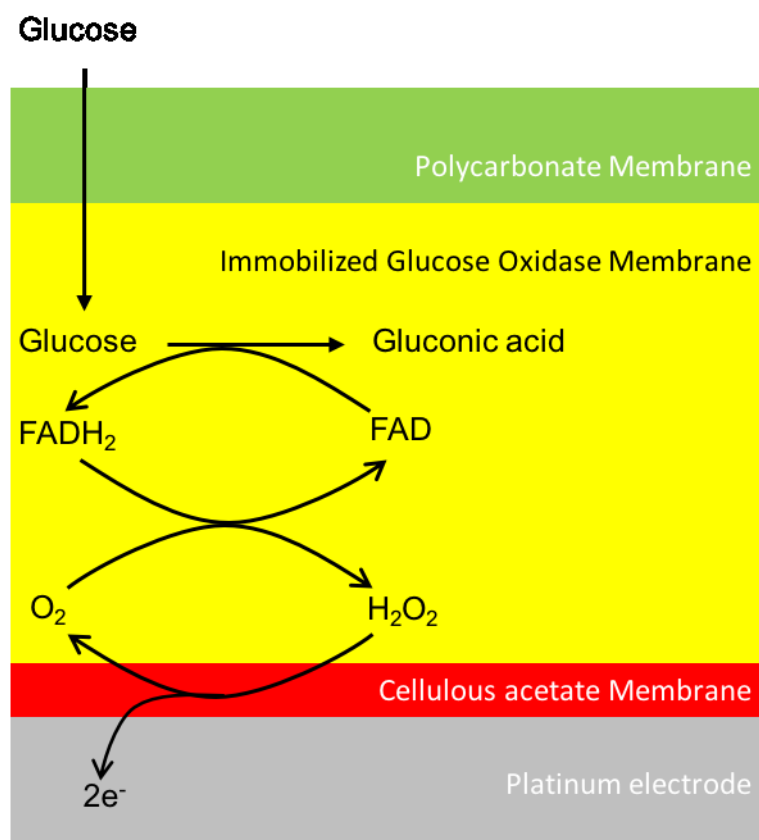


Figure 2.1 The glucose oxidation and generating electrons in membranes on the platinum electrode.

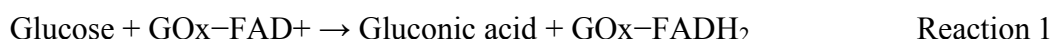
When the GOx-modified electrode is exposed to biological fluids, glucose and oxygen diffuse into the membrane containing GOx (figure 2.1). When a constant potential is applied, the current will increase when gluconic acid is formed. These signals can be used to calculate glucose concentration in biological fluids.<sup>152-153</sup>

### 2.1.1.1 First Generation of Glucose Biosensors

Glucose measurements are based on interactions between glucose and certain enzymes. Two common enzymes used for glucose sensing for self-monitoring blood glucose (SMBG) are GOx and glucose-1-dehydrogenase.<sup>149</sup> GOx is the most common enzyme for biosensors

because of its high selectivity for glucose, its low cost and stability in various conditions.<sup>149</sup>

The function of GOx for glucose detection involves the following steps: In order to act as a catalyst, GOx requires a redox cofactor, flavin adenine dinucleotide (FAD), which performs as the initial electron acceptor and is reduced to FADH<sub>2</sub> (Reaction 1).



The cofactor FAD is regenerated by its reaction with oxygen and leads to the formation of hydrogen peroxide. (Reaction 2).



Hydrogen peroxide is oxidized at the platinum electrode, which generates electrons. (Reaction 3). The electrons result in an increased current, which is related to the rate of reaction ( $v_A$ ) by equation 8, as follows.<sup>157</sup>



$$i = nFAv_A$$

where  $i$  represents the current,  $n$  represents the number of electrons transferred,  $A$  is the electrode area, and  $F$  is the Faraday constant. The rate of reaction ( $v_A$ ) of the substrate (glucose) to the surface has been found to be proportional to the surface area and the difference between the initial and final substrate (glucose) concentration. This follows Michaelis-Menten kinetics, which is a well-known enzyme kinetics equation. This can be explained using equation 9.<sup>158</sup>

$$v_A = K_L([S_0] - [S])$$

where  $K_L$  is the mass transfer coefficient,  $[S_0]$  is the initial concentration of the substrate (glucose), and  $[S]$  is the final concentration of the substrate

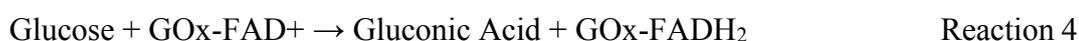
Equation 9

(glucose). The number of electrons transferred is automatically calculated using equation 8 and from the rate of reaction ( $v_A$ ) of equation 9, so that the glucose biosensor provides a glucose concentration in the blood. Therefore, the current increases as the electron transfers increase, signaling that there is more glucose present in the blood. The reduction in the oxygen

concentration is proportional to that of the glucose concentration. The glucose concentration is quantified by measuring the increment of hydrogen peroxide.<sup>159</sup> A disadvantage of the first generation of glucose biosensors was the interference of endogenous electroactive species, for example, uric acid, ascorbic acid, and drugs. Those species react with oxygen, leading the sensor to give a false measurement. Another disadvantage was an oxygen deficit, which was the restricted oxygen solubility in biological fluids. Oxidase-based devices rely on oxygen as an electron acceptor. Oxygen consumption in early glucose sensors monitored the oxidation of glucose in the presence of oxygen. However, there is a limited amount of oxygen in biological fluid and continuous oxygen consumption leads to oxygen deficits in those fluids. This leads to errors resulting from the fluctuations in oxygen partial pressure. These errors change sensor responsivity.<sup>149,155,160</sup>

### 2.1.1.2 Second Generation of Glucose Biosensors

First-generation glucose biosensors have an oxygen dependence, and they undergo oxygen deficits at low oxygen concentrations in biological fluid. This can be overcome by using redox mediators, which are a major characteristic of a second-generation glucose biosensor. Redox mediators carry electrons from the enzyme to the surface of the electrode. This redox mediator carries electrons between the FAD and the electrode surface using the following reactions:



where  $\text{M}_{(\text{ox})}$  and  $\text{M}_{(\text{red})}$  are the oxidized and reduced forms of the mediator. The glucose in the presence of GOx-FAD is oxidized to gluconic acid and GOx-FAD is reduced to GOx-FADH<sub>2</sub> (Reaction 4). The GOx-FADH<sub>2</sub> can be oxidized back to GOx-FAD by reducing the redox mediator (Reaction 5). The redox mediator is re-oxidized at the electrode to the oxidized mediator (Reaction 6 and Fig 2.2). The current is measured by the electrons and is directly

related to the amount of glucose, which is oxidized by the GOx-FAD enzyme reactions as shown in Equation 8.<sup>155</sup>

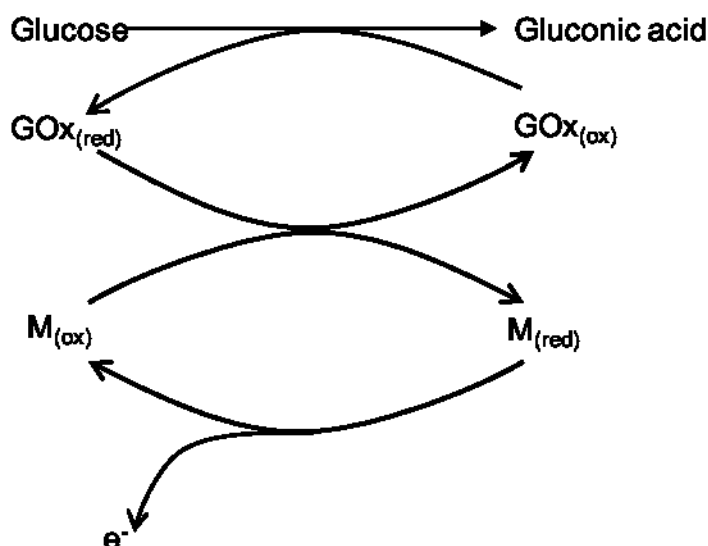


Figure 2.2 Glucose Oxidase electrochemistry in second-generation glucose biosensors' mediated system. Adapted from<sup>155</sup>. Copyright 2001, WILEY-VCH Verlag GmbH & Co. KGaA, Weinheim.

In order to be used effectively, the mediator should react rapidly with the reduced enzyme to minimize the reaction with oxygen. It should have a significant electrochemical property, such as a low redox potential, and should be nontoxic and chemically stable in oxidized and reduced forms.<sup>149,155</sup>

A variety of mediators, such as ferrocene derivatives, ferricyanide, conducting organic salts, quinines, tetrathiafulvalene (TTF), tetracyanoquinodimethane (TCNQ) and phenoxazine compounds have been widely used to improve sensing performance.<sup>157,161-163</sup> Oxygen was a physiological electron acceptor in first-generation glucose biosensors. The use of electron-carrying mediators eliminates the need for oxygen in electron transfer, and the measurements overcome the oxygen deficit problem of first-generation biosensors. These mediators can be carried out at lower potentials, which do not induce interfering reactions from coexisting electroactive species (Reaction 6).<sup>160</sup> In particular, ferrocene is a suitable mediator, which is

independent of oxygen and pH, and chemically stable and without oxygen reactivity in both oxidized and reduced forms.<sup>155,157</sup>

### 2.1.1.3 Third Generation of Glucose Biosensors

The use of mediators in glucose biosensors poses several problems. First, the mediators compete with oxygen. Although the major reaction is between the mediator and  $\text{GOx}_{(\text{red})}$ , there remains the possibility that the dissolved oxygen will compete to oxidize the  $\text{GOx}_{(\text{red})}$ . Second, the possibility exists that coexisting electroactive species such as uric acid and ascorbic acid will react with oxygen. This might give false signal and inaccurate measurement. Third, the mediator's small size and highly diffusive properties lead to a leaching problem from the intermediate region between the enzyme and electrode. This mediator leaching problem alters the biosensor response.<sup>164-167</sup> In order to overcome these drawbacks, third-generation glucose biosensors were developed. These biosensors are reagent-less and are subsequently less toxic; they are based on direct electron transfer between enzymes. The direct electron transfer is a result of the use of organic conducting salts, which are based on charge-transfer complexes.<sup>149,155</sup> The organic conducting salts, such as tetrathiafulvalene-tetracyanoquinodimethane (TTF-TCNQ), are known to mediate the electrochemistry of pyrrole-quinolinequinone enzymes (GDH-PQQ) as well as of flavoproteins, i.e., GOx. TTF functions as an electron donor and TCNQ functions as an electron acceptor. TTF-TCNQ has a specific orientation on the electrode, allowing for a direct electron transfer system.<sup>149,164</sup> Figure 2.3 shows three different generations of electrodes. The first-generation electrode was oxygen-dependent; the second-generation electrode used a redox mediator, which is oxygen-independent; and the third generation electrode used direct electron transfer between GOx and the electrode.

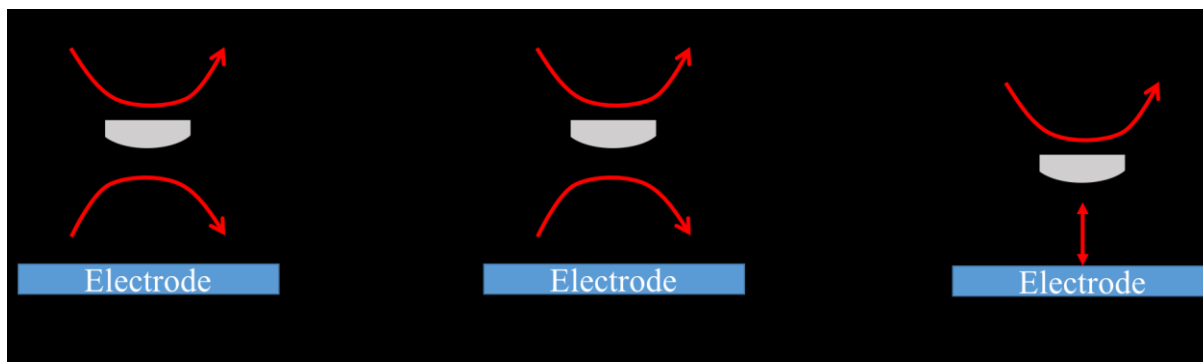


Figure 2.3 The three generation of glucose biosensors based on amperometric enzyme electrodes. A) glucose based on the use of the oxygen cofactor. B) artificial redox mediator. C) direct electron transfer between GOx and the electrode. Adapted from<sup>168</sup>. Copyright 2008, ACS Publications.

### 2.1.2 Current Glucose-Sensing Technology

The third-generation glucose biosensor made it possible to develop devices capable of home and personal use. Such devices are minimally invasive, disposable, inexpensive, accurate, and easy to use. Current glucose monitoring devices have been developed to be smaller, and provided faster and greater sensitivity.<sup>155,169</sup> The glucose monitoring system uses disposable enzyme electrode test strips. These strips contain printed working electrodes coated with reference electrodes, and with reagents such as enzymes, mediators, or stabilizers. The control meter is typically light, pocket-sized, and battery operated. Figure 2.4 shows a schematic of the commercial glucose biosensor strip. The working electrode is coated with the necessary reagents (i.e., enzyme, mediator, linking and binding agents, and stabilizer).<sup>168</sup> However, there is a problem with this glucose strip: species such as ascorbic acid and uric acid in blood can be oxidized at the same potential required to oxidize the mediator. Therefore, two working electrodes are on the strip. The first working electrode is coated with GOx and a mediator. In order to avoid an interference effect, the second working electrode has only mediator not GOx. The measure of the difference glucose concentration current is between the current at the first

working electrode and the current at the second working electrode. Both currents are measured with respect to the reference electrode.<sup>170</sup>

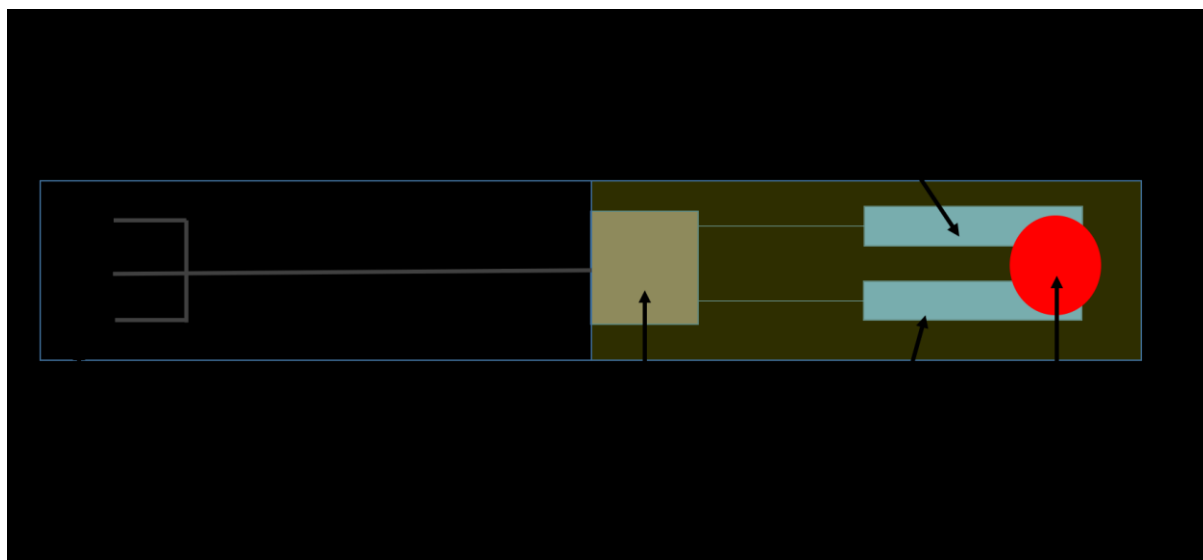


Figure 2.4 The single-use blood glucose meter strip. Adapted from <sup>170</sup>. Copyright 2008, ACS Publications.

Commercial glucose biosensors use nanomaterials on a graphite electrode with GOx adsorption. A nanomaterial-based sol-gel composite at the surface of the graphite electrode was introduced to the glucose biosensor. With their unique electrical and optical properties, and mechanical strength,<sup>171</sup> nanomaterial-based biosensors appear to be more promising than previous gel- or membrane-based biosensors.<sup>172</sup> Figure 2.5 shows the graphite electrode-based glucose sensor. A poly (glycidyl methacrylate-co-vinylferrocene) (poly (GMA-co-VFc)) film coats the graphite electrode. This graphite electrode provides the amperometric current response of poly (GMA-co-VFc)-GOx to glucose. This graphite electrode has a linear relationship with the amperometric current and glucose, the range of which is between 1 and 16 mM.<sup>173</sup> GOx immobilized on a nanomaterial-based glucose biosensor provides high selectivity, glucose responsivity, and fast glucose detection in a matter of seconds.

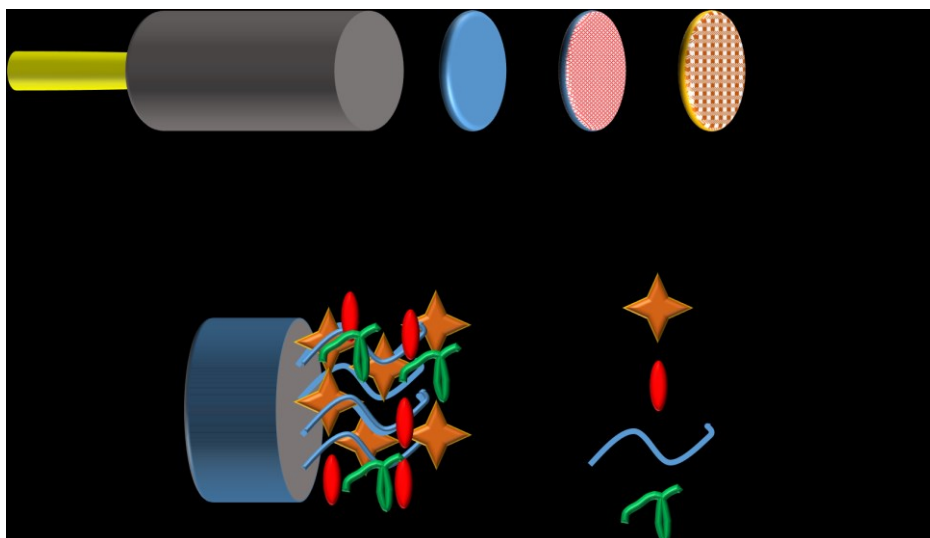


Figure 2.5 The illustration of glucose biosensing based on a graphite electrode. Adapted from <sup>173</sup>. Copyright 2014, Elsevier Inc.

The first commercial glucose biosensor product was a pen-type device made by Medisense Inc. in 1987, based on a second-generation glucose biosensor which relied on a ferrocene-derivative mediator.<sup>169,174</sup> To quickly obtain a reading of their glucose concentration, diabetes patients take their blood by pricking one of their fingers and placing their blood on the sensor strip.

The microgel-based glucose biosensor is a promising device: it is simple and can be re-used, and in these ways it avoids some of the main drawbacks of glucose biosensor technology. Microgels are easy to synthesize and inexpensive. We expect microgel-based glucose biosensor to show great performance in glucose detection.

### 2.1.3 Glucose-Responsive Microgels

Glucose-sensitive pNIPAm-based microgels have been studied by several research groups.<sup>32,175</sup> In general, hydrogel composed of poly (methacrylic acid) and poly (ethylene glycol) with immobilized GOx and phenylboronic acid derivatives-based polymers are commonly used as glucose responsive polymers.<sup>157</sup> This is because hydrogels containing GOx and polymers containing phenylboronic acid derivatives are able to interact with glucose: for

instance, interactions between GOx and glucose, and diol and boronic acid. As mentioned in Chapter 1, APBA is a phenylboronic acid derivative often used to detect glucose in pH responsive polymers. APBA has a  $pK_a$  of 8.2<sup>79</sup> and, in pNIPAm-based APBA microgels, it shows swelling behavior by changing to a pH above  $pK_a$ . At the pH 9.0 buffer, boronic acid moieties on the APBA were hydroxylated, giving the boron atoms a negative charge. pNIPAm-based APBA microgels become swollen once the pH is over the  $pK_a$  of APBA ( $\sim 8.2$ )<sup>175,176</sup> and then diols in glucose start binding to the charged boron atoms (figure 2.6). Diols bind favorably to boronic acid in a charged state.<sup>177</sup> The more that the glucose molecules bind to the charged boronic acid groups, the more the boronic acid groups are converted into the charged state to reach an equilibrium state. Furthermore, as more charged boron atoms are present, more glucose molecules can bind to charged boron atoms, thus forming a signaling cascade.<sup>175</sup>

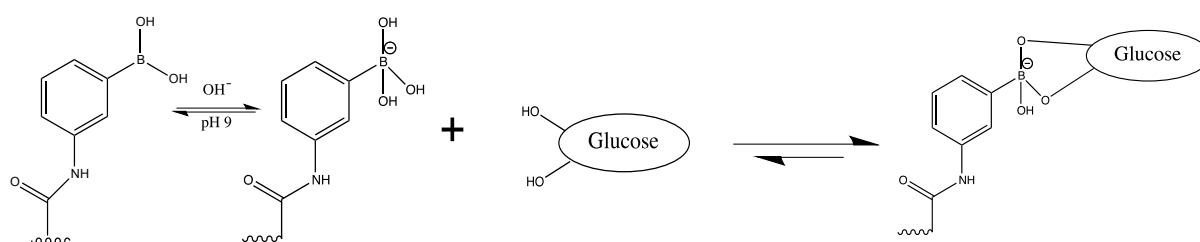


Figure 2.6 The mechanism of glucose binding to hydroxylated boronic acid at pH 9.5. Adapted from<sup>94</sup>. Copyright 2010, Springer.

In the presence of glucose molecules in a buffer solution, the binding of glucose molecules to boronic acid is preferred. The glucose binding to boronic acid promotes hydroxylation of boron atoms, so that more of the atoms become charged. Hence, Coulombic repulsion is increased in the microgel network, resulting in APBA microgels swelling.<sup>94</sup> According to previous studies, when microgels showed a swelling response, this APBA microgels-based etalon was observed as a red shift, as shown in equation 1 in Chapter 1.<sup>88</sup> In other words, APBA microgels between the two Au layers on QCM crystal became swollen and there was a change

in distance between the two Au layers (figure 2.7).<sup>87,178</sup> In this chapter, the APBA microgel's swelling behavior will be demonstrated by a resonant frequency shift.

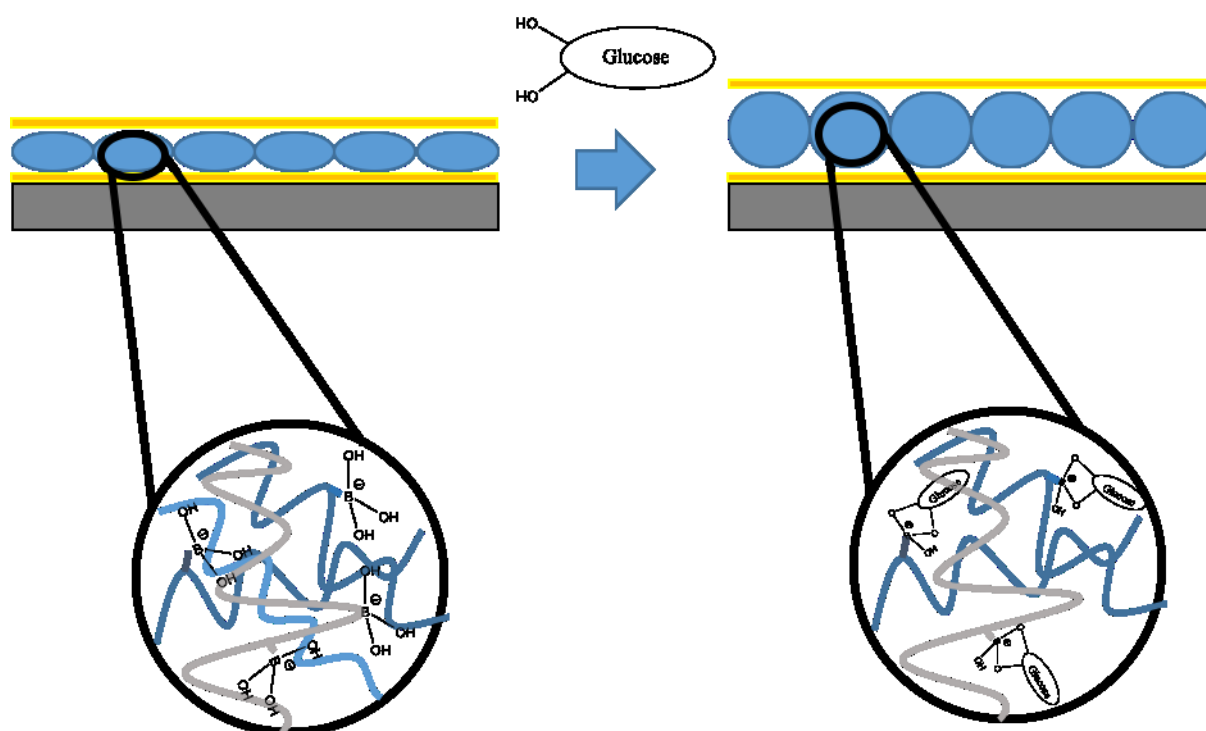


Figure 2.7 The scheme of the glucose responsivity of a pNIPAm-co-APBA microgel-based etalon at pH 9.0. Reprinted from<sup>94</sup>. Copyright 2010, Springer.

## 2.2 Materials and Methods

### *Materials*

N-isopropylacrylamide was obtained from TCI (Portland, Oregon) and purified by recrystallization hexanes (ACS reagent grade, EMD, Gibbstown, NJ) for use in the study. N,N'-methylenebisacrylamide (BIS; 99 %), ammonium persulfate (APS; 98+ %),  $\alpha$ -D-glucose (ACS reagent), and 3-(Acrylamido)phenylboronic acid (APBA, 98 %) were obtained from Sigma-Aldrich (Oakville, Ontario, Milwaukee, WI, and St. Louis, MO). Sodium bicarbonate ( $\text{NaHCO}_3$ ) and sodium carbonate ( $\text{Na}_2\text{CO}_3$ ) were obtained from Caledon Laboratories Ltd. (Rockville, Ontario). All deionized (DI) water was filtered to have a resistivity of 18.2 M $\Omega$  cm and was

obtained from a Milli-Q Plus system from Millipore (Billerica, MA). Anhydrous ethanol was purchased from Commercial Alcohols (Brampton, Ontario).

### ***Instrumentation***

Microgel-coated QCM crystals as well as etalon-coated devices were analyzed using a QCM-200 obtained from Stanford Research Systems (Sunnyvale, California). The crystal was placed into a specially designed holder, which allowed for a buffer solution at a given pH and temperature to constantly flow over the crystal at a rate of  $0.062 \text{ mL s}^{-1}$ . This flow was controlled by a FMI lab pump model RP-G150 (Oyster Bay, New York). The temperature was controlled by placing a beaker containing the buffer solution onto a Corning model PC-420D hotplate (Lowell, Massachusetts), and the solution's temperature was measured through a thermocouple. In order to change the pH of the solution, aliquots of either 0.1 M NaOH or 0.1M HCl were added to the water, and the buffer solution's pH was measured with a Jenco model 6173 pH meter (San Diego, California).

### ***Preparation of pH 9.5 buffer solution***

A 5-mM pH 9 carbonate buffer was prepared by dissolving 0.76 g  $\text{NaHCO}_3$  and 0.11 g  $\text{Na}_2\text{CO}_3$  in 2 L DI water in a volumetric flask. The pH of the resulting solution was pH 9.35, and therefore a few drops of sodium hydroxide were added to make pH 9.5.<sup>94</sup>

### ***Dynamic light scattering measurement***

Dynamic light scattering (DLS) measurement was performed using a Malvern Zetasizer Nano S. The temperature was set to 25 °C and the dispersant was set to DI water. The refractive index was set to 1.330 and the dielectric constant was 78.5. The DLS measurement was done three times per sample. For DLS measurements, low volume disposable cuvettes were used.

### ***pNIPAm-co-APBA Microgel synthesis***

#### ***1. Large pNIPAm-co-APBA microgels***

In order to demonstrate the effect of resonant frequency changes by different amounts of APBA in pNIPAm, two different pNIPAm-*co*-APBA microgels were synthesized: 10% and 15% APBA. The pNIPAm-*co*-APBA microgels were synthesized using surfactant-free, free radical precipitation as described previously with NIPAm (85 %), BIS (5 %) and ABPA (10 %), and NIPAm (80 %), BIS (5 %) and ABPA (15 %).<sup>110,116</sup> Briefly, 17.0 mmol (16.0 mmol for 15 % APBA microgel) of NIPAm monomer and 1.0 mmol of N,N- methylenebisacrylamide (BIS) as the crosslinker were added to a beaker with 100 mL of DI water. The solution was stirred by a magnetic stirrer for about 30 min. After dissolving completely, the solution was filtered by a syringe through a 0.2  $\mu\text{m}$  syringe filter into a 250 mL 3-necked round-bottom flask. The beaker was rinsed with an additional 15 mL of DI water, which was also filtered by syringe and added to the round-bottom flask. The gas inlet (needle), a reflux condenser, and a temperature probe were set up onto the round-bottom flask. To maintain the O<sub>2</sub> level, N<sub>2</sub> gas was continuously purged through the solution while being heated to 45 °C for 1.5 hour and the solution was stirred at 450 RPM. Immediately prior to initiation, 2.0 mmol (3.0 mmol for 15 % APBA) of APBA were added to the solution with 5 mL of 0.078 M ammonium persulfate (APS) solution. The temperature of the solution was then increased to 65 °C at a rate of 30 °C/h immediately following initiation and was allowed to react for four hours. After the reaction, the solution was allowed to cool down and was filtered through glass wool to get rid of large aggregate particles. The filtrate was diluted to 100 mL with DI water and 35 mL aliquots were transferred to centrifuge tubes, and centrifuged at  $\sim$  8500 relative centrifugal force (rcf) for 1h at 23 °C. The microgels precipitated at the bottom of the centrifuge tube, and the supernatant solution was successively removed, and replaced with fresh DI water. Overall, the supernatant solution was centrifuged six times to remove leftover monomer and polymer chains from the microgel mixture. After that, pure, concentrated, and very viscous microgel paste was formed and was dried using a lyophilizer (Kansas City, Missouri). The mass of microgels was (32.1 mg) and

10ml DI water was added to make a 3.21 mg/dL concentration of microgel solution. This solution was used to coat the QCM crystal. Microgels in a pH 9.3 buffer solution had a diameter of 1727.5 nm ( $\pm 19.6$  nm). The microgel diameter measurement was performed by dynamic light scattering.

### **2. Medium *pNIPAm-co-APBA* microgels**

The microgels were synthesized following the procedure used in a previous study<sup>113</sup>. A 3-neck flask was fitted with a reflux condenser, nitrogen inlet, and temperature probe, and charged with a solution of NIPAm (11.9 mmol) and BIS (0.703 mmol) in 99 mL DI water, previously filtered through a 0.2  $\mu$ m filter. The solution was N<sub>2</sub>-gas purged and allowed to heat to 70 °C over ~1.5 hour. Immediately prior to initiation, APBA (1.43 mmol) was added to the heated reaction mixture in one aliquot with APS (0.2 mmol) in 1 mL of DI water. The reaction was allowed to proceed at 70 °C for four hours under nitrogen gas. The resulting suspension was allowed to cool overnight, and then it was filtered through a Whatman #1 paper filter to remove any large aggregates. The microgel solution was then distributed into centrifuge tubes and purified via centrifugation at ~8300 rcf to form a pellet, followed by removal of the supernatant and resuspension with DI water. Overall, supernatant solution was centrifuged six times to remove left over monomer and polymer chains from the microgel mixture. After that pure, microgel paste was obtained. The microgel diameter measurement was performed by dynamic light scattering. Microgels in a pH 9.3 buffer solution had a diameter of 524 nm ( $\pm 8$  nm). The microgel diameter measurement was performed by dynamic light scattering.

### **3. Small *pNIPAm-co-APBA* microgels**

The microgels were synthesized following a previously published protocol.<sup>114</sup> A 3-neck flask was fitted with a reflux condenser, nitrogen inlet, and temperature probe, and charged with a solution of NIPAm (11.1 mmol), BIS (0.652 mmol), and sodium dodecyl sulfate (SDS, 0.2 mmol) in 190 mL DI water, previously filtered through a 0.2  $\mu$ m filter. The solution was

purged with N<sub>2</sub> and allowed to heat to 70 °C over ~1 hour. Immediately prior to initiation, APBA (1.30 mmol) was added to the heated reaction mixture in one aliquot with APS (0.3 mmol) in 10 mL of DI water. The reaction was allowed to proceed at 70 °C for four hours under a blanket of nitrogen. The resulting suspension was allowed to cool overnight, and then it was filtered through a Whatman #1 paper filter to remove any large aggregates. Approximately half of the microgel solution was then distributed into rehydrated dialysis tubing (12-14k nominal MWCO, 25 mm flat width, Fisherbrand Regenerated Cellulose, Nepan, ON) for purification. The tubes were placed into two 2 L beakers with D water and a stir bar for two weeks and the water was replaced twice daily. The cleaned microgels were semi-transparent. They were recombined and stored in a brown glass jar. The microgel diameter measurement was performed by dynamic light scattering. Microgels in pH 9.3 buffer solution had a diameter of 225 nm ( $\pm 4$  nm). The microgel diameter measurement was performed by dynamic light scattering.

### ***Optical Microscopy***

Four different microgel solutions were prepared; i) 10  $\mu$ L DI water: 150  $\mu$ L microgel solution, ii) 10  $\mu$ L water: 155  $\mu$ L microgel solution, iii) 10  $\mu$ L water: 160  $\mu$ L microgel solution, iiiii) 10  $\mu$ L water: 165  $\mu$ L microgel solution. Each microgel solution was painted on the cover glass. Microscopic images of the films were taken using an Olympus IX71 inverted microscope (Markham, Ontario) fitted with a 100 oil-immersion objective, and a 10 eyepiece, differential interference contrast (DIC) optics, and an Andor Technology iXon camera (Belfast, Ireland). A 100  $\times$  magnification booster was used where specified. Andor SOLIS v4.15.3000.0 software was used to record microscope images of the microgel films. An image of an Edmunds Industrial Optics (Barrington, NJ) PYSER-SGI scale grating (100  $\mu$ m  $\times$  2  $\mu$ m) was used to determine the scale bars.

### ***Atomic Force Microscopy***

In-liquid height analysis for a pNIPAm-*co*-APBA microgel etalon in 5 mM carbonate buffer pH 9.5 and 0.199 g/dL glucose in pH 9.5 buffer solution was performed using APBA-functionalized and APBA-exposed control samples. Images were acquired using an Asylum Research MFP 3D AFM (Santa Barbara, CA) over a 5×5- $\mu\text{m}$  area using a scan rate of 0.498 Hz, using 512 scan points and lines. The tips were Olympus TR800PSA with a resonant frequency of 24 kHz. An image was taken by using a sessile drop method first in the pH 9.5 glucose solution at ~24 °C, taken after 15min and 30min, which is the moment that what? reached the equilibrium state. For this analysis, a line was scratched into the sample using a new razor blade and the scratch was imaged. The height was determined using the software by taking 100-line blocks and measuring the height on a line trace. Four 100-line blocks were measured and averaged to get the average height and standard deviation of each image.

#### ***The effect on glucose responsivity of the amount of APBA in pNIPAm-*co*-APBA microgels***

Both pNIPAm-*co*-APBA containing 10 % and 15 % APBA microgels were prepared. The microgel synthesis was introduced above. After the pNIPAm-*co*-APBA microgel was painted on the gold electrode of QCM crystal and etalon fabrication was performed, the crystal was placed into the QCM holder. Then 100 mL of buffer solution was transferred into five different beakers using a glass pipette, and 0.06 g, 0.1 g, 0.2 g, 0.4 g, and 0.6 g of  $\alpha$ -D glucose were transferred, respectively, to the each buffer solution beaker, and stirred for 10 min until they each dissolved completely. Each glucose buffer solution in a 100 mL beaker at 25 °C was injected into the QCM holder via an inlet tube. An outlet tube of the holder was connected to the same beaker to reuse the solution. This experiment was conducted with two different microgels (10 % and 15 % pNIPAm-*co*-APBA microgels). The glucose buffer solution was added in the following order: 0.06 g, 0.1 g, 0.2 g, 0.4 g, and 0.6 g/dL.

#### ***The effect on glucose responsivity of pNIPAm-*co*-APBA microgel particle size***

The following experiment was completed to investigate whether the microgel's diameter affected its response to glucose. The pNIPAm-*co*-APBA microgel was painted on the gold electrode of QCM crystal and after the etalon fabrication was conducted, the crystal was placed into the QCM holder. The buffer solution was transferred by 100 mL glass pipette, and 0.6 g of  $\alpha$ -D glucose was transferred to the buffer solution and stirred for 10 min until it dissolved completely. This glucose buffer solution in a 100 mL beaker at 25 °C was injected into the QCM holder via an inlet tube. An outlet tube of the holder was connected to the same beaker to reuse the solution. Each diameter of pNIPAm-*co*-APBA microgels shows its glucose responsivity by a resonant frequency shift. This performance was separately conducted using pNIPAm-*co*-APBA microgels with different diameters: large, medium and small.

#### ***Ultraviolet Visible Spectroscopy***

Ultraviolet visible spectroscopy was conducted to demonstrate that the absorbance peak difference of APBA microgels depends on different glucose concentrations. Each glucose concentration (0.05 g, 0.1 g, 0.11 g, 0.125 g, 0.126 g, 0.14 g, 0.155 g, 0.175 g, 0.199 g, 0.2 g, 0.3 g, 0.4 g, 0.5 g glucose/100 mL of pH 9.5 buffer solution) was measured with a UV/VIS reflectance probe from Ocean Optics (Dunedin, Florida). Each glucose solution was taken and transferred to a cuvette and DI water. DI water in the cuvette was measured as a blank. After that, each glucose solution was added to a cuvette. A spectrum was recorded using Ocean Optics Spectra Suite Spectroscopy Software (Dunedin, Florida).

### **Formation of etalons on QCM crystals**

Etalons were fabricated as described in previous studies,<sup>87,116,110,178</sup> with some slight modifications, as detailed here. The Au electrodes of the QCM quartz crystal were rinsed with copious amounts of anhydrous ethanol and dried with N<sub>2</sub> gas. A microgel solution was pipetted only on the “large circle” Au active electrode on the QCM crystal and allowed to dry for 30 min at 35 °C. Figure 2.8 shows the pNIPAm-co-APBA microgels on the QCM crystal.

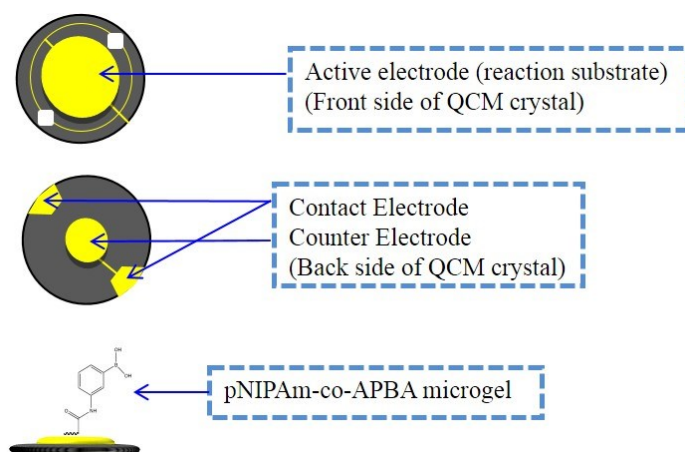


Figure 2.8 Scheme of pNIPAm-co-ABPA microgel on QCM crystal

Following drying, the microgels that had indirectly bound to the Au electrode were rinsed off with DI water, and the QCM crystal was immersed in DI water overnight at 35 °C. After soaking, the crystal was further rinsed with DI water and dried with N<sub>2</sub> gas. A monolayer microgel was adhered to the QCM crystal, such that only the Au electrode, which was coated with microgels, was exposed. The QCM crystal was then inserted into a Torr International Inc. (New Windsor, NY) thermal evaporation system model THEUPG. Two nm of Cr and 15 nm of Au were deposited only onto the Au-bound microgel layer at a rate of  $\sim 0.2 \text{ \AA s}^{-1}$  and  $\sim 0.1 \text{ \AA s}^{-1}$ , for Cr and Au, respectively. After this overlayer was applied, the crystal was removed from the vacuum chamber and immersed in DI water overnight at 35 °C.

## **2.3 Results and discussion**

### **Optical Microscopy**

We hypothesize that the single monolayer microgel gives accurate glucose responsivity by resonant frequency shift in QCM. In previous studies, the microgel painting protocol significantly enhanced homogeneity of the response in etalons.<sup>88,179</sup> The surface roughness of QCM crystal may affect the resonant frequency.<sup>106</sup> Therefore, it is necessary to find the ratio of DI water to viscous APBA microgels solution, which can make the single and homogeneous microgel layer on the QCM crystal provide a more accurate resonant frequency shift. Each of the four different microgel solutions is painted on the gold electrode on the QCM crystal. Figure 2.9 shows the microscope image.

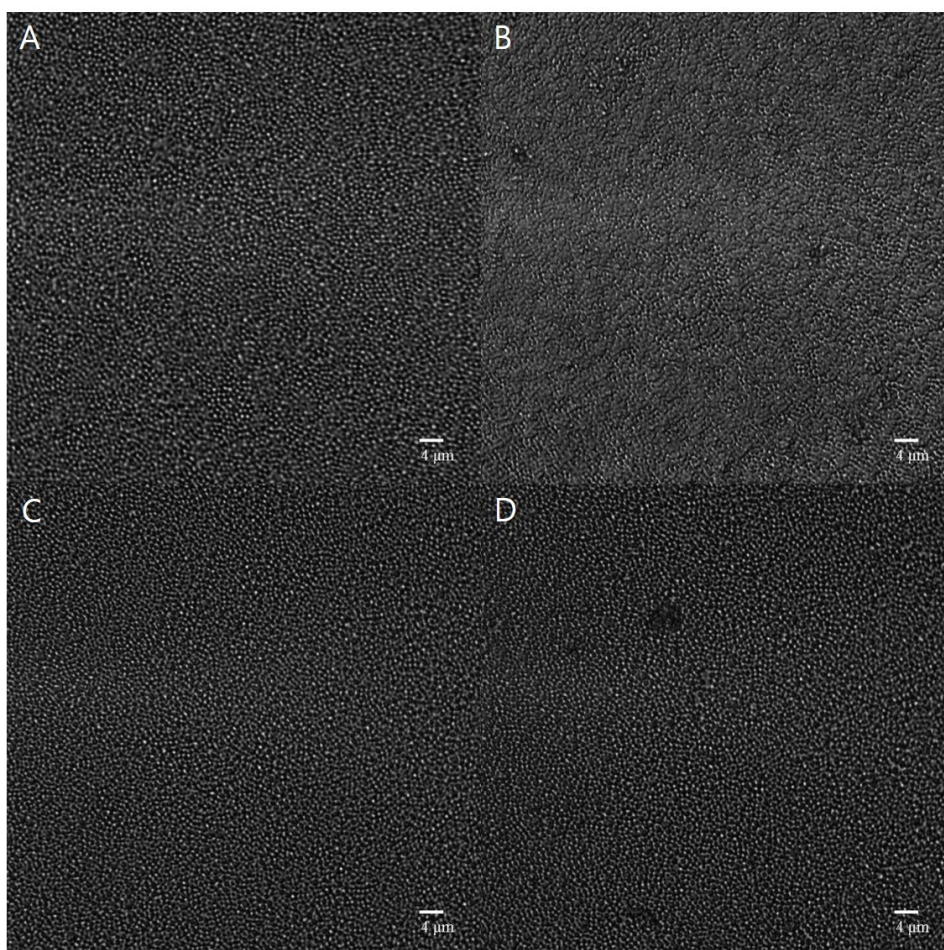


Figure 2.9 The microscopic image of pNIPAM-co-APBA microgels on the glass substrate. The microgel solutions were prepared in four different ratio: A) 10  $\mu$ L: 150  $\mu$ L. B) 10  $\mu$ L: 155  $\mu$ L. C) 10  $\mu$ L: 160  $\mu$ L. D) 10  $\mu$ L: 165  $\mu$ L ratio of DI water to APBA microgel solution.

However, we cannot see any differences in any of the cases. Each painting protocol shows a similar homogeneous layer. In this thesis, the microgel coating procedure is followed by a 10  $\mu\text{L}$ : 160  $\mu\text{L}$  ratio microgel solution as a coating protocol.

### ***Atomic Force Microscopy***

The pNIPAm-*co*-APBA microgels show their glucose responsivity by their swelling behavior. AFM imaging recorded the height of the APBA microgel layer. The height of the layer was measured after the glucose buffer solution was added after 0, 15, and 30 min. The result is shown in figure. 2.10.

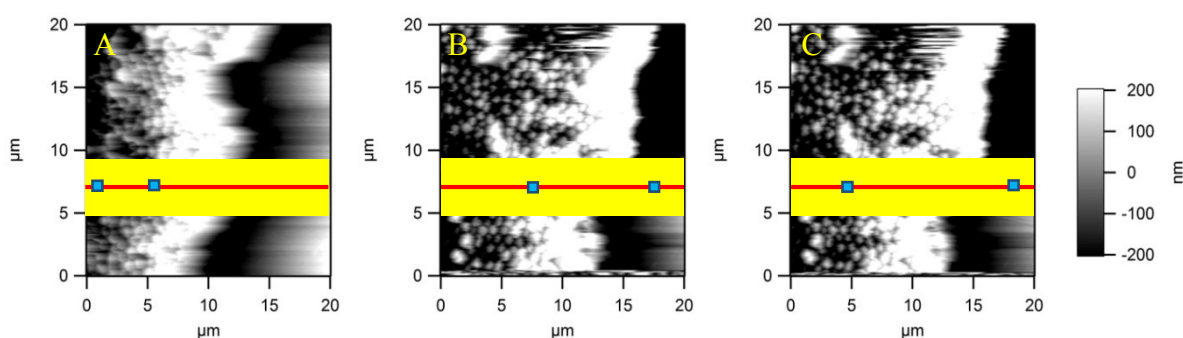


Figure 2.10 The AFM image of a APBA microgel layer after glucose solution addition A) 0min, B) 15 min, and C) 30 min. For each image, a yellow rectangle in image was measured for height analysis and averaged to obtain a standard deviation. All images are 20  $\mu\text{m}$  X 20  $\mu\text{m}$ .

We obtained an AFM image 0, 15, and 30 min after glucose was added and chose the yellow rectangular section in Figure 2.10 to measure the height difference between the microgel layer and the scratched region (see the black area on the right side of each image). The height analysis of the microgel layer in the etalon shows that the thickness of the microgel layer increased after the glucose solution was added. The glucose molecules bound to the pNIPAm-*co*-APBA microgels and the microgels swelled. Consequently, the distance of the microgel layer between the two Au layers in the etalon increased due to swelling. After 0.199 g/dL of a glucose buffer solution was added, the microgel particles started to swell. Each microgel particle's size increased in 0, 15 and 30 min, according to height measurements. The results can be seen in figures 2.11-2.13.

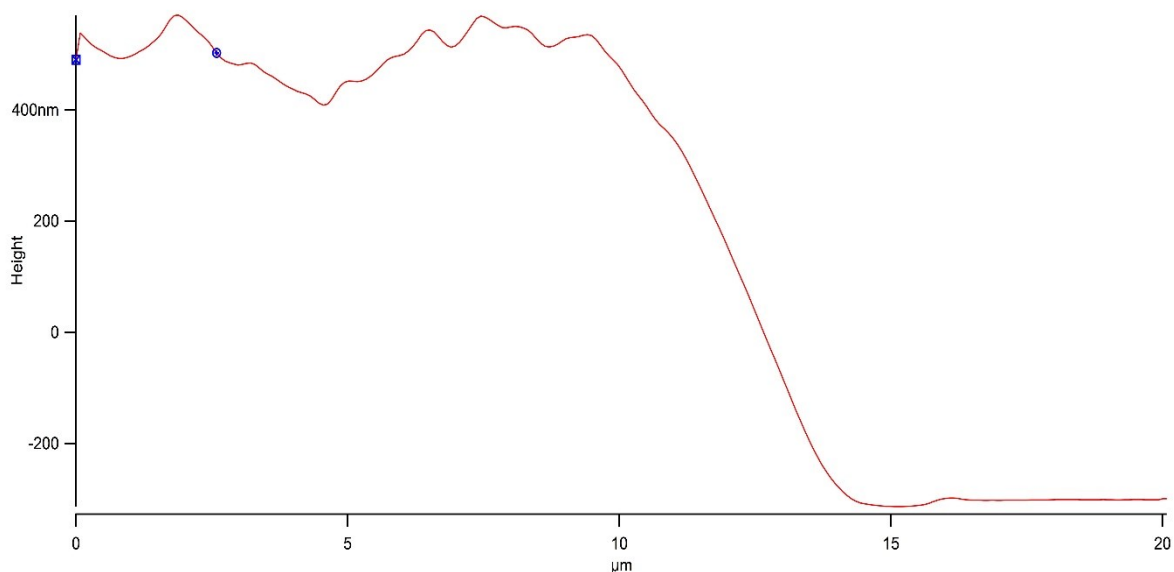


Figure 2.11 The height of the pNIPAm-*co*-APBA microgel layer on the QCM crystal before glucose was added. The height was 900 nm ( $\pm 40$  nm). The two blue points correspond to figure 2.10 A) two blue points.

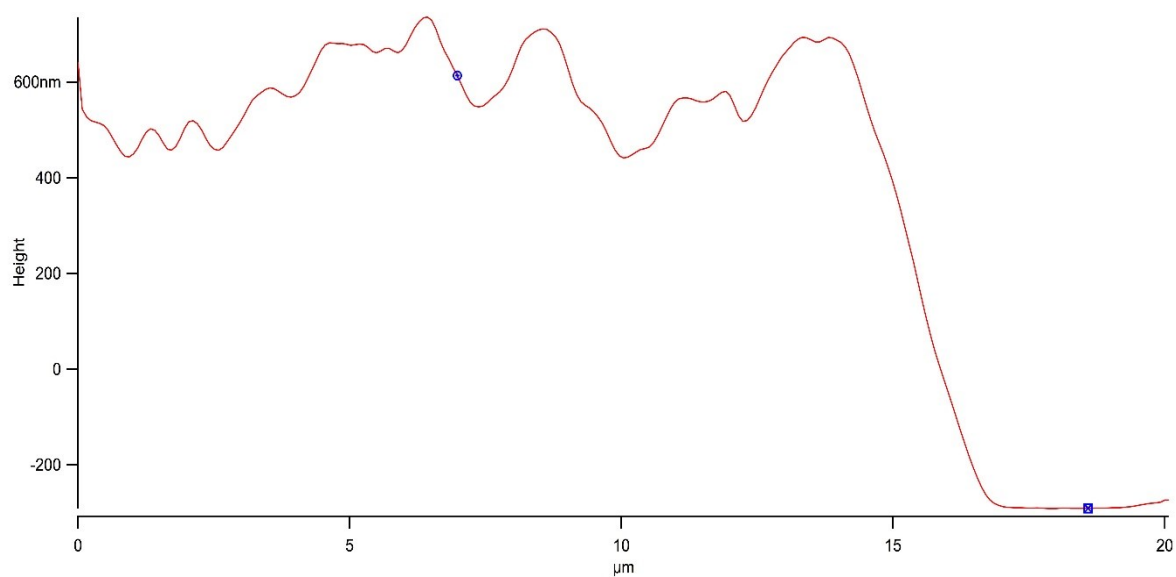


Figure 2.12 The height of the pNIPAm-*co*-APBA microgel layer on the QCM crystal 15 min after glucose was added. The height was 980 nm ( $\pm 100$  nm). The two blue points correspond to figure 2.10 B) blue points.

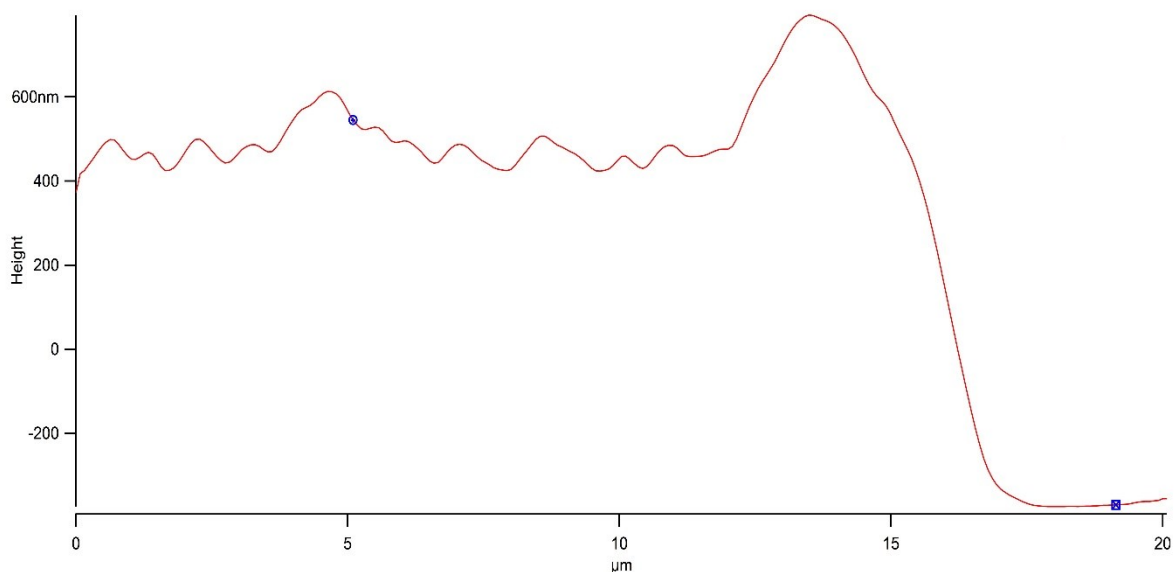


Figure 2.13 The height of the pNIPAm-*co*-APBA microgel layer on the QCM crystal after 30 min glucose addition. The height was 1100 nm ( $\pm 150$  nm). The two blue points correspond to figure 2.10 C) two blue points.

The pNIPAm-*co*-APBA microgel etalon exhibited a total change in (+) 200 nm. The initial height of the APBA etalon in pH 9.5 buffer solutions was 900 nm ( $\pm 40$  nm) but after 15 min and 30 min, it was 980 nm ( $\pm 100$  nm) and 1100 nm ( $\pm 150$  nm) respectively.

When the pNIPAm-*co*-APBA microgel was exposed to glucose, the glucose molecules bound to the charged boronic acid groups. This binding effect caused the microgel swelling and the microgel layer increased. The 0.199 g/dL glucose solution increases the microgel layer's thickness by 200 nm. Next, we look at how UV-VIS can be used to show how different glucose concentrations affect pNIPAm-*co*-APBA-based etalon microgels' glucose responsivity.

### ***Ultraviolet-Visible Spectroscopy (UV-VIS)***

We investigated the microgel's glucose responsivity to different glucose concentrations using UV-VIS. As the incident light passed through the microgel's solution in a cuvette, Mie scattering occurred in the microgel. Mie scattering is described as the scattering intensity functions for spherical particles with radii similar to or larger than the scattering wavelength. Mie scattering depends on the size of particles. Larger diameter particles show stronger

scattering if they have the same refractive index.<sup>180</sup> However, small particles with a high refractive index show stronger scattering than large particles with a low refractive index and vice versa. In general, increases in the refractive index induced by the collapsed pNIPAm will lead to an increase in the scattering/absorbance.<sup>177</sup> In keeping with this phenomenon, as the microgels in the water start to swell, they become capable of absorbing water in the cuvette. One explanation for this is that as more glucose bound to the microgels, the absorbance became close to that of DI water, which means that the microgels' refractive index was close to the DI water's refractive index. Also, this can be explained by Mie scattering: the larger diameter pNIPAm with a low refractive index has weak Mie scattering and transmittance increases, so absorbance decreases. Figure 2.14 shows the UV-VIS spectra.

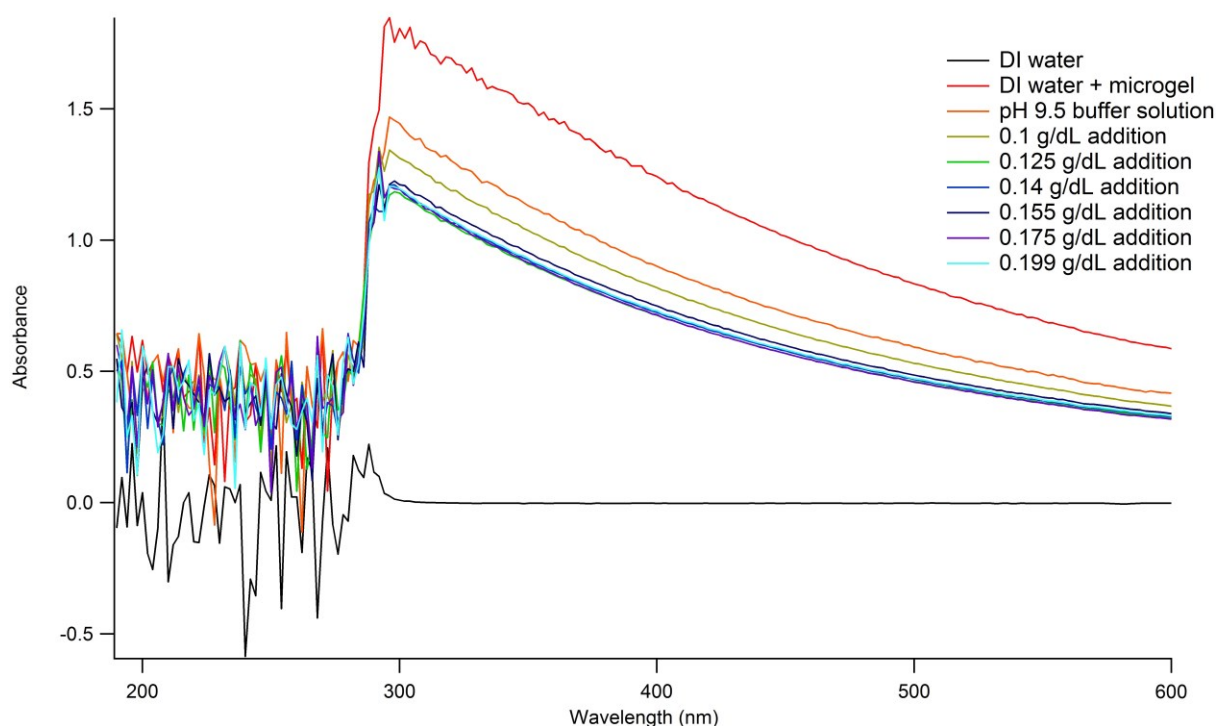


Figure 2.14 UV-VIS absorption spectra of pH 9.5 buffer solutions containing pNIPAm-*co*-APBA microgels before and after the addition of the indicated amount of glucose.

DI water absorbance was a blank and pNIPAm-*co*-APBA microgels in DI water are at the top of the spectrum (shown as red line in Figure 2.12). Hypothetically, the highest concentration of glucose buffer solution makes the largest pNIPAm-*co*-APBA microgel particles and

provides the lowest absorbance. However, we find a decrease in absorbance ranging from the microgel in DI water to the microgel with 0.14 g/dL of added glucose. After that point, the absorbance values were all the same in the rest of the glucose concentrations. In order to investigate more specifically, the variation of the absorbance at 300nm is shown in figure. 2.15.

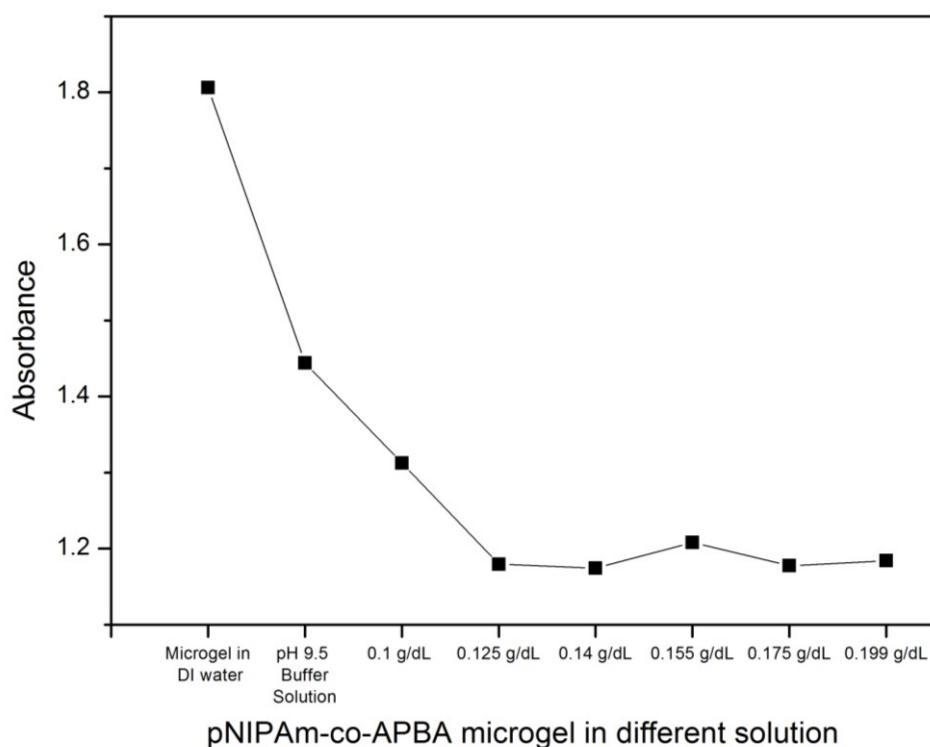


Figure 2.15 The variation of the absorbance at 300nm as a function of glucose addition.

This figure illustrates that the response showed a decreasing absorbance in the range of until 0.125 g/dL glucose buffer solution. After a 0.125 g/dL point, the QCM device did not show glucose sensitivity up to a 0.199 g/dL glucose concentration.

### ***The Amount of APBA in pNIPAm Microgels Affects Resonance Frequency***

We also investigated the way in which the amount of APBA in the microgels influenced the microgels' response to glucose addition. The more boronic acid groups in pNIPAm-co-APBA microgels, the better the glucose responsivity. Eventually, the sensitivity of glucose detection will be enhanced. The amount of APBA in pNIPAm microgels that affects resonance

frequency is performed by both pNIPAm-*co*- (10 % and 15 %) APBA microgels. Figure 2.16 shows the data.

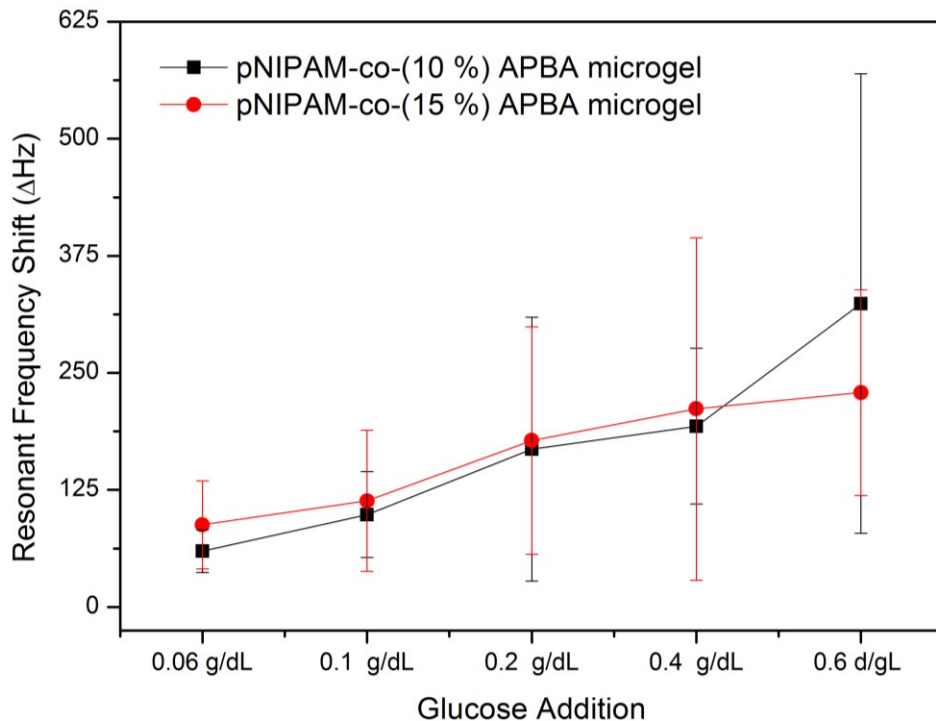


Figure 2.16 The resonant frequency shift of pNIPAm containing 10 % and 15 % APBA with different amounts of glucose added

We believe that more APBA in pNIPAm microgels show high resonant frequency shifts because microgels have more binding sites for glucose. The pNIPAm-*co*-(15 %) APBA microgels were expected to show a higher resonant frequency shift in all concentrations. However, in the entire range, there was no significant resonant frequency shift difference between 10 % and 15 % pNIPAm-*co*-APBA microgels. Furthermore, the error in both microgels was significant. Each glucose addition was conducted consecutively. Then the microgel was saturated at certain points. It was challenging to paint the microgel on the QCM crystal, as 15 % of APBA microgels dry fast and easily break the microgel layer. Because of painted microgel layer's stability, the conventional pNIPAm-*co*- (10 %) APBA microgel will be used in following sections and in Chapter 3. Also, in order to avoid obtaining high errors, it

is necessary to add strong acid to remove glucose molecules in the microgel network after each glucose concentration was added. As shown in figure 2.6, the charged boron atom is formed once the pH is over the  $pK_a$  of boronic acid. Therefore, the pH is much lower than the  $pK_a$  of boronic acid, the reverse reaction occurs, and glucose molecules are removed from the microgel network.

### ***Microgel Diameter Size Affects Glucose Responsiveness***

We investigated how the diameter of pNIPAm-*co*-APBA microgels influences their response to glucose addition. We assumed that the large particle microgel has a higher binding affinity between boronic acid groups and glucose molecules. It is expected that the largest particle pNIPAm-*co*-APBA microgels will give the highest resonant frequency shift. In contrast, the smallest particle will give lowest resonant frequency shift. Three different pNIPAm-*co*-APBA microgel particle sizes, in relation to their resonant frequency shift, are investigated under the same concentration of glucose buffer solution. Table 2.1 shows the results.

Table 2.1 The resonant frequency shift in different diameter pNIPAm-*co*-APBA microgels after 0.6 g/dL of glucose buffer solution (pH 9.5).

Particle	Large	Medium	Small
Size of Microgel	1728 nm ( $\pm 19$ nm)	524 nm ( $\pm 8$ nm)	225 nm ( $\pm 4$ nm)
Resonant frequency shift (Hz)	182.15	-3.65	-69.97

The microgel diameter determines how many glucose molecules can bind to boronic acid groups in APBA microgels. With this logic, medium- and small-sized microgels have a smaller amount of glucose molecules attached to them compared to large-sized microgels. Large-diameter APBA microgels showed a positive resonant frequency shift value after glucose addition. However, medium- and small-diameter APBA microgels showed a negative resonant frequency shift value. After glucose bound to a microgel, the medium and small particles were

saturated faster compared to the large particles. The faster saturation led to an increase in the viscosity of the microgels, a decrease in frequency and a negative resonant frequency shift value. This led us to conclude that the large-diameter APBA microgels are excellent candidates for glucose detection.

## **2.4 Conclusions**

Generally pNIPAm-*co*-APBA microgels are used for many glucose detection applications because boronic acid groups have glucose-binding properties.<sup>32,178</sup> Theoretically, we found that higher glucose concentration causes the pNIPAm-*co*-APBA to swell more. AFM measured the height of the microgel layer on the QCM crystal. We found that different glucose concentrations affected microgels' glucose sensitivity. To investigate the microgel's glucose sensitivity, we used UV/VIS spectrums, increasing the concentration of the glucose buffer solution in specific concentrations, ranging from 0.1 g/dL to 0.125 g/dL. Furthermore, between 10% and 15% APBA in a pNIPAm microgel did not show a significant difference in resonant frequency shifts. Since pNIPAm-*co*- (15 %) APBA microgel has stability issues when the coating is applied onto the QCM crystal, pNIPAm-*co*- (10 %) APBA microgels is more suitable for experiments. The diameter of the microgel affects the resonant frequency shift. Only large particle microgels show a positive resonant frequency shift. Medium and small particle microgels show negative resonant frequency shifts. In conclusion, our microgel-modified QCM device has been tailored to use large pNIPAm-*co*- (10 %) APBA microgels, because large particles are suitable for glucose detection.

## CHAPTER 3      MICROGEL MODIFIED QUARTZ CRYSTAL MICROBALANCES AS A GLUCOSE SENSOR

### 3.1 Introduction

In this chapter, we will discuss the performance of quartz crystal microbalances (QCM) that are modified with poly (N-isopropylacrylamide)-co-3-acrylamidophenylboronic acid (pNIPAm-*co*-APBA) microgels to detect glucose. In Chapter 2, we showed how the microgel layers respond to glucose, which was revealed using atomic force microscopy (AFM) and ultraviolet-visible spectroscopy (UV/VIS). This characterization helped us to obtain the accurate resonant frequency shift when the pNIPAm-*co*-APBA microgels detected glucose molecules. Also in Chapter 2, we showed that glucose responsivity is affected by the amount of APBA in a microgel, and the microgel's diameter. We found that large particles of pNIPAm-*co*-(10 %) APBA microgel enable the QCM to respond to glucose. In this chapter, we will discuss, in detail, the investigation of the performance of pNIPAm-*co*-APBA microgels' glucose selectivity and reproducible glucose detection.

We investigated the selectivity of glucose-sensing devices using sugars similar to glucose, but which contain diols. We then determined that the QCM-based devices can be reused multiple times to analyze the amount of glucose in a sample. Figure 2.6 in Chapter 2 shows the mechanism of glucose binding to boronic acid, a bond that is very strong at a high pH. That is, the binding of the glucose to APBA is favored when the pH is above the  $pK_a$  of boronic acid (8.2).<sup>94</sup> In this chapter, we introduce a method for reversing the reaction by exposing the microgel layers to a low pH solution. We hypothesize that this will allow the glucose to be removed from the APBA. Since the glucose/APBA binding mechanism is strongly favored at high pH, it is necessary to expose the microgels to strong acid for 1.5 h to remove the glucose molecules in the microgel.

As I pointed out in previous chapters, pNIPAm-based microgels have many advantages including low cost, and they can be easily used to fabricate sensor devices (i.e., etalons). By fabricating etalons on QCM devices, it is possible to generate novel glucose sensors that have an enhanced response to glucose.

## **3.2 Materials and Methods**

### ***Materials***

N-isopropylacrylamide was obtained from TCI (Portland, OR) and purified using recrystallization hexanes (ACS reagent grade, EMD, Gibbstown, NJ). N,N'-methylenebisacrylamide (BIS; 99 %), ammonium persulfate (APS; 98+ %),  $\alpha$ -D-glucose (ACS reagent), 3-(Acrylamido)phenylboronic acid (APBA, 98 %), sodium chloride, and sodium hydroxide were obtained from Sigma-Aldrich (Oakville, Ontario; Milwaukee, WI; and St. Louis, MO). Sodium bicarbonate ( $\text{NaHCO}_3$ ) and sodium carbonate ( $\text{Na}_2\text{CO}_3$ ) were obtained from Caledon Laboratories Ltd. (Rockville, Ontario). All deionized water was filtered to have a resistivity of 18.2 M $\Omega$  cm and was obtained from a Milli-Q Plus system from Millipore (Billerica, MA). Anhydrous ethanol was purchased from Commercial Alcohols (Brampton, Ontario).

### ***Instrumentation***

Microgel-coated QCM crystals as well as the etalon-coated devices were analyzed using a QCM-200 obtained from Stanford Research Systems (Sunnyvale, California). The crystal was placed into a specially designed holder, which allowed for a buffer solution of a given pH and temperature for constant flow over the crystal at a rate of 0.062 mL s<sup>-1</sup>. The flow was controlled by a FMI lab pump model RP-G150 (Oyster Bay, New York). The temperature was controlled by placing a beaker containing a buffer solution onto a Corning model PC-420D hotplate (Lowell, Massachusetts), and measured through a thermocouple that was placed in an

outlet tube. The buffer solution pH was measured with a Jenco model 6173 pH meter (San Diego, California).

### ***Preparation of pH 9.5 buffer solution***

A 5-mM pH 9 carbonate buffer was prepared by dissolving 0.76 g NaHCO<sub>3</sub> and 0.11 g Na<sub>2</sub>CO<sub>3</sub> in 2 L of deionized H<sub>2</sub>O in a volumetric flask. The pH of the resulting solution was 9.35, and so a few drops of sodium hydroxide were added to make a pH of 9.5.<sup>94</sup> The ionic strength of this buffer solution was 0.06 mM.

### ***pNIPAm-co-APBA microgels synthesis***

The pNIPAm-co-APBA microgels were synthesized using surfactant-free, free radical precipitation with NIPAm (85 %), BIS (5 %), and ABPA (10 %) as described in Chapter 2.<sup>110,116</sup> Briefly, 17.0 mmol of NIPAm monomer and 1.0 mmol of N,N- methylenebisacrylamide (BIS) as the crosslinker were added to a beaker with 100 mL of deionized water. The solution was stirred by a magnetic stirrer for about 30 min. After the reactants completely dissolved, the solution was filtered by a syringe through a 0.2 μm syringe filter into a 250 mL three-necked round bottom flask. The beaker was rinsed with an additional 15 mL of deionized water, which was also filtered by a syringe and added to the round-bottom flask. The gas inlet (needle), a reflux condenser, and a temperature probe were set up onto the round-bottom flask. In order to maintain an environment with a low O<sub>2</sub> concentration, N<sub>2</sub> gas was purged into the reaction solution while the solution was heated to 45 °C for 1.5 hour and stirred at 450 RPM. Immediately prior to initiation, 2.0 mmol of APBA were added to the solution with 5 mL of 0.078 M ammonium persulfate (APS, initiator) solution. The temperature of solution was then increased to 65 °C at a rate of 30 °C/h immediately following initiation, and the solution was allowed to react for four hours. After the reaction, the solution was allowed to cool down and was filtered through glass wool to remove large aggregate particles from the solution. The filtrate was diluted to 100 mL with deionized water and 35 mL of aliquots were transferred to

centrifuge tubes, and centrifuged at around 8500 relative centrifugal force for 1 h at 23 °C. The microgels were forced to the bottom of the centrifuge tube, and the supernatant solution was removed, and replaced with fresh DI water. Overall, the supernatant solution was centrifuged six times to remove leftover monomer and polymer chains from the microgel mixture. After the purification, the microgels were centrifuged once again, the supernatant was removed, leaving behind highly concentrated microgels at the bottom of the tube.

### ***Etalon Fabrication***

Etalons were fabricated as indicated in Chapter 2. The Au electrodes of the QCM were rinsed with a copious amount of anhydrous ethanol and dried with N<sub>2</sub> gas. A microgel solution (10 μL water:160 μL viscous microgel solution) was spread over the QCMs "large Au active electrode" using a pipette. The solution was allowed to dry for 30 min at 35 °C. After drying, the microgels that indirectly bound to the Au electrode were rinsed off with DI water, and the QCM crystal was immersed in DI water overnight at 35 °C. Following soaking, the crystal was further rinsed with DI water and dried with N<sub>2</sub> gas, which yielded a single microgel layer on the Au electrode. To generate the etalon, the QCM crystal was inserted into a Torr International Inc. (New Windsor, NY) thermal evaporation system model THEUPG. Two nm of Cr and 15 nm of Au were deposited only onto the Au-bound microgel layer at a rate of ~0.2 Ås<sup>-1</sup> and ~0.1 Ås<sup>-1</sup>, respectively. After application of this overlayer, the crystal was subsequently removed from the vacuum chamber and immersed in DI water overnight at 35 °C.

### ***Selectivity Performance***

Sucrose and galactose were used as interfering species to determine the selectivity of the devices for glucose. After pNIPAm-co-APBA microgels were painted on the QCM's gold electrode and the etalons completely fabricated, the crystal was placed into the QCM holder. One-hundred mL of buffer solution was transferred into four different beakers using a 100 mL glass pipette. Then, 0.11 g, 0.14 g, 0.175 g, and 0.199 g of α-D glucose were added to the each

beaker, respectively, and stirred for 10 min until dissolving completely. Each glucose buffer solution in a 100 mL beaker at 25 °C was introduced into the QCM holder via an inlet tube. An outlet tube of the holder was connected to the same beaker to recirculate the solution. The order of adding the glucose buffer solution was 0.11 g, 0.14 g, 0.175 g, and 0.199 g. The entire procedure described above was applied and repeated for sucrose and galactose.

During the selectivity performance, the QCM crystal was placed into the QCM holder. We did not take it out to rinse it or for the next addition. The entire protocol was consecutive. We could determine that the QCM device was completely rinsed and ready for the next addition after adding 0.1 M HCl solution and the pH 9.5 buffer solution, and when the resonant frequency ( $f$ ) reached a frequency similar to what it had been initially ( $f_i$ ).

### ***Reproducibility Performance***

The regeneration performance was investigated using the following protocol. The pNIPAm-co-APBA microgels were painted on the QCM's gold electrode to perfectly fabricate etalons, and the crystal was placed into the QCM holder. Glucose buffer solutions with different concentrations were prepared. One hundred mL of buffer solution were transferred into seven beakers using a glass pipette. Each of 0.05 g, 0.11 g, 0.125 g, 0.14 g, 0.155 g, 0.175 g and 0.199 g of  $\alpha$ -D glucose was added to each beaker, and stirred for 10 min until dissolving completely. Each glucose buffer solution in a 100 mL beaker at 25 °C was introduced into the QCM holder via an inlet tube. An outlet tube of the holder was connected to the same beaker to recirculate the solution. The initial resonant frequency was measured from the buffer solution without glucose. After the initial resonant frequency was measured, a 0.05 g/dL glucose buffer solution was added and we waited until the resonant frequency reached a plateau. After the plateau was reached, for 1.5 h, 0.1 M HCl solution (pH 3.0) was added to remove the glucose molecules and then 200 mL of the buffer solution (pH 9.5) were added again to make the initial resonant frequency. Once the resonant frequency reached a magnitude similar to that of the initial

frequency, a 0.05 g/dL buffer solution was added. This addition was repeated until the resonant frequency shift stabilized. The entire procedure was repeated for 0.11g/dL, 0.125 g/dL, 0.14 g/dL, 0.155 g/dL, 0.175 g/dL, and 0.199 g/dL glucose buffer solution, respectively. A new pNIPAm-co-APBA microgel based etalon crystal was used for each concentration.

This reproducibility protocol was as follows:

- i) pH 9.5 buffer solution was introduced to the microgels and resonant frequency ( $f_i$ ) was stabilized.
- ii) First addition of each concentration of glucose buffer solution was introduced to the microgels.
- iii) Resonant frequency shift occurred and eventually stabilized.
- iv) 0.1 M HCl was introduced to the microgels to remove glucose molecules.
- v) pH 9.5 buffer solution was introduced to the microgels to make initial resonant frequency ( $f_i$ ).
- vi) The next addition of each concentration of glucose buffer solution was introduced to the microgels and steps iii to vi were repeated until the resonant frequency shift ( $\Delta Hz$ ) stabilized.

### 3.3 Results and Discussion

A functioning microgel-based glucose sensor requires three features: 1) the microgels must show glucose responsivity; 2) they must have glucose selectivity; and 3) they must be regenerative. The Serpe group was able to demonstrate the glucose responsivity of pNIPAm-*co*-APBA microgels both visually and spectrally.<sup>94</sup> In the spectral sense, the etalon's reflectance peaks show a red shift, and the hydrodynamic diameter increases in response to glucose addition<sup>32</sup>. This leads to a visible color change from green to red.<sup>94</sup> In Chapter 2, the pNIPAm-*co*-APBA microgels-modified QCM showed glucose responsivity by increasing resonant frequency. In this chapter, we investigate two different features of microgels: glucose selectivity, and the reproducibility of glucose detection in our microgel-based device. These features enable pNIPAm-*co*-APBA microgels to be used as glucose sensors.

#### 3.3.1 Selectivity Performance

As detailed in Chapter 2, human blood contains not only glucose but other components, such as oxygen, uric acid, and ascorbic acid.<sup>181</sup> The glucose sensor should target glucose. To provide a more accurate diabetes diagnosis, it should have minimal interference with other components. There are several reasons to investigate glucose selectivity. One reason is to determine whether other sugars that have structures similar to glucose's (e.g., they contain diols such as galactose and fructose (Fig 3.1)), are capable of binding to the APBA microgels. By comparing the resonant frequency shifts of the three sugars, we can determine which sugar binds most strongly to the APBA-modified microgels.

The boronic acid-sugar interaction was first discovered in 1874 and demonstrated mechanistically in the 1940s as a reversible covalent interaction between the charged phenylboronic acid groups and cis-diol groups on polyols.<sup>182-185</sup>

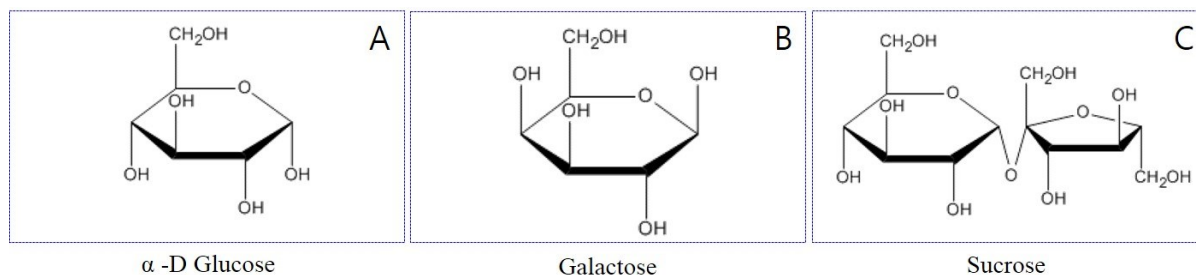


Figure 3.1 The Molecular Structure of A)  $\alpha$ -D Glucose, B) Galactose, and C) Sucrose.

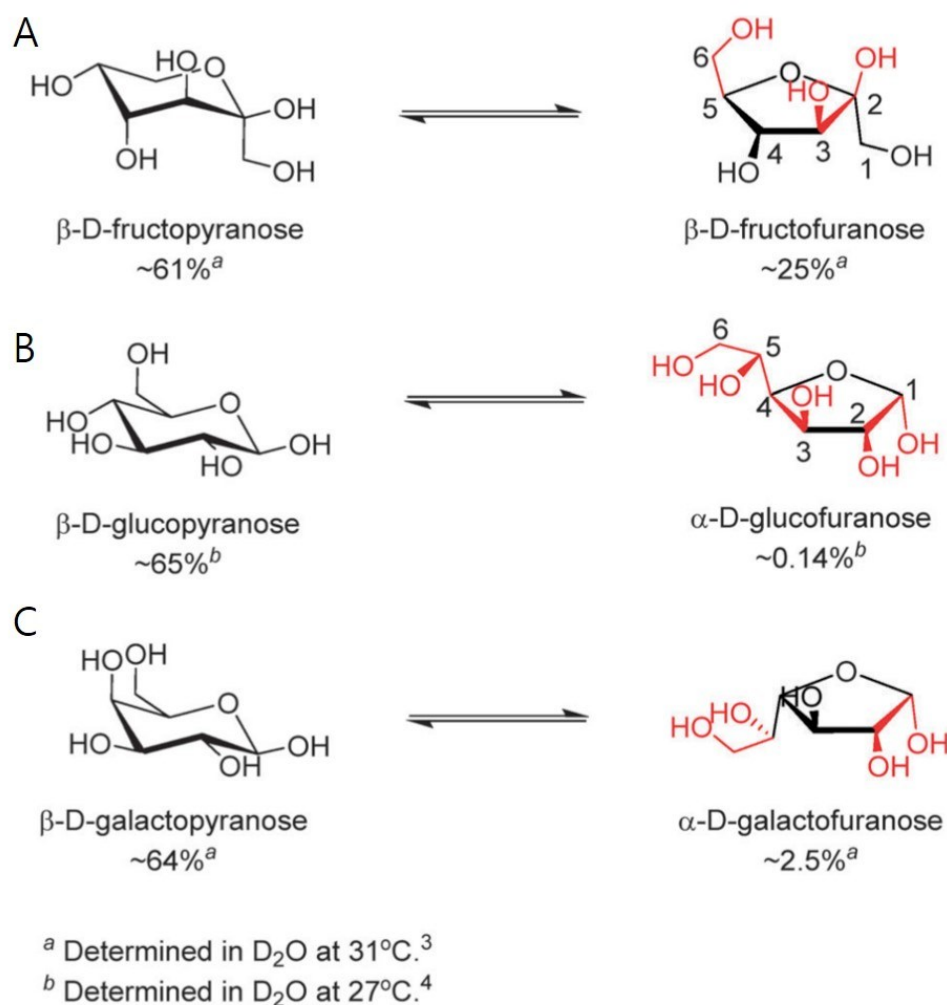


Figure 3.2 Equilibria between the favorable form (left) and the form that contains a syn-periplanar anomeric hydroxyl pair (right) of D-fructose A), D-glucose B) and D-galactose C). Highlighting in red indicates the potential boronic acid-binding sites. Positions for hydroxyl groups are numbered in  $\beta$ -D-fructofuranose and  $\alpha$ -D-glucofuranose. Reprinted from <sup>185</sup>. Copyright © 2013. Published by The Royal Society of Chemistry.

The binding affinity of phenylboronic acids with monosaccharides were observed in the following order: fructose > galactose > mannose > glucose.<sup>183</sup> The Wu et al. showed that carbohydrates exist in two forms in water: dominant and less dominant. The less dominant form contains syn-periplanar hydroxyl groups. The more syn-periplanar forms that a sugar has, the better its binding affinity with boronic acid. Fructose had the highest syn-periplanar form in D<sub>2</sub>O (25 %), galactose was 2.5 %, and glucose was 0.14 % (figure 3.2).<sup>185</sup> The monosaccharide-based sensors performed poorly because carbohydrates lack the syn-periplanar form in D<sub>2</sub>O. Although the lack of the syn-periplanar sugar form is a drawback of monosaccharide-based sensors, a multivalent ligand system provides a compensatory mechanism. B-O-C bonds are monovalent, but the interaction between a single boronic acid and diol is divalent because there are two B-O-C bonds between boronic acid and the diol. Generally, a single boronic acid has two or three B-O-C bonds as a valence. The fructose isomer,  $\beta$ -D-fructofuranose, uses a boronic acid binding as a monovalent ligand, while  $\alpha$ -D-glucofuranose is a divalent ligand able to bind two boronic acid species at the 1,2 and 3,5,6 positions (Fig 3.2 B).<sup>185</sup> Although two boronic acid moieties can generally bind to fructose in fructose's  $\beta$ -pyranose form, this bond was observed only with excess fructose or at a high concentration of boronic acid.<sup>186</sup> Unfortunately, this condition is not compatible with glucose biosensor use. The difference in the number of valences for glucose and fructose has aided in the development of boronic acid-based sensors because both diboronic and polyboronic acid systems (boronic acid based polymer) offer enhanced glucose selectivity, which allows the acid to bind more strongly with glucose than with fructose. Moreover, triggering the number of valences for glucose allows more enhanced selectivity for glucose in boronic-acid based sensors.<sup>185-186</sup>

It is expected that the pNIPAm-*co*-APBA-microgels-etalon device will be based on Wu's study<sup>185</sup> and is highly selective to glucose. The pNIPAm-*co*-APBA microgels exhibit a resonant frequency shift in response to glucose, sucrose, and galactose. Compared to the respective

resonant frequency shift ( $\Delta\text{Hz}$ ), we can determine that the sugar, which has highest resonant frequency shift, has the highest selectivity for pNIPAm-*co*-APBA microgels. As each buffer has the same ionic strength, we assume that the ions are not influencing the microgels. Figure 3.3 shows the resonant frequency shift corresponding to the increased concentration of each sugar (glucose, sucrose, and galactose) in the buffer solution.

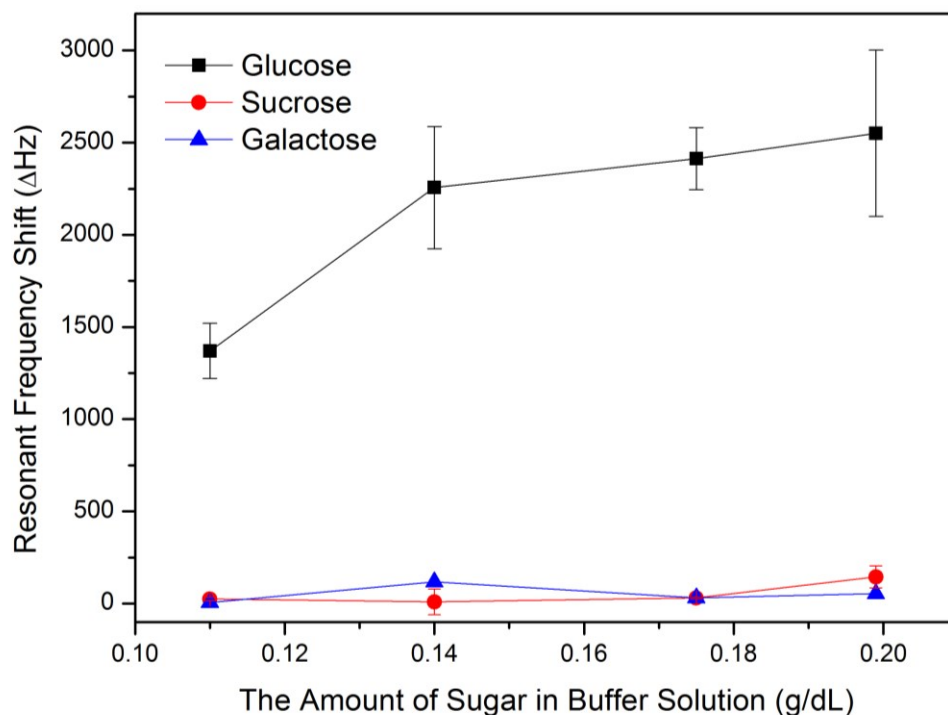


Figure 3.3 The selectivity performance in pNIPAm-*co*-APBA microgels. Glucose-, sucrose-, and galactose-responsive measurement by resonant frequency shift. Each point indicates 0.11 g/dL, 0.14 g/dL, 0.175 g/dL, and 0.199 g/dL (left to right) of glucose buffer solution (pH 9.5) introduced into microgels.

The pNIPAm-*co*-APBA-microgels-based QCM shows different resonant frequency shifts by different sugar concentrations of the buffer solution. Only glucose showed an increasing resonant frequency shift. Sucrose and galactose showed a stabilized resonant frequency shift. The fact that pNIPAm-*co*-APBA microgels contain “polyboronic” acid that shows enhanced glucose selectivity suggests that the pNIPAm-*co*-APBA-microgels-etalon-based device is

highly selective to glucose. This device's high glucose selectivity means that we can offer a new platform: a pNIPAm-co-APBA microgel-based glucose sensor.

### 3.3.2 Reproducibility Performance

The purpose of this investigation was to show that a pNIPAm-co-APBA-microgels-etalon-modified QCM device can provide consistent results after multiple uses. The reproducibility performance demonstrated how many times the microgel-modified QCM device could show glucose responsivity. Repeated addition of each concentration of the glucose buffer solution was conducted until the resonant frequency shift was stable. The stable frequency signaled that the microgels were saturated, and no more glucose molecules could bind to them. After the glucose buffer solution (pH 9.5) was introduced into the QCM holder, the glucose molecules began binding to boronic acid groups in pNIPAm-co-APBA microgels. The resonant frequency then increased due to the microgels' swelling. After the glucose molecules were removed from the microgel by adding 0.1 M HCl, the rinsed microgels on the QCM device showed a number of reproducible resonant frequency shifts. This means that the microgels were able to be reused multiple times for glucose detection. Each error was calculated using the standard deviation from the average of each glucose concentration's resonant frequency shift. Figure 3.4 shows the resonant frequency shift recorded after the addition of 0.05 g/dL and 0.11 g/dL of glucose buffer solution.

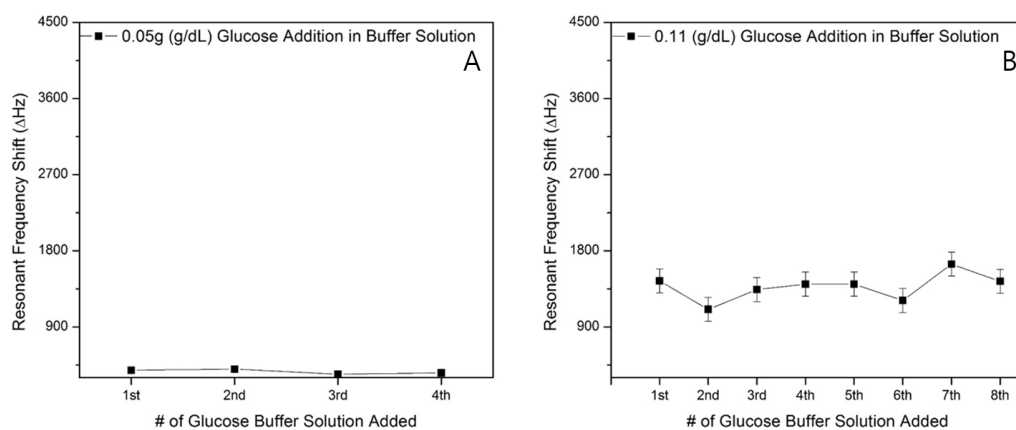


Figure 3.4 The resonant frequency shift for each A) 0.05 g/dL and B) 0.11 g/dL of glucose buffer solution (pH 9.5) added at 25 °C.

Each 0.05 g/dL of glucose buffer solution added showed a range of 345 Hz ~400 Hz. The average is 370 Hz ( $\pm 20$  Hz). The 0.11 g/dL of glucose buffer solution provides a higher resonant frequency shift than does 0.05 g/dL. The pNIPAm-*co*-APBA microgels showed glucose responsivity until the eighth addition of the glucose buffer solution. The resonant frequency shift showed a range of 1100 Hz ~ 1650 Hz and an average shift of 1380 Hz ( $\pm 140$  Hz). When we added 0.11 g/dL of glucose buffer solution, the resonant frequency shift increased four times more than it did when we added 0.05 g/dL of solution. The 0.05 g/dL and 0.11 g/dL additions resulted in reproducible resonant frequency shifts that were four and eight times, respectively.

After the 0.125 g/dL and 0.14 g/dL additions of glucose buffer solution, both resonant frequency shifts increased more than when 0.05 and 0.11 g/dL were added. Figure 3.5 shows the resonant frequency shifts for both concentrations.

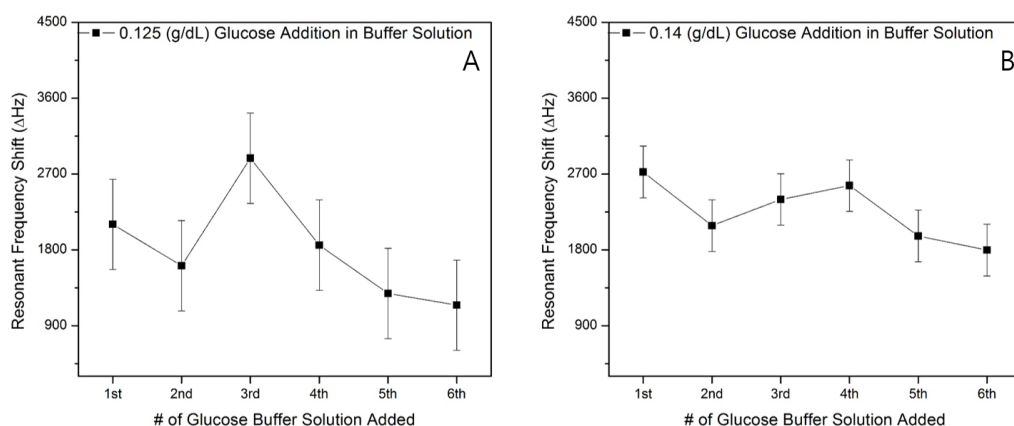


Figure 3.5 The resonant frequency shift for each A) 0.125 g/dL and B) 0.140 g/dL of glucose buffer solution (pH 9.5) added at 25 °C.

The 0.125 g/dL and 0.140 g/dL glucose additions reproduced the resonant frequency shift six times. The resonant frequency shifts ranged from 1250 Hz ~ 2750 Hz with an average of 1800 Hz ( $\pm 540$  Hz), and 1750 Hz ~ 2750 Hz with an average of 2300 Hz ( $\pm 310$  Hz) in the 0.125 and 0.14 g/dL glucose buffer solution, respectively.

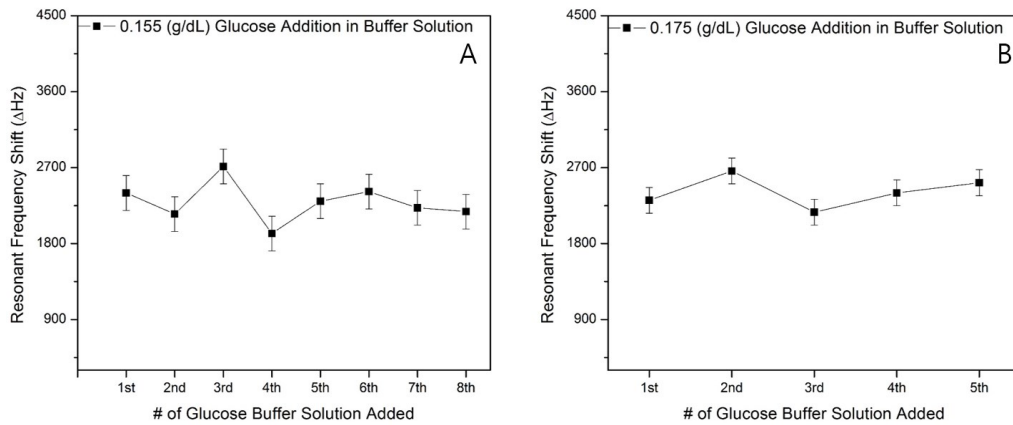


Figure 3.6 The resonant frequency shift for each A) 0.155 g/dL and B) 0.175 g/dL of glucose buffer solution (pH 9.5) added at 25 °C.

The glucose concentration increased again in 0.155 g/dL and 0.175 g/dL. With the same addition protocol as before, the magnitude of the resonant frequency shift increased and 0.155 g/dL and 0.175 g/dL glucose addition reproduced the resonant frequency shift eight times and five times, respectively. Figure 3.6 shows both concentration glucose buffer solutions added to pNIPAm-co-APBA microgels and their resonant frequency shifts. The resonant frequency shift increased in a range of 2000 Hz ~ 2700 Hz with an average of 2300 Hz ( $\pm$ 210 Hz) in the 0.155 g/dL buffer solution, and in a range of 2200 Hz ~ 2700 Hz with an average of 2400 Hz ( $\pm$ 150 Hz) in the 0.175 g/dL buffer solution.

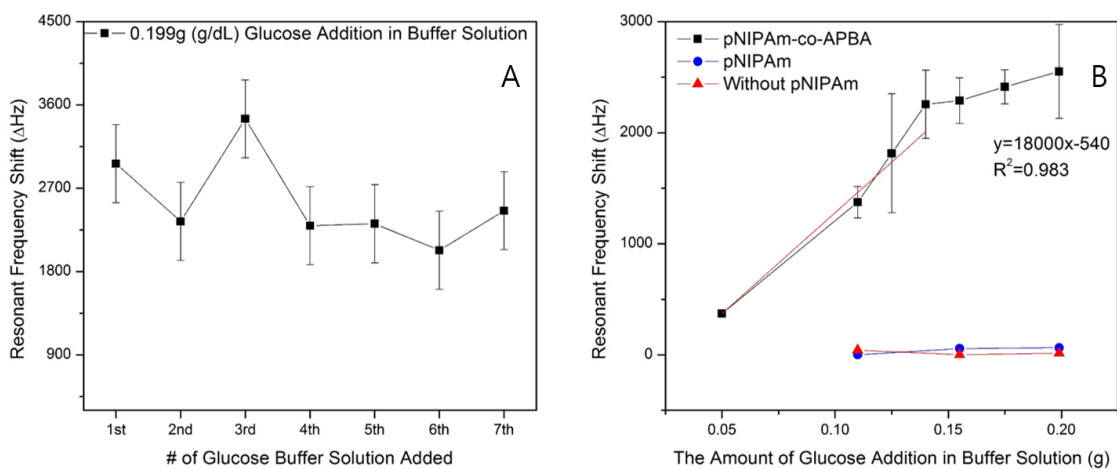


Figure 3.7 The resonant frequency shift for each A) 0.199 g/dL of glucose buffer solution (pH 9.5) added and B) The average resonant frequency shift in all ranges of glucose added to the buffer solution at 25 °C

The last addition was 0.199 g/dL of glucose buffer solution. The entire resonant frequency shift for each glucose concentration is shown in Fig 3.7 A). The higher concentration of glucose buffer solution leads to the lowest viscosity and greatest swelling in the pNIPAm-co-APBA microgels. This promotes the QCM oscillation and increases the resonant frequency shifts.<sup>57</sup> Adding 0.199 g/dL of a glucose buffer solution shows the resonant frequency shift in a range of 2000 Hz ~ 3400 Hz with an average of 260 Hz ( $\pm 420$  Hz). In figure 3.7 B), the 0.05 g/dL to 0.14 g/dL range showed a linear relationship between the resonant frequency shift and glucose concentration with a 0.983 R<sup>2</sup> value. After the 0.14 g/dL point, the results were the same.

It was challenging to obtain a low standard deviation in reproducible resonant frequency shifts. That is because during the adding acid protocol to remove glucose molecules, we cannot determine that the glucose molecules are completely removed from the microgels' network, which leads to an inaccurate resonant frequency shift and, consequently, a high standard deviation. The overall results are shown in Table 3.1.

Table 3.1 The resonant frequency shift in different glucose concentrations and the reproducibility of each concentration

Concentration (g/dL)	Resonant frequency shift ( $\Delta$ Hz)	The number of times microgel can be reproduced
$5.00 \times 10^{-2}$	372 ( $\pm 21$ )	4
$1.10 \times 10^{-1}$	1380 ( $\pm 140$ )	8
$1.25 \times 10^{-1}$	1820 ( $\pm 540$ )	6
$1.40 \times 10^{-1}$	2260 ( $\pm 310$ )	6
$1.55 \times 10^{-1}$	2290 ( $\pm 210$ )	8
$1.75 \times 10^{-1}$	2410 ( $\pm 150$ )	5
$1.99 \times 10^{-1}$	2550 ( $\pm 420$ )	7

Table 3.1 showed that the resonant frequency shift increases concurrently with increases in the glucose concentration. Also, our microgel-modified QCM can be reused at least six times for glucose detection. Also, the QCM device shows a linear relationship ranging from 0.05

g/dL to 0.14 g/dL between the glucose concentration and resonant frequency shift. The linear relationship in those ranges can be explained by equation 10, below.

$$y = 18000 (\pm 1400)x - 540 (\pm 70)$$

The previous glucose-responsive pNIPAm-based microgel studies Equation 10 demonstrated that the hydrodynamic radius of the microgels' ( $R_h$ ) value increases dramatically as the glucose concentration increases.<sup>37,53</sup> Additionally, in the pNIPAm-co-APBA microgel-etalon device, when glucose binds to the microgel, the resultant swelling increases the thickness of the microgel layer, which is between the two Au layers.<sup>37,53</sup> Through the selectivity and reproducibility performances, our microgel-based QCM device shows glucose selectivity and is reusable for glucose detection.

### 3.4 Conclusions

The pNIPAm-co-APBA-microgel-etalon-modified QCM device shows great performance for glucose detection. Using a binding mechanism between boronic acid groups and glucose molecules turns microgels into glucose-responsive material. The presence of boronic acid groups in the microgels shows a higher selectivity to glucose than to other carbohydrates such as sucrose and galactose. Also, this microgel-modified QCM device shows reproducible resonant frequency shifts. To obtain accurate resonant frequency shifts during QCM device regeneration, it is necessary to remove the glucose molecules from the microgels. In order to observe consistency in the resonant frequency shifts, it is necessary to develop a rinsing protocol. The microgel-modified QCM device can be used for glucose detection at least six times. Their inexpensive material, specific analyte selectivity, and reusable properties make pNIPAm microgels a new platform and promising material for biosensing applications.

## CONCLUSIONS

Chapter 1 provided a general concept of stimuli-responsive polymers and introduced pNIPAm microgels. The chapter showed how pNIPAm-based microgels with different comonomers show stimuli responsivity, and that etalon fabrication provides enhanced sensitivity of stimuli in the microgel system. The chapter introduced a QCM-based sensor that functions by using changes in the mass of coating material on the QCM crystal.

Chapter 2 showed that pNIPAm with 3-aminophenylboronic acid (APBA) microgels are glucose-responsive. The boronic acid groups in pNIPAm microgels were able to bind to diols in glucose. Several methods were suggested to homogeneously coat the microgel on QCM crystal, but we did not find a better way to do this. Also, to find an enhanced glucose sensitivity, we tested the amount of APBA in microgels and the different diameters of the microgels to see how they affected the resonant frequency shifts. We determined that 10% of a pNIPAm-*co*-APBA microgel with a large diameter (1727.5 nm) was the appropriate microgel for glucose detection.

In Chapter 3, we looked at the performances of pNIPAm-*co*-APBA-microgels-based-etalon QCM device glucose selectivity and reproducible resonant frequency shift. The QCM device reproduced resonant frequency shifts multiple times with glucose addition and was highly selective to glucose and not to other sugars such as sucrose and galactose. As a result of both performances, the relationship between glucose concentration and the resonant frequency shift showed a linear trend with a 0.983  $r^2$  value in the range of 0.05 g/dL to 0.14 g/dL.

## FUTURE DIRECTION

As discussed in Chapter 2, a poly (N-isopropylacrylamide)-*co*-3-(acrylamido) phenylboronic acid microgel (pNIPAm-*co*-APBA) showed glucose sensitivity. Chapter 2 showed how the microgel system provides enhanced glucose sensitivity. It also showed that the resonant frequency shift is easily affected by surface conditions on a quartz crystal microbalance (QCM) crystal. To obtain accurate glucose sensitivity using resonant frequency, it is also necessary to further investigate coating a microgel monolayer on QCM crystal. To demonstrate a coated microgel layer on the QCM crystal, it is necessary to take scanning electron microscope or transmission electron microscope images of the microgel layer on the QCM crystal. Furthermore, the way in which different glucose concentrations affect microgels' glucose responsivity by ultraviolet-visible spectroscopy needs to be very specific. The UV-VIS results showed decreased absorbance in specific glucose concentrations. However, after 0.14 g/dL glucose was added, the UV-VIS results did not show any glucose sensitivity. This means that we need to investigate what happens when much higher glucose concentrations are added, and how UV-VIS will show the absorbance.

Chapter 3 examined pNIPAm-*co*-APBA microgel's glucose selectivity and reproducible resonant frequency shift. Sucrose is a disaccharide, so we also need to use the other common monosaccharide, fructose, for glucose selectivity. This will allow us to compare glucose selectivity in only monosaccharides. Also, other interference species, such as different ionic strength and proteins in blood, affect resonant frequency shifts. After we find all of the interference species effects, the QCM device could be more precise and accurate.

During the reproducibility performance, one QCM crystal measured the resonant frequency shift for one concentration. Overall, seven different QCM crystals were used for seven different glucose concentrations. During the measurement of resonant frequency, the

QCM crystal was in the QCM holder and was not taken out. The results contained huge errors, and it is necessary to investigate the source of those errors. Each glucose concentration was measured by several different QCM crystals to obtain their average number of reproducibility.

It is also necessary to learn how many times the microgel-modified QCM device is reusable for each concentration. The data we had been collecting until the resonant frequency shifts stabilized had been useful data. After the shifts stabilized, the data generated was not useful. The question is, had we resumed adding glucose, might we once again have been able to generate useful data? It is important, therefore, that we define the criteria of reusability of our QCM device for glucose detection. Doing so will provide the answer to that question, and ensure that our device is reliable. Defining the criteria of reusability of our QCM device for glucose detection might provide the answer to that question. Once we define that criteria, our device can be considered reliable.

## REFERENCES

1. Adhikari, B.; Majumdar, S., Polymers in sensor applications. *Progress in Polymer Science* **2004**, *29* (7), 699-766.
2. Wang, X.; Uchiyama, S., *Polymers for Biosensors Construction*. 2013.
3. Park, M.; Tsai, S.-L.; Chen, W., Microbial Biosensors: Engineered Microorganisms as the Sensing Machinery. *Sensors (Basel, Switzerland)* **2013**, *13* (5), 5777-5795.
4. Newman, J.; Setford, S., Enzymatic biosensors. *Mol Biotechnol* **2006**, *32* (3), 249-268.
5. Sadana, A., Antigen-Antibody Binding Kinetics for Biosensors: The Fractal Dimension and the Binding Rate Coefficient. *Biotechnology Progress* **1995**, *11* (1), 50-57.
6. Janata, J.; Bezegh, A., CHEMICAL SENSORS. *Anal. Chem.* **1988**, *60* (12), R62-R74.
7. Arlett, J. L.; Myers, E. B.; Roukes, M. L., Comparative advantages of mechanical biosensors. *Nature nanotechnology* **2011**, *6* (4), 203-215.
8. Fernández-Sánchez, C.; McNeil, C. J.; Rawson, K.; Nilsson, O., Disposable Noncompetitive Immunosensor for Free and Total Prostate-Specific Antigen Based on Capacitance Measurement. *Anal. Chem.* **2004**, *76* (19), 5649-5656.
9. Lee, L.; Nordman, E.; Johnson, M.; Oldham, M., A Low-Cost, High-Performance System for Fluorescence Lateral Flow Assays. *Biosensors* **2013**, *3* (4), 360.
10. Sajid, M.; Kawde, A.-N.; Daud, M., Designs, formats and applications of lateral flow assay: A literature review. *Journal of Saudi Chemical Society*.
11. Perry, e. a., *Enzyme-Linked Immunosorbent Assay (ELISA)*. Sinauer Associates: 2002; Vol. 1st Edition.
12. Rich, R. L.; Myszka, D. G., Advances in surface plasmon resonance biosensor analysis. *Current Opinion in Biotechnology* **2000**, *11* (1), 54-61.
13. Markey, F., What is SPR anyway. *BIA journal* **1999**, *6*, 14-17.

14. Madeira, A.; Vikeved, E.; Nilsson, A.; Sjögren, B.; Andrén, P. E.; Svenningsson, P., Identification of Protein-Protein Interactions by Surface Plasmon Resonance followed by Mass Spectrometry. In *Current Protocols in Protein Science*, John Wiley & Sons, Inc.: 2001.
15. Teh, H. F.; Peh, W. Y. X.; Su, X.; Thomsen, J. S., Characterization of Protein–DNA Interactions Using Surface Plasmon Resonance Spectroscopy with Various Assay Schemes. *Biochemistry* **2007**, *46* (8), 2127-2135.
16. Salamon, Z.; Cowell, S.; Varga, E.; Yamamura, H. I.; Hruby, V. J.; Tollin, G., Plasmon Resonance Studies of Agonist/Antagonist Binding to the Human  $\delta$ -Opioid Receptor: New Structural Insights into Receptor-Ligand Interactions. *Biophysical Journal* **2000**, *79* (5), 2463-2474.
17. Geitmann, M.; Danielson, U. H., Studies of substrate-induced conformational changes in human cytomegalovirus protease using optical biosensor technology. *Analytical Biochemistry* **2004**, *332* (2), 203-214.
18. Ruummele, J. A.; Hall, W. P.; Ruvuna, L. K.; Van Duyne, R. P., A Localized Surface Plasmon Resonance Imaging Instrument for Multiplexed Biosensing. *Anal. Chem.* **2013**, *85* (9), 4560-4566.
19. Haes, A. J.; Hall, W. P.; Chang, L.; Klein, W. L.; Van Duyne, R. P., A Localized Surface Plasmon Resonance Biosensor: First Steps toward an Assay for Alzheimer's Disease. *Nano Letters* **2004**, *4* (6), 1029-1034.
20. Nguyen, H. H.; Park, J.; Kang, S.; Kim, M., Surface Plasmon Resonance: A Versatile Technique for Biosensor Applications. *Sensors (Basel, Switzerland)* **2015**, *15* (5), 10481-10510.
21. Kim, M.; Jung, S. O.; Park, K.; Jeong, E.-J.; Joung, H.-A.; Kim, T.-H.; Seol, D.-W.; Chung, B. H., Detection of Bax protein conformational change using a surface plasmon resonance imaging-based antibody chip. *Biochemical and Biophysical Research Communications* **2005**, *338* (4), 1834-1838.

22. Uludag, Y.; Tothill, I. E., Cancer Biomarker Detection in Serum Samples Using Surface Plasmon Resonance and Quartz Crystal Microbalance Sensors with Nanoparticle Signal Amplification. *Anal. Chem.* **2012**, *84* (14), 5898-5904.
23. Murphy, L., Biosensors and bioelectrochemistry. *Current Opinion in Chemical Biology* **2006**, *10* (2), 177-184.
24. Cabane, E.; Zhang, X.; Langowska, K.; Palivan, C.; Meier, W., Stimuli-Responsive Polymers and Their Applications in Nanomedicine. *Biointerphases* **2012**, *7* (1-4), 1-27.
25. Zhang, L.; Xu, T.; Lin, Z., Controlled release of ionic drug through the positively charged temperature-responsive membranes. *Journal of Membrane Science* **2006**, *281* (1-2), 491-499.
26. Hu, J.; Liu, S., Responsive Polymers for Detection and Sensing Applications: Current Status and Future Developments. *Macromolecules* **2010**, *43* (20), 8315-8330.
27. Wang, W.; Chen, C.; Qian, M.; Zhao, X. S., Aptamer biosensor for protein detection using gold nanoparticles. *Analytical Biochemistry* **2008**, *373* (2), 213-219.
28. Islam, M.; Ahiabu, A.; Li, X.; Serpe, M., Poly (N-isopropylacrylamide) Microgel-Based Optical Devices for Sensing and Biosensing. *Sensors* **2014**, *14* (5), 8984.
29. Ward, M. A.; Georgiou, T. K., Thermoresponsive Polymers for Biomedical Applications. *Polymers (20734360)* **2011**, *3* (3), 1215-1242.
30. Dissemond, J.; Witthoff, M.; Brauns, T. C.; Haberer, D.; Goos, M., pH-Wert des Milieus chronischer Wunden. *Hautarzt* **2003**, *54* (10), 959-965.
31. Schmaljohann, D., Thermo- and pH-responsive polymers in drug delivery. *Advanced Drug Delivery Reviews* **2006**, *58* (15), 1655-1670.
32. Hoare, T.; Pelton, R., Engineering Glucose Swelling Responses in Poly(N-isopropylacrylamide)-Based Microgels. *Macromolecules* **2007**, *40* (3), 670-678.
33. Qiu, Y.; Park, K., Environment-sensitive hydrogels for drug delivery. *Advanced Drug Delivery Reviews* **2001**, *53* (3), 321-339.

34. Yao, K.; Tang, C.; Zhang, J.; Bunyard, C., Degradable and salt-responsive random copolymers. *Polymer Chemistry* **2013**, *4* (3), 528-535.
35. Priya, B.; Viness, P.; Yahya, E. C.; Lisa, C. d. T., Stimuli-responsive polymers and their applications in drug delivery. *Biomedical Materials* **2009**, *4* (2), 022001.
36. Suzuki, Y.; Tanihara, M.; Nishimura, Y.; Suzuki, K.; Kakimaru, Y.; Shimizu, Y., A new drug delivery system with controlled release of antibiotic only in the presence of infection. *Journal of Biomedical Materials Research* **1998**, *42* (1), 112-116.
37. Miyata, T.; Jikihara, A.; Nakamae, K.; Hoffman, A. S., Preparation of poly(2-glucosyloxyethyl methacrylate)-concanavalin A complex hydrogel and its glucose-sensitivity. *Macromolecular Chemistry and Physics* **1996**, *197* (3), 1135-1146.
38. Ulijn, R. V.; Bibi, N.; Jayawarna, V.; Thornton, P. D.; Todd, S. J.; Mart, R. J.; Smith, A. M.; Gough, J. E., Bioresponsive hydrogels. *Materials Today* **2007**, *10* (4), 40-48.
39. Fischel-Ghodsian, F.; Brown, L.; Mathiowitz, E.; Brandenburg, D.; Langer, R., Enzymatically controlled drug delivery. *Proceedings of the National Academy of Sciences of the United States of America* **1988**, *85* (7), 2403-2406.
40. Kim, H.; Cohen, R. E.; Hammond, P. T.; Irvine, D. J., Live Lymphocyte Arrays for Biosensing. *Advanced Functional Materials* **2006**, *16* (10), 1313-1323.
41. Thorogate, R.; Moreira, J. C. S.; Jickells, S.; Miele, M. M. P.; Daniel, B., A novel fluorescence-based method in forensic science for the detection of blood in situ. *Forensic Science International: Genetics* **2** (4), 363-371.
42. Abu-Salah, K. M.; Zourob, M. M.; Mouffouk, F.; Alrokayan, S. A.; Alaamery, M. A.; Ansari, A. A., DNA-Based Nanobiosensors as an Emerging Platform for Detection of Disease. *Sensors (Basel, Switzerland)* **2015**, *15* (6), 14539-14568.
43. Kawai, M.; Matsutera, E.; Kanda, H.; Yamaguchi, N.; Tani, K.; Nasu, M., 16S Ribosomal DNA-Based Analysis of Bacterial Diversity in Purified Water Used in Pharmaceutical

Manufacturing Processes by PCR and Denaturing Gradient Gel Electrophoresis. *Applied and Environmental Microbiology* **2002**, *68* (2), 699-704.

44. Ali, M. M.; Su, S.; Filipe, C. D. M.; Pelton, R.; Li, Y., Enzymatic manipulations of DNA oligonucleotides on microgel: towards development of DNA-microgel bioassays. *Chemical Communications* **2007**, (43), 4459-4461.

45. Zhao, Y.; Zhao, X.; Tang, B.; Xu, W.; Li, J.; Hu, J.; Gu, Z., Quantum-Dot-Tagged Bioresponsive Hydrogel Suspension Array for Multiplex Label-Free DNA Detection. *Advanced Functional Materials* **2010**, *20* (6), 976-982.

46. Miyata, T.; Asami, N.; Urugami, T., A reversibly antigen-responsive hydrogel. *Nature* **1999**, *399* (6738), 766-769.

47. Li, X.; Serpe, M. J., Bioresponsive Hydrogels and Microgels. In *Chemistry of Bioconjugates*, John Wiley & Sons, Inc.: 2014; pp 370-386.

48. Stayton, P. S.; Shimoboji, T.; Long, C.; Chilkoti, A.; Ghen, G.; Harris, J. M.; Hoffman, A. S., Control of protein-ligand recognition using a stimuli-responsive polymer. *Nature* **1995**, *378* (6556), 472-474.

49. Langer, R.; Vacanti, J., Tissue engineering. *Science* **1993**, *260* (5110), 920-926.

50. Shoichet, M. S., Polymer Scaffolds for Biomaterials Applications. *Macromolecules* **2010**, *43* (2), 581-591.

51. Yamato, M.; Okano, T., Cell sheet engineering. *Materials Today* **2004**, *7* (5), 42-47.

52. Yamada, N.; Okano, T.; Sakai, H.; Karikusa, F.; Sawasaki, Y.; Sakurai, Y., Thermo-responsive polymeric surfaces; control of attachment and detachment of cultured cells. *Die Makromolekulare Chemie, Rapid Communications* **1990**, *11* (11), 571-576.

53. You, J.-O.; Auguste, D. T., Feedback-regulated paclitaxel delivery based on poly(N,N-dimethylaminoethyl methacrylate-co-2-hydroxyethyl methacrylate) nanoparticles. *Biomaterials* **2008**, *29* (12), 1950-1957.

54. van de Wetering, P.; Moret, E. E.; Schuurmans-Nieuwenbroek, N. M. E.; van Steenbergen, M. J.; Hennink, W. E., Structure–Activity Relationships of Water-Soluble Cationic Methacrylate/Methacrylamide Polymers for Nonviral Gene Delivery. *Bioconjugate Chemistry* **1999**, *10* (4), 589-597.
55. Kavetskii, R. E.; Osinskii, S. P.; Bubnovskaya, L. N., Activation of glycolysis in tumor tissue by inorganic phosphate at low pH values. *Bull Exp Biol Med* **1979**, *87* (3), 277-278.
56. You, J.-O.; Auguste, D. T., Nanocarrier Cross-Linking Density and pH Sensitivity Regulate Intracellular Gene Transfer. *Nano Letters* **2009**, *9* (12), 4467-4473.
57. Chaterji, S.; Kwon, I. K.; Park, K., Smart Polymeric Gels: Redefining the Limits of Biomedical Devices. *Progress in polymer science* **2007**, *32* (8-9), 1083-1122.
58. Wong, J. E.; Gaharwar, A. K.; Müller-Schulte, D.; Bahadur, D.; Richtering, W., Dual-stimuli responsive PNiPAM microgel achieved via layer-by-layer assembly: Magnetic and thermoresponsive. *Journal of Colloid and Interface Science* **2008**, *324* (1–2), 47-54.
59. Thevenot, J.; Oliveira, H.; Sandre, O.; Lecommandoux, S., Magnetic responsive polymer composite materials. *Chemical Society Reviews* **2013**, *42* (17), 7099-7116.
60. Corpart, J. M.; Candau, F., Aqueous solution properties of ampholytic copolymers prepared in microemulsions. *Macromolecules* **1993**, *26* (6), 1333-1343.
61. Buenger, D.; Topuz, F.; Groll, J., Hydrogels in sensing applications. *Progress in Polymer Science* **2012**, *37* (12), 1678-1719.
62. Groll, J.; Amirgoulova, E. V.; Ameringer, T.; Heyes, C. D.; Röcker, C.; Nienhaus, G. U.; Möller, M., Biofunctionalized, Ultrathin Coatings of Cross-Linked Star-Shaped Poly(ethylene oxide) Allow Reversible Folding of Immobilized Proteins. *Journal of the American Chemical Society* **2004**, *126* (13), 4234-4239.

63. Branco, M. C.; Nettesheim, F.; Pochan, D. J.; Schneider, J. P.; Wagner, N. J., Fast Dynamics of Semiflexible Chain Networks of Self-Assembled Peptides. *Biomacromolecules* **2009**, *10* (6), 1374-1380.
64. Gander, B.; Gurny, R.; Doelker, E.; Peppas, N., Effect of Polymeric Network Structure on Drug Release from Cross-Linked Poly(Vinyl Alcohol) Micromatrices. *Pharm Res* **1989**, *6* (7), 578-584.
65. Biswal, D.; Hilt, J. Z., Microscale analysis of patterning reactions via FTIR imaging: Application to intelligent hydrogel systems. *Polymer* **2006**, *47* (21), 7355-7360.
66. Dalton, P. D.; Hostert, C.; Albrecht, K.; Moeller, M.; Groll, J., Structure and Properties of Urea-Crosslinked Star Poly[(ethylene oxide)-ran-(propylene oxide)] Hydrogels. *Macromolecular Bioscience* **2008**, *8* (10), 923-931.
67. Oh, K. S.; Oh, J. S.; Choi, H. S.; Bae, Y. C., Effect of Cross-Linking Density on Swelling Behavior of NIPA Gel Particles. *Macromolecules* **1998**, *31* (21), 7328-7335.
68. Atta, A. M.; Arndt, K. F., Temperature and pH sensitive ionic hydrogels based on new crosslinkers. *Polymers for Advanced Technologies* **2005**, *16* (6), 442-450.
69. Cheng, H.; Zhang, G., Thermally Sensitive Microgels: From Basic Science to Applications. In *Hydrogel Micro and Nanoparticles*, Wiley-VCH Verlag GmbH & Co. KGaA: 2012; pp 1-32.
70. Hu, L.; Sarker, A. K.; Islam, M. R.; Li, X.; Lu, Z.; Serpe, M. J., Poly (N-isopropylacrylamide) microgel-based assemblies. *Journal of Polymer Science Part A: Polymer Chemistry* **2013**, *51* (14), 3004-3020.
71. Wu, C.; Zhou, S., Thermodynamically Stable Globule State of a Single Poly(N-isopropylacrylamide) Chain in Water. *Macromolecules* **1995**, *28* (15), 5388-5390.
72. Wu, C.; Zhou, S., First Observation of the Molten Globule State of a Single Homopolymer Chain. *Physical Review Letters* **1996**, *77* (14), 3053-3055.

73. Nayak, S.; Lyon, L. A., Soft Nanotechnology with Soft Nanoparticles. *Angewandte Chemie International Edition* **2005**, *44* (47), 7686-7708.
74. Schild, H. G., Poly(N-isopropylacrylamide): experiment, theory and application. *Progress in Polymer Science* **1992**, *17* (2), 163-249.
75. Saunders, B. R.; Vincent, B., Microgel particles as model colloids: theory, properties and applications. *Advances in Colloid and Interface Science* **1999**, *80* (1), 1-25.
76. Smith, M. H.; Lyon, L. A., Tunable Encapsulation of Proteins within Charged Microgels. *Macromolecules* **2011**, *44* (20), 8154-8160.
77. Hu, X.; Tong, Z.; Lyon, L. A., Multicompartment Core/Shell Microgels. *Journal of the American Chemical Society* **2010**, *132* (33), 11470-11472.
78. Debord, J. D.; Lyon, L. A., On the Unusual Stability of Succinimidyl Esters in pNIPAm-AAc Microgels. *Bioconjugate Chemistry* **2007**, *18* (2), 601-604.
79. Hoffman, A.; Stayton, P.; Press, O.; Murthy, N.; Lackey, C.; Cheung, C.; Black, F.; Campbell, J.; Fausto, N.; Kyriakides, T.; Bornstein, P., Bioinspired polymers that control intracellular drug delivery. *Biotechnol. Bioprocess Eng.* **2001**, *6* (4), 205-212.
80. Still, T.; Chen, K.; Alsayed, A. M.; Aptowicz, K. B.; Yodh, A. G., Synthesis of micrometer-size poly(N-isopropylacrylamide) microgel particles with homogeneous crosslinker density and diameter control. *Journal of Colloid and Interface Science* **2013**, *405*, 96-102.
81. Hu, X.; Tong, Z.; Lyon, L. A., Control of Poly(N-isopropylacrylamide) Microgel Network Structure by Precipitation Polymerization near the Lower Critical Solution Temperature. *Langmuir : the ACS journal of surfaces and colloids* **2011**, *27* (7), 4142-4148.
82. Okay, O.; Funke, W., Conditions of microgel formation in homogeneous anionic polymerization of 1,4-divinylbenzene. *Die Makromolekulare Chemie* **1990**, *191* (7), 1565-1573.

83. Pelton, R., Temperature-sensitive aqueous microgels. *Advances in Colloid and Interface Science* **2000**, 85 (1), 1-33.
84. Khan, A., Preparation and characterization of N-isopropylacrylamide/acrylic acid copolymer core-shell microgel particles. *Journal of Colloid and Interface Science* **2007**, 313 (2), 697-704.
85. Pich, A.; Richtering, W., Microgels by Precipitation Polymerization: Synthesis, Characterization, and Functionalization. In *Chemical Design of Responsive Microgels*, Pich, A.; Richtering, W., Eds. Springer Berlin Heidelberg: 2011; Vol. 234, pp 1-37.
86. Lee, A.; Tsai, H. Y.; Yates, M. Z., Steric Stabilization of Thermally Responsive N-isopropylacrylamide Particles by Poly(vinyl alcohol). *Langmuir : the ACS journal of surfaces and colloids* **2010**, 26 (23), 18055-18060.
87. Sorrell, C. D.; Carter, M. C. D.; Serpe, M. J., Color Tunable Poly (N-Isopropylacrylamide)-co-Acrylic Acid Microgel-Au Hybrid Assemblies. *Advanced Functional Materials* **2011**, 21 (3), 425-433.
88. Sorrell, C. D.; Serpe, M. J., Reflection Order Selectivity of Color-Tunable Poly(N-isopropylacrylamide) Microgel Based Etalons. *Advanced Materials* **2011**, 23 (35), 4088-4092.
89. Michael, J., Poly (N-Isopropylacrylamide) Microgel-Based Etalons for Optical Sensing. *Journal of Analytical & Bioanalytical Techniques* **2012**.
90. Su, S.; Ali, M. M.; Filipe, C. D. M.; Li, Y.; Pelton, R., Microgel-Based Inks for Paper-Supported Biosensing Applications. *Biomacromolecules* **2008**, 9 (3), 935-941.
91. Parasuraman, D.; Leung, E.; Serpe, M., Poly (N-isopropylacrylamide) microgel based assemblies for organic dye removal from water: microgel diameter effects. *Colloid Polym Sci* **2012**, 290 (11), 1053-1064.
92. Kiser, P. F.; Wilson, G.; Needham, D., A synthetic mimic of the secretory granule for drug delivery. *Nature* **1998**, 394 (6692), 459-462.

93. Hoare, T.; Pelton, R., Charge-Switching, Amphoteric Glucose-Responsive Microgels with Physiological Swelling Activity. *Biomacromolecules* **2008**, *9* (2), 733-740.
94. Sorrell, C.; Serpe, M., Glucose sensitive poly (N-isopropylacrylamide) microgel based etalons. *Anal Bioanal Chem* **2012**, *402* (7), 2385-2393.
95. Parasuraman, D.; Sarker, A. K.; Serpe, M. J., Poly(N-Isopropylacrylamide)-Based Microgels and Their Assemblies for Organic-Molecule Removal from Water. *ChemPhysChem* **2012**, *13* (10), 2507-2515.
96. Hoare, T.; Pelton, R., Impact of Microgel Morphology on Functionalized Microgel–Drug Interactions. *Langmuir* **2008**, *24* (3), 1005-1012.
97. Sigolaeva, L. V.; Gladyr, S. Y.; Gelissen, A. P. H.; Mergel, O.; Pergushov, D. V.; Kurochkin, I. N.; Plamper, F. A.; Richtering, W., Dual-Stimuli-Sensitive Microgels as a Tool for Stimulated Spongelike Adsorption of Biomaterials for Biosensor Applications. *Biomacromolecules* **2014**, *15* (10), 3735-3745.
98. Schmidt, S.; Zeiser, M.; Hellweg, T.; Duschl, C.; Fery, A.; Möhwald, H., Adhesion and Mechanical Properties of PNIPAM Microgel Films and Their Potential Use as Switchable Cell Culture Substrates. *Advanced Functional Materials* **2010**, *20* (19), 3235-3243.
99. Islam, M. R.; Ahiabu, A.; Li, X.; Serpe, M. J., Poly (N-isopropylacrylamide) Microgel-Based Optical Devices for Sensing and Biosensing. *Sensors (Basel, Switzerland)* **2014**, *14* (5), 8984-8995.
100. Contreras-Cáceres, R.; Sánchez-Iglesias, A.; Karg, M.; Pastoriza-Santos, I.; Pérez-Juste, J.; Pacifico, J.; Hellweg, T.; Fernández-Barbero, A.; Liz-Marzán, L. M., Encapsulation and Growth of Gold Nanoparticles in Thermoresponsive Microgels. *Advanced Materials* **2008**, *20* (9), 1666-1670.

101. John, H. O. H.; Jeffrey, H. H., Adsolubilization: Some Expected and Unexpected Results. In *Surfactant Adsorption and Surface Solubilization*, American Chemical Society: 1996; Vol. 615, pp 49-66.
102. Wu, W.; Zhou, S., Hybrid micro-/nanogels for optical sensing and intracellular imaging. *Nano Reviews* **2010**, *1*, 10.3402/nano.v1i0.5730.
103. Delair, T.; Meunier, F.; Elaïssari, A.; Charles, M.-H.; Pichot, C., Amino-containing cationic latex–oligodeoxyribonucleotide conjugates: application to diagnostic test sensitivity enhancement. *Colloids and Surfaces A: Physicochemical and Engineering Aspects* **1999**, *153* (1–3), 341-353.
104. Nayak, S.; Lee, H.; Chmielewski, J.; Lyon, L. A., Folate-mediated cell targeting and cytotoxicity using thermoresponsive microgels. *Journal of the American Chemical Society* **2004**, *126* (33), 10258-10259.
105. Luo, Q.; Liu, P.; Guan, Y.; Zhang, Y., Thermally Induced Phase Transition of Glucose-Sensitive Core–Shell Microgels. *ACS Applied Materials & Interfaces* **2010**, *2* (3), 760-767.
106. Cheng, C. I.; Chang, Y.-P.; Chu, Y.-H., Biomolecular interactions and tools for their recognition: focus on the quartz crystal microbalance and its diverse surface chemistries and applications. *Chemical Society Reviews* **2012**, *41* (5), 1947-1971.
107. Janshoff, A.; Steinem, C., Quartz Crystal Microbalance for Bioanalytical Applications. *Sensors Update* **2001**, *9* (1), 313-354.
108. O’Sullivan, C. K.; Guilbault, G. G., Commercial quartz crystal microbalances – theory and applications. *Biosensors and Bioelectronics* **1999**, *14* (8–9), 663-670.
109. Höök, F. Development of a novel QCM technique for protein adsorption studies. Ph.D Thesis, Chalmers University of Technology and Goteborg University, 1997.

110. Johnson, K. C. C.; Mendez, F.; Serpe, M. J., Detecting solution pH changes using poly (N-isopropylacrylamide)-co-acrylic acid microgel-based etalon modified quartz crystal microbalances. *Analytica Chimica Acta* **2012**, *739*, 83-88.
111. Marx, K. A., Quartz Crystal Microbalance: A Useful Tool for Studying Thin Polymer Films and Complex Biomolecular Systems at the Solution–Surface Interface. *Biomacromolecules* **2003**, *4* (5), 1099-1120.
112. Keiji Kanazawa, K.; Gordon, J. G., The oscillation frequency of a quartz resonator in contact with liquid. *Analytica Chimica Acta* **1985**, *175*, 99-105.
113. Bianco, M.; Aloisi, A.; Arima, V.; Capello, M.; Ferri-Borgogno, S.; Novelli, F.; Leporatti, S.; Rinaldi, R., Quartz crystal microbalance with dissipation (QCM-D) as tool to exploit antigen–antibody interactions in pancreatic ductal adenocarcinoma detection. *Biosensors and Bioelectronics* **2013**, *42*, 646-652.
114. Modin, C.; Stranne, A.-L.; Foss, M.; Duch, M.; Justesen, J.; Chevallier, J.; Andersen, L. K.; Hemmersam, A. G.; Pedersen, F. S.; Besenbacher, F., QCM-D studies of attachment and differential spreading of pre-osteoblastic cells on Ta and Cr surfaces. *Biomaterials* **2006**, *27* (8), 1346-1354.
115. QCM 100- Quartz Crystal Microbalance Theory and Calibration. Stanford Research Systems: U.S.A, 2009.
116. Islam, M. R.; Johnson, K. C. C.; Serpe, M. J., Microgel-based etalon coated quartz crystal microbalances for detecting solution pH: The effect of Au overlayer thickness. *Analytica Chimica Acta* **2013**, *792*, 110-114.
117. Parra, A.; Casero, E.; Pariente, F.; Vázquez, L.; Lorenzo, E., Cholesterol oxidase modified gold electrodes as bioanalytical devices. *Sensors and Actuators B: Chemical* **2007**, *124* (1), 30-37.

118. Takeda, S.; Ozaki, H.; Hattori, S.; Ishii, A.; Kida, H.; Mukasa, K., Detection of Influenza Virus Hemagglutinin with Randomly Immobilized Anti-Hemagglutinin Antibody on a Carbon Nanotube Sensor. *Journal of Nanoscience and Nanotechnology* **2007**, *7* (3), 752-756.
119. Croll, T. I.; O'Connor, A. J.; Stevens, G. W.; Cooper-White, J. J., Controllable Surface Modification of Poly(lactic-co-glycolic acid) (PLGA) by Hydrolysis or Aminolysis I: Physical, Chemical, and Theoretical Aspects. *Biomacromolecules* **2004**, *5* (2), 463-473.
120. Pastorino, L.; Caneva Soumetz, F.; Giacomini, M.; Ruggiero, C., Development of a piezoelectric immunosensor for the measurement of paclitaxel. *Journal of Immunological Methods* **2006**, *313* (1-2), 191-198.
121. Pastorino, L.; Disawal, S.; Nicolini, C.; Lvov, Y. M.; Erokhin, V. V., Complex catalytic colloids on the basis of firefly luciferase as optical nanosensor platform. *Biotechnology and Bioengineering* **2003**, *84* (3), 286-291.
122. Prime, K.; Whitesides, G., Self-assembled organic monolayers: model systems for studying adsorption of proteins at surfaces. *Science* **1991**, *252* (5009), 1164-1167.
123. Su, X., Covalent DNA Immobilization on Polymer-Shielded Silver-Coated Quartz Crystal Microbalance Using Photobiotin-Based UV Irradiation. *Biochemical and Biophysical Research Communications* **2002**, *290* (3), 962-966.
124. Brochu, H.; Vermette, P., Liposome Layers Characterized by Quartz Crystal Microbalance Measurements and Multirelease Delivery. *Langmuir* **2007**, *23* (14), 7679-7686.
125. Chen, K.-S.; Chen, S.-C.; Lin, H.-R.; Yan, T.-R.; Tseng, C.-C., A novel technique to immobilize DNA on surface of a quartz crystal microbalance by plasma treatment and graft polymerization. *Materials Science and Engineering: C* **2007**, *27* (4), 716-724.
126. Papadopoulou-Bouraoui, A.; Barrero-Moreno, J.; Lejeune, M.; Bretagnol, F.; Manso, M.; Valsesia, A.; Colpo, P.; Gilliland, D.; Ceccone, G.; Rossi, F., *Sensors and Materials* **2006**, *18* (353), 366.

127. Zeng, H.; Wang, H.; Chen, F.; Xin, H.; Wang, G.; Xiao, L.; Song, K.; Wu, D.; He, Q.; Shen, G., Development of quartz-crystal-microbalance-based immunosensor array for clinical immunophenotyping of acute leukemias. *Analytical Biochemistry* **2006**, *351* (1), 69-76.
128. Cooper, M. A.; Singleton, V. T., A survey of the 2001 to 2005 quartz crystal microbalance biosensor literature: applications of acoustic physics to the analysis of biomolecular interactions. *Journal of Molecular Recognition* **2007**, *20* (3), 154-184.
129. Janshoff, A.; Steinem, C.; Sieber, M.; Galla, H. J., Specific binding of peanut agglutinin to GM1-doped solid supported lipid bilayers investigated by shear wave resonator measurements. *Eur Biophys J* **1996**, *25* (2), 105-113.
130. Caruso, F.; Furlong, D. N.; Kingshott, P., Characterization of Ferritin Adsorption onto Gold. *Journal of Colloid and Interface Science* **1997**, *186* (1), 129-140.
131. Guilbault, G. G., Determination of formaldehyde with an enzyme-coated piezoelectric crystal detector. *Anal. Chem.* **1983**, *55* (11), 1682-1684.
132. Guilbault, G. G.; Jordan, J. M.; Scheide, E., Analytical Uses of Piezoelectric Crystals: A Review. *C R C Critical Reviews in Analytical Chemistry* **1988**, *19* (1), 1-28.
133. Tang, D.; Li, Q.; Tang, J.; Su, B.; Chen, G., An enzyme-free quartz crystal microbalance biosensor for sensitive glucose detection in biological fluids based on glucose/dextran displacement approach. *Analytica Chimica Acta* **2011**, *686* (1-2), 144-149.
134. Wang, Y.; Chalagalla, S.; Li, T.; Sun, X.-l.; Zhao, W.; Wang, P. G.; Zeng, X., Multivalent interaction-based carbohydrate biosensors for signal amplification. *Biosensors and Bioelectronics* **2010**, *26* (3), 996-1001.
135. Karamollaoğlu, İ.; Öktem, H. A.; Mutlu, M., QCM-based DNA biosensor for detection of genetically modified organisms (GMOs). *Biochemical Engineering Journal* **2009**, *44* (2-3), 142-150.

136. Mutlu, S.; Saber, R.; Koçum, C.; Piskin, E., An Immunosensor: Immobilization of Anti-HBs Antibody on Glow-Discharge Treated Piezoelectric Quartz Crystal for HBs-Ag Detection. *Analytical Letters* **1999**, *32* (2), 317-334.
137. Saber, R.; Mutlu, S.; Pişkin, E., Glow-discharge treated piezoelectric quartz crystals as immunosensors for HSA detection. *Biosensors and Bioelectronics* **2002**, *17* (9), 727-734.
138. Zhou, X. C.; Huang, L. Q.; Li, S. F. Y., Microgravimetric DNA sensor based on quartz crystal microbalance: comparison of oligonucleotide immobilization methods and the application in genetic diagnosis. *Biosensors and Bioelectronics* **2001**, *16* (1–2), 85-95.
139. Chang., B.; Zhao., T. *Quartz Crystal Microbalance study of DNA immobilization and hybridization for DNA sensor development*; Michigan State University,: 2008.
140. Rodahl, M.; Höök, F.; Krozer, A.; Brzezinski, P.; Kasemo, B., Quartz crystal microbalance setup for frequency and Q-factor measurements in gaseous and liquid environments. *Review of Scientific Instruments* **1995**, *66* (7), 3924-3930.
141. Höök, F.; Rodahl, M.; Brzezinski, P.; Kasemo, B., Energy Dissipation Kinetics for Protein and Antibody–Antigen Adsorption under Shear Oscillation on a Quartz Crystal Microbalance. *Langmuir* **1998**, *14* (4), 729-734.
142. Nomura, T.; Hattori, O., Determination of micromolar concentrations of cyanide in solution with a piezoelectric detector. *Analytica Chimica Acta* **1980**, *115*, 323-326.
143. Stockbridge, C. D., *Effect of Hydrostatic Pressure on Rotated Y-Cut Quartz Crystal Resonators*. Plenum Press: New York, 1966; Vol. 5, p 179-191.
144. High Blood Sugar. *Total Health Life* May 4, 2011, 2005.
145. Walls, R.; Ratey, J. J.; Simon, R. I., *Rosen's Emergency Medicine: Expert Consult Premium Edition*. St. Louis: Mosby., 2009.
146. Department of Health information of healthy New York, The important of controlling blood sugar.

[https://www.health.ny.gov/diseases/conditions/diabetes/controlling\\_blood\\_sugar\\_importance.htm](https://www.health.ny.gov/diseases/conditions/diabetes/controlling_blood_sugar_importance.htm) (accessed September 30).

147. Hidekatsu Yanai; Hiroki Adachi; Hisayuki Katsuyama; Sumie Moriyama; Hamasaki, H.; Sako., A., Causative anti-diabetic drugs and the underlying clinical factors for hypoglycemia in patients with diabetes. *World J Diabetes* **2015**, *6* (1), 30-36.

148. Schrier, R. W., *The internal medicine casebook real patients, real answers*. 3rd edition ed.; Lippincott Williams & Wilkins: Philadelphia, 2007; p 119.

149. Yoo, E.-H.; Lee, S.-Y., Correction: Yoo, E.H., et al. Glucose Biosensors: An Overview of Use in Clinical Practice. *Sensors* 2010, *10*, 4558–4576. *Sensors (Basel, Switzerland)* **2010**, *10* (5), 1-2.

150. *American Diabetes Association. Diagnosis and classification of diabetes mellitus.*; 2010; pp 62-69.

151. Diabetes: How to Use Insulin. *American Family Physician* Aug, 1, 1999, pp 649-651.

152. Habermüller, K.; Mosbach, M.; Schuhmann, W., Electron-transfer mechanisms in amperometric biosensors. *Fresenius J Anal Chem* **2000**, *366* (6-7), 560-568.

153. Pearson, J. E.; Gill, A.; Vadgama, P., Analytical aspects of biosensors. *Annals of Clinical Biochemistry* **2000**, *37* (2), 119-145.

154. Clark, L. C.; Lyons, C., ELECTRODE SYSTEMS FOR CONTINUOUS MONITORING IN CARDIOVASCULAR SURGERY. *Annals of the New York Academy of Sciences* **1962**, *102* (1), 29-45.

155. Wang, J., Glucose Biosensors: 40 Years of Advances and Challenges. *Electroanalysis* **2001**, *13* (12), 983-988.

156. Updike, S. J.; Hicks, G. P., The Enzyme Electrode. *Nature* **1967**, *214* (5092), 986-988.

157. Chaubey, A.; Malhotra, B. D., Mediated biosensors. *Biosensors and Bioelectronics* **2002**, *17* (6–7), 441-456.

158. Berendsen, W. R.; Lapin, A.; Reuss, M., Investigations of Reaction Kinetics for Immobilized Enzymes—Identification of Parameters in the Presence of Diffusion Limitation. *Biotechnology Progress* **2006**, *22* (5), 1305-1312.
159. Rahman, M. M.; Saleh Ahammad, A. J.; Jin, J.-H.; Ahn, S. J.; Lee, J.-J., A Comprehensive Review of Glucose Biosensors Based on Nanostructured Metal-Oxides. *Sensors (Basel, Switzerland)* **2010**, *10* (5), 4855-4886.
160. Liu J.; J., W., Improved design for the glucose biosensor. *Food technology and biotechnology*. **2001**, *39*, 55–58.
161. Shichiri, M.; Yamasaki, Y.; Kawamori, R.; Hakui, N.; Abe, H., WEARABLE ARTIFICIAL ENDOCRINE PANCREAS WITH NEEDLE-TYPE GLUCOSE SENSOR. *The Lancet* **1982**, *320* (8308), 1129-1131.
162. Cass, A. E. G.; Davis, G.; Francis, G. D.; Hill, H. A. O.; Aston, W. J.; Higgins, I. J.; Plotkin, E. V.; Scott, L. D. L.; Turner, A. P. F., Ferrocene-mediated enzyme electrode for amperometric determination of glucose. *Anal. Chem.* **1984**, *56* (4), 667-671.
163. Frew, J. E.; Hill, H. A. O., Electrochemical biosensors. *Anal. Chem.* **1987**, *59* (15), 933A-944A.
164. Palmisano, F.; Zambonin, P. G.; Centonze, D.; Quinto, M., A Disposable, Reagentless, Third-Generation Glucose Biosensor Based on Overoxidized Poly(pyrrole)/Tetrathiafulvalene– Tetracyanoquinodimethane Composite. *Anal. Chem.* **2002**, *74* (23), 5913-5918.
165. Yokoyama, K.; Tamiya, E.; Karube, I., Performance of an Integrated Biosensor Composed of a Mediated and an Oxygen-Based Glucose Sensor Under Unknown Oxygen Tension. *Analytical Letters* **1989**, *22* (15), 2949-2959.
166. Foulds, N. C.; Lowe, C. R., Enzyme entrapment in electrically conducting polymers. Immobilisation of glucose oxidase in polypyrrole and its application in amperometric glucose

sensors. *Journal of the Chemical Society, Faraday Transactions 1: Physical Chemistry in Condensed Phases* **1986**, 82 (4), 1259-1264.

167. Kajiya, Y.; Sugai, H.; Iwakura, C.; Yoneyama, H., Glucose sensitivity of polypyrrole films containing immobilized glucose oxidase and hydroquinonesulfonate ions. *Anal. Chem.* **1991**, 63 (1), 49-54.

168. Wang, J., Electrochemical Glucose Biosensors. *Chemical Reviews* **2008**, 108 (2), 814-825.

169. J.K., K.; C.C., R., Important features of blood glucose meters. *J Am Pharm Assoc* **1988**, 38 (2), 210-219.

170. Harris, D. C., *Quantitative chemical analysis*. New York, N.Y. : W.H. Freeman and Co., c2007.

7th ed.: 2007.

171. Su, S.; Wu, W.; Gao, J.; Lu, J.; Fan, C., Nanomaterials-based sensors for applications in environmental monitoring. *Journal of Materials Chemistry* **2012**, 22 (35), 18101-18110.

172. Salimi, A.; Compton, R. G.; Hallaj, R., Glucose biosensor prepared by glucose oxidase encapsulated sol-gel and carbon-nanotube-modified basal plane pyrolytic graphite electrode. *Analytical Biochemistry* **2004**, 333 (1), 49-56.

173. Dervisevic, M.; Çevik, E.; Şenel, M., Development of glucose biosensor based on reconstitution of glucose oxidase onto polymeric redox mediator coated pencil graphite electrodes. *Enzyme and Microbial Technology* **2015**, 68, 69-76.

174. Matthews, D. R.; Bown, E.; Watson, A.; Holman, R. R.; Steemson, J.; Hughes, S.; Scott, D., PEN-SIZED DIGITAL 30-SECOND BLOOD GLUCOSE METER. *The Lancet* **1987**, 329 (8536), 778-779.

175. Zhang, Y.; Guan, Y.; Zhou, S., Synthesis and Volume Phase Transitions of Glucose-Sensitive Microgels. *Biomacromolecules* **2006**, 7 (11), 3196-3201.

176. Matsumoto, A.; Yoshida, R.; Kataoka, K., Glucose-Responsive Polymer Gel Bearing Phenylborate Derivative as a Glucose-Sensing Moiety Operating at the Physiological pH. *Biomacromolecules* **2004**, *5* (3), 1038-1045.
177. Springsteen, G.; Wang, B., A detailed examination of boronic acid–diol complexation. *Tetrahedron* **2002**, *58* (26), 5291-5300.
178. Sorrell, C. D.; Carter, M. C. D.; Serpe, M. J., A “Paint-On” Protocol for the Facile Assembly of Uniform Microgel Coatings for Color Tunable Etalon Fabrication. *ACS Applied Materials & Interfaces* **2011**, *3* (4), 1140-1147.
179. Jones, C. D.; Lyon, L. A., Synthesis and Characterization of Multiresponsive Core–Shell Microgels. *Macromolecules* **2000**, *33* (22), 8301-8306.
180. Cohen, A.; Derr, V. E.; McNice, G. T.; Cupp, R. E., Measurement of Mie Scattering Intensities from Monodispersed Spherical Particles as a Function of Wavelength. *Appl. Opt.* **1973**, *12* (4), 779-782.
181. Ginsberg, B. H., Factors Affecting Blood Glucose Monitoring: Sources of Errors in Measurement. *Journal of diabetes science and technology (Online)* **2009**, *3* (4), 903-913.
182. Böeseken, J., The use of Boric Acid for the Determination of the Configuration of Carbohydrates. In *Advances in Carbohydrate Chemistry*, Pigman, W. W.; Wolfro, M. L., Eds. Academic Press: 1949; Vol. Volume 4, pp 189-210.
183. Lorand, J. P.; Edwards, J. O., Polyol Complexes and Structure of the Benzeneboronate Ion. *The Journal of Organic Chemistry* **1959**, *24* (6), 769-774.
184. Vignon, L., *C. R. Acad. Sci.* **1874**, *78*, 148-149.
185. Wu, X.; Li, Z.; Chen, X.-X.; Fossey, J. S.; James, T. D.; Jiang, Y.-B., Selective sensing of saccharides using simple boronic acids and their aggregates. *Chemical Society Reviews* **2013**, *42* (20), 8032-8048.

186. Norrild, J. C.; Eggert, H., Boronic acids as fructose sensors. Structure determination of the complexes involved using  $^1\text{JCC}$  coupling constants. *Journal of the Chemical Society, Perkin Transactions 2* **1996**, (12), 2583-2588.